FAST NUMERICAL SOLUTION OF EXTERIOR HELMHOLTZ PROBLEMS WITH RADIATION BOUNDARY CONDITION BY IMBEDDING

A DISSERTATION
SUBMITTED TO THE PROGRAM IN SCIENTIFIC COMPUTING AND COMPUTATIONAL MATHEMATICS
AND THE COMMITTEE ON GRADUATE STUDIES
OF STANFORD UNIVERSITY
IN PARTIAL FULFILLMENT OF THE REQUIREMENTS
FOR THE DEGREE OF
DOCTOR OF PHILOSOPHY

By
Oliver G. Ernst
October 1994

I certify that I have read this dissertation and that in my opinion it is fully adequate, in scope and in quality, as a dissertation for the degree of Doctor of Philosophy.

Prof. Gene H. Golub
(Principal Adviser)

I certify that I have read this dissertation and that in my opinion it is fully adequate, in scope and in quality, as a dissertation for the degree of Doctor of Philosophy.

Prof. Joseph B. Keller

I certify that I have read this dissertation and that in my opinion it is fully adequate, in scope and in quality, as a dissertation for the degree of Doctor of Philosophy.

Prof. George C. Papanicolaou

Approved for the University Committee on Graduate Studies:

Dean of Graduate Studies

Abstract

The development of efficient solution algorithms for Poisson's equation on domains allowing for separation of variables prompted research towards extending these algorithms to domains of general shape. The resulting numerical techniques are known as imbedding methods or capacitance matrix methods. In this dissertation, we develop capacitance matrix methods for exterior boundary value problems for the Helmholtz equation, a second-order elliptic PDE which governs time-harmonic wave propagation.

Solutions of exterior Helmholtz problems must satisfy an asymptotic boundary condition at infinity in order to be uniquely determined. We incorporate this boundary condition into the discretization by posing the Dirichlet-to-Neumann (DtN) condition, an exact non-local boundary condition, on a circular artificial boundary. A fast Helmholtz solver of complexity $\mathcal{O}(nm \log n)$ can then be obtained for the resulting discrete problem on an $m \times n$ grid when the underlying computational domain is an annulus or a disk.

This fast solver is used as the main computational ingredient in two capacitance matrix methods. We introduce both a direct finite-difference based method as well as an iterative variant based on a finite-element discretization. Imbedding methods relate the discrete problem on the original domain to a suitable discrete problem on an auxiliary domain for which a fast solver is available. This relation is described by the capacitance matrix, a dense square matrix whose computation and factorization incurs substantial overhead. The direct method is efficient for problems with many right hand sides, since this overhead is amortized over several subproblems. In the iterative variant, the computation of the capacitance matrix is avoided altogether,

since the iterative solver used requires the matrix only for the formation of matrix-vector products, which can be computed without explicitly computing the matrix.

The resulting algorithms are applied to plane wave-scattering problems on several two-dimensional geometries.

Acknowledgements

First and foremost, I would like to express my gratitude to my adviser Prof. Gene Golub for the role he has played in bringing about this thesis project and in helping me to embark on a carreer in numerical analysis. From encouraging me to come to apply to Stanford's Scientific Computing and Computational Mathematics program while I was still a student in Germany, to the generosity with which he made it possible for me to attend conferences as a graduate student from very early on to the care he took in introducing me to countless researchers in the field, Gene has been a constant benign force in my life as a graduate student at Stanford. It is largely due to him that the atmosphere surrounding the SCCM program is such a pleasant one.

I wish to thank Prof. George Papanicolaou and Prof. Joe Keller for taking the time to serve on my reading committee and for many helpful discussions and advice on my work. I also thank Prof. Andrew Stuart for being on my oral exam committee and Prof. Peter Pinsky for chairing the exam.

It is a pleasure to acknowledge financial support for my thesis project from Dassault Aviation, France and especially to thank Dr. Jacques Périaux for continued support, encouragement and inspiration. I also thank Dr. Gérard Meurant for suggesting the thesis topic.

I thank Prof. Joe Oliger and Prof. Bob Street who provided financial support during my first year at Stanford and I am also gratful to Prof. Bob Dutton for financial support during my last summer at Stanford and for generously providing access to the IBM SP1 in his lab on which the computations in this thesis were performed.

My time at Stanford was very much enriched by the SCCM students I've had the pleasure of working with. There has always been a very friendly climate among the students here as well as a tradition of mutual support and encouragement. Special thanks goes to my office mates Marcus Grote, Gabriel Lord, Amala Mahadevan and Liliana Borcea for their friendship and long discussions on numerical analysis.

I also owe thanks to SCCM's system administrator/secretary/student services coordinator Mary Washburn, whose superb management of SCCM's computer system and guiding hand through the intricacies of Stanford's administration made for very smooth sailing. Mary was also a constant source of good cheer and has become a friend I will miss.

Finally, I would like to thank my wife Susanne for her love, companionship and infinite support throughout our time at Stanford and for putting up with my working hours and my preoccupation with $\Delta + k^2$ during the often strenuous phases of graduate student life.

This is probably also the proper place to thank the person who got me on the 'math track' in the first place, my mathematics teacher Werner Bakowsky at the Okengymnasium in Offenburg, Germany, who didn't think seventh grade was too early to introduce us to the group axioms.

Contents

List of Tables

List of Figures

Chapter 1

Introduction

1.1 History of Imbedding Methods

This section is intended to provide an overview of the development of imbedding techniques for boundary value problems over the last 25 years. It is by no means complete, but it does summarize the literature that gave the basis for the research contained in this thesis.

1.1.1 Fast Poisson Solvers

Fast Poisson solvers, from which imbedding methods derive their efficiency, were developed in the mid 1960s. They are efficient implementations of the method of separation of variables known from the theory of partial differential equations. Numerical algorithms based on separation of variables techniques had been in use before, but these all had higher complexities than what are now known as fast Poisson solvers. Just as in the continuous case, the differential operator and the boundary conditions of the boundary value problem need to separate and the underlying domain must be rectangular in a suitable coordinate system in order for the method to be applicable. It is the constraints on the domain and the boundary conditions which imbedding algorithms attempt to circumvent.

There are basically two different approaches used in fast Poisson solvers, one relying on the fast Fourier transform, the other on block cyclic reduction. The FFT-based algorithm cf. [61], sometimes referred to as *matrix decomposition*, diagonalizes the problem in one of the variables by exploiting the fact that multiplying with the eigenfunctions in that variable can be accomplished by a discrete sine, cosine or complete Fourier transform, depending on whether Dirichlet, Neumann or periodic boundary conditions are imposed. In conrast, *block cyclic reduction*, also known as *odd-even reduction*, eliminates blocks of unknowns such that the blocks of the reduced systems are polynomials in the blocks of the original coefficient matrix, the block dimension of the reduced system being roughly halved at each step so that a divide-and-conquer type algorithm results. The polynomials involved are Chebyshev polynomials, the zeros of which are known, so that the reduced systems can typically be factored by shifting tridiagonal matrices by these zeros times the identity. The odd-even reduction algorithm was suggested to R. Hockney by G. Golub, who had discovered the method as a technique for solving systems with tridiagonal coefficient matrices [55]. The algorithm is highly unstable when used in its block variant for higher dimensional boundary value problems on large meshes and it was a modification due to O. Buneman [21] that resulted in a practical method. Both the matrix decomposition and the cyclic reduction algorithms have a complexity of $\mathcal{O}(nm \log n)$ on an $m \times n$ rectangular grid with with a constant less than ten. A combination of the two algorithms due to R. Hockney known as FACR reduces this complexity further to $\mathcal{O}(mn \log\log n)$. All these techniques are described in Buzbee, Golub and Nielson [22].

Some survey articles for fast Poisson solvers are [32, 22, 102, 101, 62]. A library of fast Poisson solver software for two and three-dimensional problems for rectangular, circular and spherical geometries can be found on NETLIB in the software package named FISHPAK which was developed by P. Swarztrauber and R. Sweet.

1.1.2 Origins of the Capacitance Matrix Method

The origin of the capacitance matrix method is probably a classical technique used in electrostatics, where it is known as the “capacity matrix method”. It describes the linear relationship between the electrostatic potential at given points due to a system of point charges of various magnitudes. A background reference for this idea, which dates back to Maxwell, is Sommerfeld [98]. Note, however, that the classical capacity matrix corresponds to the inverse of what is usually called the capacitance matrix in the context of imbedding methods.

Curiously enough, the term capacity matrix ("Kapazitätsmatrix") is also used in a 1952 paper by Hermann Weyl [106] titled "The Capacity of Radiation Fields" in which an existence proof is given for the exterior Helmholtz problem using the method of integral equations (cf. [83]). The term capacity matrix is used there to refer to the bijective linear operator between the null spaces of the second-kind Fredholm integral operators belonging to the double layer potential and its transpose. This operator serves as a tool for constructing a solution.

1.1.3 The Numerical Method

To the author's knowledge, the first papers describing imbedding methods for numerically solving elliptic boundary value problems appeared in 1970, one by R. Hockney [62], the other by A. George [43].

Hockney's paper describes the solution of Poisson's equation on a rectangle with various types of linear boundary conditions. In addition, the solution is fixed at certain points inside the domain which he calls "interior electrodes". The problem is first solved ignoring the interior electrodes, resulting in a non-zero residual at these points. A correction to this first solution causing the residual to vanish also at the interior electrodes is then sought as the solution to the same linear system with the right hand side, or source term, modified at these points. This procedure can be interpreted in the electrostatic setting as placing point charges at the interior electrodes in such a way that the proper correction is obtained. These point charges are the solution to a dense system of linear equations. Here also, the term "capacity matrix" is used for the *inverse* of the corresponding coefficient matrix. The fast solver used is the FFT diagonalization combined with cyclic reduction used to solve the tridiagonal systems of the transformed equations. According to [55], the suggestion of seeking a numerical analogue to this engineering tool is due to Buneman.

In [43], A. George considers the Dirichlet problem for Poisson's equation on a doubly connected domain bounded internally and externally by axis-aligned rectangles. He introduces two imbedding methods, the first being Hockney's method, and also develops iterative variants of these which avoid computing the capacitance matrix. The capacitance matrices are symmetric and positive definite for this problem, so that the conjugate gradient method can be used for the iteration. The term "iterative imbedding algorithm" is also introduced here.

The fact that using the conjugate gradient method when applicable to solve the capacitance matrix equation corresponds to solving the original system with the conjugate gradient algorithm preconditioned with a 'nearby' matrix for which a fast solver is available is also mentioned in [28].

1.1.4 Matrix Formulations

A rather general matrix formulation of the capacitance matrix idea is presented in Buzbee et al. [23] in 1971. The authors consider the case where the coefficient matrix A of the linear system to be solved differs in p rows from a matrix B for which a fast solver is available. It is shown that, if B is nonsingular, then consistency of the system to be solved implies consistency of the capacitance matrix equation. A capacitance matrix algorithm for the case of rank-deficient B with nonsingular A is also introduced. The issue of when to imbed and when to split the domain into subdomains is also raised here.

The condition number of the capacitance matrix is analyzed in [113] and the bound $\kappa(C) \leq \max\{k_1, k_2\}\kappa(A)\kappa(B)$ is derived where $A = B + UV^T$ and $k_1 = (\|U\|\|U^\dagger\|)^2$, $k_2 = (\|V^T\|(V^T)^\dagger\|)^2$. In the context of elliptic boundary problems in two dimensions discretized with mesh width parameter h, the condition number of the discretization matrices is proportional to h^{-2}, so that this bound can become quite large. An extensive survey of updating techniques for the inverse of a matrix can be found in [57].

1.1.5 Application to Differential Equations

The development of the matrix algorithms into a practical tool for solving a large class elliptic boundary value problems for partial differential equations is due in large part to O. Widlund and his co-workers, who began making use of properties of the underlying continuous operators to obtain faster and more stable capacitance matrix algorithms. The first in this sequence of papers seems to be [107] in which the relation of the technique of separation of variables and methods of potential theory to the previously developed matrix algorithms are explored. The next big step came with the 1976 paper by Proskurowski and Widlund [89], where the capacitance matrix method was used to solve (positive definite) Helmholtz equations of the form $-\Delta u + cu = f,\ 0 < c =$ const. on bounded non-rectangular domains. The key observation made in this work is the formal analogy of solving discrete Poisson equations by the capacitance matrix method based on the Woodbury formula with the single-layer Ansatz of the method of integral equations for solving the continuous problem. In the theory of the integral equations of potential theory, it is known that the single-layer Ansatz leads to a first-kind Fredholm integral equation, which is ill-posed since the solution operator is unbounded. Any discretization of this equation should thus be progressively more ill-conditioned as the mesh is refined. This phenomenon, which the authors verify in numerical tests, causes them to seek a discrete analog of what in the integral equations theory leads to a well-posed problem, namely using a double-layer or dipole Ansatz. The resulting method yields capacitance matrices for the Dirichlet problem which are uniformly well-conditioned with respect to the mesh size. This well-conditioning is exploited by using the conjugate gradient method applied to the normal equations to solve the capacitance matrix equation, where the uniformly low condition number guarantees uniformly fast convergence rates of this iterative method. A detailed convergence analysis of finite-difference capacitance matrix methods for the Dirichlet and Neumann problems for Poisson's equation is perfomed by A. Shieh in [95] and [96]. The Proskurowski and Widlund algorithm was extended to three-dimensional problems by O'Leary and Widlund in [86]. Short survey articles on these type of methods can be found in [107, 108, 87, 88].

Proskurowski and Widlund also developed a finite element capacitance matrix method for Laplace's equation in [90]. This work was carried on by Börgers and Widlund in a series of papers [16], [17] and [15]. Finite element capacitance matrix methods for self-adjoint positive definite elliptic problems were also developed by M. Dryja in [33], [34] and [35]. In [34], it is shown how setting up the auxiliary problem in the imbedding algorithm as a Dirichlet problem on one side of the imbedding interface and a Neumann problem on the other leads to capacitance matrices whose spectra are bounded independently of the mesh size. This idea was later also used in domain decomposition algorithms for iterative substructuring [109, 11, 12, 13].

A domain imbedding method for the Stokes equations is developed by Börgers in [14].

Another approach that uses integral equation techniques to obtain imbedding apgorithms for the Laplace and Biharmonic operators is given by A. Mayo in [81].

A comparison of the capacitance matrix method with other methods for solving the discrete problem such as multigrid methods and the precondirioned conjugate gradient method is carried out in Chan and Saied [24].

1.1.6 The French School

A large body of literature on domain imbedding methods comes from workers in France centered around R. Glowinski, P. Joly, J. Périaux and their colleagues. Their general approach lies usually in formulating the imbedding problem as a control problem [5, 4, 6] and applying techniques of exact controllability such as J.L. Lions' Hilbert Uniqueness Method [19, 20]. See also [30] for a least-squares formulation and [31] for an approach using Lagrange multipliers. Error estimates for domain imbedding algorithms are contained in [49].

1.1.7 Soviet Literature

It should also be mentioned that there is a large body of work on imbedding methods which was done in the former Soviet Union, where the method is known as the "Method of Fictitious Domains". Some representative papers treating elliptic problems including the Helmholtz equation are [1, 2, 3, 38, 78, 75], which also contain more references.

1.1.8 CMM in CFD and EM

The capacitance matrix method was applied by D. Martin [79] to several classical problems in potential incompressible flow and it was shown how additional constraints such as the Kutta condition at the trailing edge of an airfoil could be incorporated into the method. Young et al. [114] use an approach similar to the capacitance matrix method in the context of an adaptive finite element method for flow and electromagnetics problems. Bespalov et al. [10] carry out a comparison between the finite element method on unstructured meshes versus an imbedding approach applied to the potential flow around an airfoil. They conclude that, for an equal number of mesh points and for equal accuracy, the imbedding method is faster; only when a mesh optimizer is used is the unstrucured mesh approach competitive.

In work closely related to this thesis, Bespalov [9] uses an imbedding method to design a preconditioner for an iterative method to solve the discrete Helmholtz equation for plane wave scattering problems.

1.2 The Helmholtz Equation

In this section, we collect various well-known results on the mathematical theory of the Helmholtz equation and its solutions. We will describe both the classical theory of twice continuously differentiable solutions and some results on weak solutions as will be needed for the finite element method in Chapter 3.

1.2.1 Problem Statement

Let $D \subset \mathbb{R}^2$ be a bounded domain with boundary $\Gamma = \partial D$ cf. Figure 1.1. We shall assume throughout that Γ is of class C^2, although the theory collected below has been generalized to surfaces with less smoothness, in particular to those with corners. This, however, entails technical complications which are beyond the scope of this thesis. This will not prevent us from applying the algorithms developed also

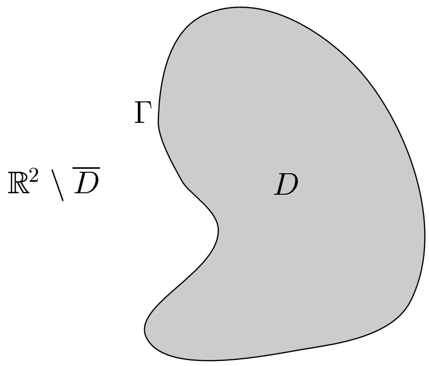

Figure 1.1: An exterior domain

to domains with corners later on. In applications, the domain D usually represents an obstacle at which an incident wave field is scattered and for this reason we shall refer to D synonymously as the *obstacle* or *scatterer*. Given data $g : \Gamma \to \mathbb{C}$, we seek a function $u : \mathbb{R}^2 \setminus \overline{D} \to \mathbb{C}$ which satisfies

$$\Delta u(x) + k^2 u(x) = 0, \qquad x \in \mathbb{R}^2 \setminus \overline{D} \tag{1.1}$$

$$Bu(x) = g(x), \qquad x \in \Gamma \tag{1.2}$$

$$u_r - iku = o(r^{-\frac{1}{2}}), \qquad \text{uniformly as } r = |x| \to \infty. \tag{1.3}$$

Equation (1.1) is known as the *reduced wave equation* or *Helmholtz equation* so named in honor of the German physicist Hermann Ludwig Ferdinand von Helmholtz for his pioneering work on the mathematical theory of acoustics and electromagnetics. The operator Δ denotes the Laplacian and the parameter $k \in \mathbb{C}$ is called the *wave number* and is related to the frequency λ of the underlying wave by $k\lambda = 2\pi$. We choose the sign of k such that $\mathrm{Im}(k) \geq 0$, but we are mainly interested in the case of real k which models propagating waves, whereas a nonzero imaginary part of k results in waves which are attenuated. The operator B in (1.2) stands for a linear combination of the function and its normal derivative resulting in a Dirichlet, Neumann or Robin boundary condition on the obstacle boundary. The third condition (1.3) is the Sommerfeld radiation condition which, mathematically, is required in order that the exterior problem have a unique solution and, physically, specifies that the solution u

be an outgoing wave. More is said on the interpretation of the Sommerfeld radiation condition in Section 1.2.5.

The function spaces in which the data and solution live depend on whether one considers classical or weak solutions. We will mention both in the following. Also, in view of the applications we are interested in where the equation is forced by boundary data due to an incident wave, we focus on the homogeneous Helmholtz equation, although we note that the theory and numerical algorithms to be developed apply equally well when a source term is present on the right hand side of (1.1).

1.2.2 The Method of Integral Equations

The Helmholtz equation can of course be treated using the theory of boundary value problems for second order elliptic partial differential equations cf. [85, 112, 44]. However, in light of the close connection between the numerical techniques to be developed in this thesis and the theory of (boundary) integral equations for the Helmholtz equation, we will only give a short summary of the results we need coming from the latter.

As in the classical potential theoretic case where $k = 0$, the first rigorous existence and uniqueness results concerning boundary value problems for the Helmholtz equation came from the theory of integral equations. Our summary closely follows the monograph [26] by Colton and Kress, where proofs of all the theorems cited in this section can be found unless indicated otherwise. In the classical theory, solutions satisfying (1.1)-(1.3) are sought in the space $C^2(\mathbb{R}^2 \setminus \overline{D}) \cap C(\mathbb{R}^2 \setminus D)$ in case of the Dirichlet problem. For exterior Neumann and Impedance (Robin) boundary value problems, u is additionally required to possess a normal derivative at the boundary *in the sense of uniform convergence*, i.e. the limit

$$\frac{\partial u}{\partial n}(x) := \lim_{\substack{h \to 0 \\ h > 0}} n(x) \cdot \nabla u(x - hn(x))$$

should exist uniformly on Γ, $n(x)$ being the unit outward normal to Γ at $x \in \Gamma$. We also assume $g \in C(\Gamma)$ for the data.

The integral equation method is based on seeking solutions of the Helmholtz equation in either of the forms

$$v(x) = (\widetilde{S}\varphi)(x) := \int_\Gamma \Phi(x,y)\varphi(y)\, ds_y, \qquad x \notin \Gamma \tag{1.4}$$

or

$$w(x) = (\widetilde{K}\psi)(x) := \int_\Gamma \frac{\partial\Phi(x,y)}{\partial n(y)}\psi(y)\, ds_y, \qquad x \notin \Gamma \tag{1.5}$$

where

$$\Phi(x,y) = \frac{i}{4}H_0^{(1)}(k|x-y|), \qquad x \neq y$$

is the free-space Green's function of the Helmholtz equation and $H_0^{(1)}$ is the first-kind Hankel function of order zero. The functions $\varphi, \psi \in C(\Gamma)$ are often referred to as *densities* and $\widetilde{S}$ and $\widetilde{K}$ are the single- and double-layer operators, respectively. The functions $v = \widetilde{S}\varphi$ and $w = \widetilde{K}\psi$ in (1.4) and (1.5), known as the single- and double-layer potential, respectively, are both analytic solutions of the Helmholtz equation which satisfy the Sommerfeld radiation condition. Their behavior as x approaches the boundary Γ is summarized in the following relations known as the *jump conditions.* For functions defined in a neighborhood of Γ we define for $x \in \Gamma$

$$u_+(x) = \lim_{\substack{y\to x \\ y\in\mathbb{R}^2\setminus\overline{D}}} u(y) \qquad \text{and} \qquad u_-(x) = \lim_{\substack{y\to x \\ y\in D}} u(y).$$

Theorem 1.2.1 *The layer potentials (1.4) and (1.5) have the following properties:*

1. *The single-layer potential v with density $\varphi \in C(\Gamma)$ is uniformly Hölder continuous throughout $\mathbb{R}^2$ with $\|v\|_{\alpha,\mathbb{R}^2} \leq C(\alpha,\Gamma)\|\varphi\|_{\alpha,\Gamma}$ for all $0 < \alpha < 1$ and some constant $C(\alpha,\Gamma)$ depending on α and Γ. In particular, v is continuous across Γ.*

2. *The double-layer potential w with density $\psi \in C(\Gamma)$ can be continuously extended from D to $\overline{D}$ and from $\mathbb{R}^2 \setminus \overline{D}$ to $\mathbb{R}^2 \setminus D$ with limiting values*

$$w_\pm(x) = \int_\Gamma \frac{\partial\Phi(x,y)}{\partial n(y)}\psi(y)\, ds_y \pm \frac{1}{2}\psi(x), \quad x \in \Gamma.$$

The integral exists as an improper integral.

3. *For the single-layer potential v with density $\varphi \in C(\Gamma)$ there holds*

$$\frac{\partial v_\pm}{\partial n}(x) = \int_\Gamma \frac{\partial \Phi(x,y)}{\partial n(x)} \varphi(y)\, ds_y \mp \frac{1}{2}\varphi(x), \quad x \in \Gamma$$

where again the integral exists as an improper integral and the normal derivative is understood in the sense of uniform convergence of

$$\frac{\partial v_\pm}{\partial n}(x) := \lim_{\substack{h \to 0 \\ h>0}} \frac{\partial v(x + hn(x))}{\partial n(x)}.$$

4. *For the double-layer potential w with density $\psi \in C(\Gamma)$ there holds*

$$\frac{\partial w_+}{\partial n}(x) = \frac{\partial w_-}{\partial n}(x), \quad x \in \Gamma.$$

Using these jump conditions, we can drive the integral equation which the density needs to satisfy in order that the resulting potential solve the exterior boundary value problem under consideration. The classical Ansatz is to seek the solution of the exterior Dirichlet problem in the form of a double-layer potential while the exterior Neumann problem is sought as a single-layer potential, the reason being that switching the two approaches would lead to first-kind Fredholm integral equations which are ill-posed. Beginning with the exterior Dirichlet problem, we see that, in order for $v(x) = g(x),\ x \in \Gamma$, we must have,

$$g(x) = w_+(x) = \int_\Gamma \frac{\partial \Phi(x,y)}{\partial n(y)} \psi(y)\, ds_y \pm \frac{1}{2}\psi(x), \quad x \in \Gamma \tag{1.6}$$

according to Theorem 1.2.1. Correspondingly, for the exterior Neumann problem, the boundary condition requires

$$g(x) = \frac{\partial v_+}{\partial n}(x) = \int_\Gamma \frac{\partial \Phi(x,y)}{\partial n(x)} \varphi(y)\, ds_y \mp \frac{1}{2}\varphi(x), \quad x \in \Gamma. \tag{1.7}$$

Multiplying through by two in both equations, we obtain the classical integral equations

$$(I + K)\psi = 2g \tag{1.8}$$

$$(I - K^*)\varphi = -2g \tag{1.9}$$

in which the integral operators K and K^* are defined as

$$(K\psi)(x) := 2\int_\Gamma \frac{\partial\Phi(x,y)}{\partial n(y)}\psi(y)\, ds_y, \qquad x\in\Gamma \tag{1.10}$$

$$(K^*\varphi)(x) := 2\int_\Gamma \frac{\partial\Phi(x,y)}{\partial n(x)}\varphi(y)\, ds_y, \qquad x\in\Gamma. \tag{1.11}$$

We shall also have use for two other integral operators defined as

$$(S\varphi)(x) := 2\int_\Gamma \Phi(x,y)\varphi(y)\, ds_y, \qquad x\in\Gamma \tag{1.12}$$

$$(T\psi)(x) := 2\frac{\partial}{\partial n(x)}\int_\Gamma \frac{\partial\Phi(x,y)}{\partial n(y)}\psi(y)\, ds_y, \qquad x\in\Gamma. \tag{1.13}$$

The operator S is also called the single-layer operator, K the double-layer operator and T is known as the hyper-singular operator. Before stating the following theorem summarizing the mapping properties of these operators, we introduce the appropriate domain for T as the linear subspace $\mathcal{N}(\Gamma)$ of all $\varphi\in C(\Gamma)$ such that the double-layer potential with φ as density has continuous normal derivatives on both sides of Γ.

Theorem 1.2.2 *The mapping properties of the integral operators S, K, K^* and T are as follows:*

1. *The operators S, K and K^* are compact in $C(\Gamma)$ and $C^{0,\alpha}(\Gamma)$ for $0<\alpha<1$. All three map $C(\Gamma)$ into $C^{0,\alpha}(\Gamma)$ continuously. S and K map $C^{0,\alpha}(\Gamma)$ into $C^{1,\alpha}(\Gamma)$ continuously.*

2. *S is self-adjoint and K and K^* are mutually adjoint in the dual system defined on $C(\Gamma)\times C(\Gamma)$ with*

$$\langle\varphi,\psi\rangle = \int_\Gamma \varphi\psi\, ds, \quad \varphi,\psi\in\Gamma.$$

3. *The operator T is self-adjoint and unbounded from $\mathcal{N}(\Gamma)$ to $C(\Gamma)$. T is bounded from $C^{1,\alpha}(\Gamma)$ to $C^{0,\alpha}(\Gamma)$.*

In the impedance boundary value problem, the boundary condition on Γ is given by

$$\frac{\partial u}{\partial n} + \lambda u = g \quad \text{on } \Gamma$$

with $\lambda \in C(\Gamma)$. When a solution is sought as a single-layer potential, the corresponding density $\varphi \in C^(\Gamma)$ needs to solve the integral equation

$$\varphi - K^*\varphi - \lambda S\varphi - -2g. \tag{1.14}$$

The integral equation method thus reduces the three exterior boundary value problems considered to the three integral equations (1.8), (1.9), and (1.14). Since S and K are compact operators, the solvability of these integral equations is completely described by the Fredholm alternative, which states that, for compact adjoint operators A and A^*, the operators $I+A$ and $I+A^*$ are *either* both bijections *or* their null-spaces have the same dimension and their ranges consist of all functions which are orthogonal to the null-space of the adjoint operator. The adjoints of the operators $I+K$ and $I-K^*$ appearing in the integral equations for the exterior Dirichlet and Neumann problems turn out to be the corresponding integral equations for the densities of the single-layer Ansatz for the interior Neumann problem and the double-layer Ansatz for the interior Dirichlet problem, respectively. Thus, the first part of the Fredholm alternative guarantees existence for the solutions of the exterior problem whenever we have uniqueness for the corresponding interior problems. Uniqueness holds for all but a sequence of positive wave numbers k accumulating only at infinity which depend on the domain and are known as *interior Neumann eigenvalues* in the first case and *interior Dirichlet eigenvalues* in the second case. For these values of k, the second part of the Fredholm alternative applies and the solutions of the integral equations are no longer unique, even though the exterior boundary value problems themselves remain uniquely solvable. The uniqueness situation for the single-layer solution of the (exterior) impedance problem reduces to that of the single-layer solution of the (exterior) Neumann problem since the null-spaces of $I-K^*$ and $I-K^*-\lambda S$ coincide for continuous λ.

1.2.3 Modified Integral Equations

The previous section shows that the non-uniqueness problems with the classical integral equations for the exterior Helmholtz problems are an artifact of the solution method and not rooted in the nature of the problem itself. In particular, these difficulties result from assuming the solution to exist in the rather special form of one of the two layer potentials, a somewhat ad hoc assumption that just happens to work in almost all cases. There are many remedies that address the non-uniqueness issue, one of which is to use a combined single- and double-layer Ansatz in place of the pure single- or double layer potential (cf. [26]), another is to replace the kernel Φ with a modified kernel $\widehat{\Phi}$ chosen so that uniquely solvable integral equations result for all wave numbers. We briefly describe the second method since it is related to the imbedding algorithms that follow. This approach is based on work by Jones [65] and Ursell [104, 105].

The results of the classical theory remain unchanged if, instead of the free-space Green's function Φ, another fundamental solution $\widehat{\Phi} = \Phi + \Psi$ is used to define the single- and double-layer potentials (1.4) and (1.5). This is the case e.g. if Ψ is chosen so that it is analytic in a region containing Γ as well as the exterior domain. In particular, since the added function Ψ is then continuous on Γ, the integral operators $\widehat{S}$, $\widehat{K}$ and $\widehat{K}^*$ obtained by substituting $\widehat{\Phi}$ for Φ in (1.12), (1.10) and (1.11) are again compact so that the Fredholm theory remains valid. For an interior region D which is connected and contains the origin, Ursell [104] suggested using the Green's function $\widehat{\Phi}_a$ for the exterior Helmholtz problem with respect to a ball $B(0, a) \subset D$ of radius a centered at the origin such that its boundary is a positive distance ℓ away from Γ. In order that this Green's function be of any more use than Φ, the resulting integral equations should be solvable for all positive wave numbers k, and this is achieved by requiring $\widehat{\Phi}_a$ to satisfy the dissipative boundary condition

$$\frac{\partial \widehat{\Phi}_a(x,y)}{\partial n(x)} + \eta \widehat{\Phi}_a(x,y) = 0, \quad |x| = a \tag{1.15}$$

with a complex number η such that $\mathrm{Im}(\eta) > 0$. If $\widehat{\Phi}_a$ is written as $\widehat{\Phi}_a = \Phi + \Psi$, then $\Psi = \Psi(x, y)$ satisfies the Helmholtz equation with respect to the variable x for each parameter value y such that $x, y > a, x \neq y$, the Sommerfeld radiation condition and the boundary condition

$$\frac{\partial \Psi(x,y)}{\partial n(x)} + \eta \Psi(x,y) = -\frac{\partial \Phi(x,y)}{\partial n(x)} - \eta \Phi(x,y) = 0, \quad |x| = a$$

for all y with $|y| > a$. Making use of the addition theorem for $H_0^{(1)}$

$$H_0^{(1)}(k|x-y|) = \sum_{n\in\mathbb{Z}} J_n(k|x|)H_n^{(1)}(k|y|)e^{in\vartheta}, \quad |y| > |x|$$

in which ϑ is the angle between x and y, a separation of variables Ansatz for $\Psi(\cdot, y)$ gives

$$\Psi(x,y) = \sum_{n\in\mathbb{Z}} a_n(y)H_n^{(1)}(k|x|)e^{in\vartheta}, \quad a < |x| < |y|$$

so that the coefficients $a_n(y)$ are determined by

$$a_n(y)[kH_n^{(1)'}(ka) + \eta H_n^{(1)}(ka)] = -H_n^{(1)}(k|y|)[kJ_n'(ka) + \eta J_n(ka)], \quad n \in \mathbb{Z}.$$

By having chosen η to have positive imaginary part, we can show that the expression $kH_n^{(1)'}(ka)+\eta H_n^{(1)}(ka)$ is non-zero for all $ka > 0$. Were this not the case for a particular value of ka, then the conjugate expression would also vanish, and, multiplying the former by $\overline{H_n^{(1)}(ka)}$ and the latter by $H_n^{(1)}(ka)$ and subtracting the two would yield

$$k(H_n^{(1)'}(ka)\overline{H_n^{(1)}(ka)} - \overline{H_n^{(1)'}(ka)}H_n^{(1)}(ka)) = (\overline{\eta} - \eta)|H_n^{(1)}(ka)|^2$$

which, using the Wronskian identity for the first- and second-kind Hankel functions

$$H_n^{(1)'}(z)H_n^{(2)}(z) - H_n^{(2)'}(z)H_n^{(1)}(z) = \frac{4i}{\pi z},$$

would become

$$\frac{2}{\pi a} = -\mathrm{Im}(\eta)|H_n^{(1)}(ka)|^2,$$

a contradiction if $\mathrm{Im}(\eta) > 0$.

Thus, the modified Green's function $\widehat{\Phi}_a$ is well defined for all k. A simple argument involving Green's theorem shows that, on the region D_a bounded externally by Γ and internally by the circle $r = a$ (or any other smooth curve lying strictly inside D), vanishing Dirichlet *or* Neumann data on Γ together with the dissipative boundary condition (1.15) on $r = a$ imply that a solution of the Helmholtz equation vanish identically.

To see that the modified kernel leads to uniquely solvable integral equations, assume the homogeneous modified equation $(I + \widehat{K})\psi = 0$ has a non-trivial solution

ψ_0. This implies along with Theorem 1.2.1 that the corresponding modified double-layer potential $\widehat{w}$ vanishes identically in the exterior of Γ and consequently so does the outside limiting value of its normal derivative on Γ. Since the double-layer potential has continuous normal derivatives across Γ, the inside limiting value of the normal derivative vanishes also, and hence $\widehat{w}$ solves the Helmholtz equation on D_a with zero Neumann data on Γ and the dissipative boundary condition $\partial\widehat{w}/\partial n + \eta\widehat{w} = 0$ on $r = a$. But this now implies $\widehat{w} \equiv 0$ and thus $\psi_0 = 0$, a contradiction. The Neumann and impedance problems are treated in the same manner.

The approach above involved adding an infinite series to Φ to obtain uniquely solvable integral equations. Jones [65] has shown that, with a modified Green's function of the general form

$$\begin{aligned}\widehat{\Phi}(x,y) = \Phi(x,y) &+ a_0 H_0^{(1)}(k|x|)H_0^{(1)}(k|y|) \\ &+ \sum_{m=1}^{M} a_m H_m^{(1)}(k|x|)H_m^{(1)}(k|y|)\cos m\vartheta_x \cos m\vartheta_y \\ &+ \sum_{n=1}^{N} b_n H_n^{(1)}(k|x|)H_n^{(1)}(k|y|)\sin n\vartheta_x \sin n\vartheta_y\end{aligned}$$

with coefficients a_m and b_n satisfying certain mild conditions, one can construct corresponding integral operators with unique solutions for all k in a real interval $0 < k < k_{M,N}$, where $k_{M,N}$ grows with M and N.

In the following, we shall develop fast Helmholtz solvers for the solution of the radiative Helmholtz problem on the exterior of a ball and use these fast solvers in a capacitance matrix method. The resulting capacitance matrix will then be a discrete analog of the modified integral equation with kernel $\widehat{\Phi}_a$. The fact that the modified Green's function is represented by an infinite series will not trouble us, since the evaluation of the modified Green's function occurs implicitly as one application of the fast Helmholtz solver.

Finally, we cite the Green's representation theorem for solutions of the Helmholtz equation, which we will make use of in Chapter 3 to obtain representations of Dirichlet to Neumann maps in terms of the classical integral operators.

Theorem 1.2.3 *Let $u \in C^2(D) \cap C(\overline{D})$ be a solution of the Helmholtz equation*

$$\Delta u + k^2 u = 0$$

in D possessing a normal derivative on Γ in the sense of uniform convergence. Then

$$\int_\Gamma \left\{ u(x)\frac{\partial \Phi(x,y)}{\partial n(y)} - \Phi(x,y)\frac{\partial u}{\partial n} \right\} ds_y = \begin{cases} -u(x), & x \in D \\ 0, & x \in \mathbb{R}^2 \setminus \overline{D}. \end{cases}$$

Let $u \in C^2(\mathbb{R}^2 \setminus \overline{D}) \cap C(\mathbb{R}^2 \setminus D)$ be a solution of the Helmholtz equation

$$\Delta u + k^2 u = 0$$

in D possessing a normal derivative on Γ in the sense of uniform convergence and satisfying the Sommerfeld radiation condition. Then

$$\int_\Gamma \left\{ u(x)\frac{\partial \Phi(x,y)}{\partial n(y)} - \Phi(x,y)\frac{\partial u}{\partial n} \right\} ds_y = \begin{cases} 0, & x \in D \\ u(x), & x \in \mathbb{R}^2 \setminus \overline{D}. \end{cases}$$

In particular, the representation theorem shows that any solution to the Helmholtz equation can be represented as a combination of a single- and a double-layer potential, each with a different density.

1.2.4 Extension to Weak Solutions

The finite element method introduced in Chapter 3 is based on a variational formulation of the exterior Helmholtz problem and thus necessitates the introduction of functions possessing weak differentiability properties, i.e. Sobolev spaces. We summarize the regularity properties of solutions of the boundary value problems as well as the mapping properties of the integral operators in appropriate Sobolev spaces in this section.

Weak solutions are sought in a space of functions with finite energy. For exterior problems, this space is usually taken to be

$$\mathscr{W}(\mathbb{R}^2 \setminus \overline{D}) := \left\{ u \in H^1_{loc}(\mathbb{R}^2 \setminus \overline{D}) : \frac{\partial u}{\partial r} - iku = o(r^{-\frac{1}{2}}) \text{ as } r \to \infty \right\}.$$

Since we are considering the Helmholtz equation with constant coefficients, the regularity theory for elliptic boundary value problems (cf. [85]) guarantees that solutions of the Helmholtz equation are analytic outside a disk containing the obstacle. Thus, the radiation condition makes sense.

A regularity theorem for the boundary value problems of interest is given by

Theorem 1.2.4 *Let $D \subset \mathbb{R}^2$ be a bounded region with C^2-boundary Γ, $g \in H^{\frac{1}{2}}(\Gamma)$, $\eta \in L^\infty(\Gamma)$ and $h \in H^{-\frac{1}{2}}(\Gamma)$. Then the three exterior boundary value problems for the Helmholtz equation*

$$\Delta u + k^2 u = 0$$

on the domain $\mathbb{R}^2 \setminus \overline{D}$ with one of the three boundary conditions

$$\begin{aligned} u = g \;\; on\; \Gamma, & \qquad \text{(Dirichlet problem)} \\ \frac{\partial u}{\partial n} = h \;\; on\; \Gamma, & \qquad \text{(Neumann Problem)} \\ or\; \frac{\partial u}{\partial n} - \eta u = h \;\; on\; \Gamma, & \qquad \text{(Impedance Problem)} \end{aligned}$$

admit unique solutions $u \in \mathscr{W}(\mathbb{R}^2 \setminus \overline{D})$. If the data possesses the additional regularity $g \in H^{\frac{3}{2}}(\Gamma)$ or $h \in H^{\frac{1}{2}}(\Gamma)$, then the the solutions lie also in the space $H^2_{loc}(\mathbb{R}^2 \setminus \overline{D})$.

It can be derived e.g. from the theorem which follows. See also [70] or [112]. The following theorem taken from [70] describes the mapping properties of the integral and potential operators in Sobolev spaces.

Theorem 1.2.5 *Let the boundary be C^∞-smooth. Then the following holds.*

1. *The operators S, K, K^* and T can be extended to bounded operators between*

$$S, K, K^* : H^s(\Gamma) \to H^{p+1}(\Gamma) \; for\; all\; p \in \mathbb{R}$$
$$T : H^{p+1}(\Gamma) \to H^p(\Gamma) \; for\; all\; p \in \mathbb{R}$$

2. *The potential operators $\widetilde{S}$ and $\widetilde{K}$ given by*

$$\varphi \mapsto \widetilde{S}\varphi = \int_\Gamma \Phi(\cdot, y)\varphi(y) ds_y$$

and

$$\psi \mapsto \widetilde{K}\psi = \int_\Gamma \frac{\partial \Phi(\cdot, y)}{\partial n(y)} \psi(y) ds_y$$

can be extended to continuous operators between

$$\widetilde{S} : H^p(\Gamma) \to H^{p+\frac{3}{2}}(D) \text{ and } H_{loc}^{p+\frac{3}{2}}(\mathbb{R}^2 \setminus \overline{D}), \text{ respectively}$$
$$\widetilde{K} : H^p(\Gamma) \to H^{p+\frac{1}{2}}(D) \text{ and } H_{loc}^{p+\frac{1}{2}}(\mathbb{R}^2 \setminus \overline{D}), \text{ respectively}$$

for all $p \in \mathbb{R}$.

We note that the smoothness assumptions on Γ can be relaxed, for details cf. [68, 69]

The jump conditions of Theorem 1.2.1 can also be extended to the Sobolev space setting, this is described in [68].

1.2.5 The Sommerfeld Radiation Condition

The Sommerfeld radiation condition is needed as an extra boundary condition for exterior Helmholtz problems in order for the solution to be uniquely determined. A simple two-dimensional example illustrating this point is given by considering the problem of solving the Helmholtz equation $\Delta u + k^2 u = 0$ on the exterior of the disk of radius a centered at the origin subject to the boundary condition $u(a, \theta) = g = const.$ The solution is any purely radial function satisfying the Bessel equation of order zero

$$u_{rr} + \frac{1}{r} u_r + k^2 u = 0.$$

Two linearly independent solutions of this equation are the zero-th order Hankel functions $H_0^{(1)}(kr)$ and $H_0^{(2)}(kr)$ of the first and second kind, respectively. Thus, two distinct solutions of the boundary value problem are given by

$$u_1(r) = \frac{g}{H_0^{(1)}(ka)} H_0^{(1)}(kr) \qquad \text{and} \qquad u_2(r) = \frac{g}{H_0^{(2)}(ka)} H_0^{(2)}(kr).$$

Physically, the first solution u_1 represents an outgoing wave while u_2 represents an incoming wave. Of the two, only u_1 satisfies the Sommerfeld radiation condition, which follows from the asymptotic behavior of the Hankel functions for large argument

$$H_0^{(1,2)}(kr) = \sqrt{\frac{2}{\pi kr}} \exp\left[\pm i\left(kr - \frac{\pi}{4}\right)\right]\left\{1 + \mathcal{O}\left(\frac{1}{kr}\right)\right\}, \quad r \to \infty.$$

Thus, adding the Sommerfeld condition to the boundary value problem makes the solution unique.

The radiation condition is attributed to Arnold Sommerfeld, who formulated it in a 1912 paper [97] on the Green's function of the Helmholtz equation. Beginning with the observation that, in contrast to the potential theoretic limit ($k = 0$), the Helmholtz equation possesses free-space eigenfunctions vanishing at infinity, Sommerfeld concludes that vanishing at infinity is not a sufficiently strong condition to uniquely determine solutions of exterior boundary value problems for the Helmholtz equation. Sommerfeld explains this by interpreting solutions of the Helmholtz equation as the spatial part of time-harmonic solutions of the wave equation. By distinguishing outgoing and incoming propagating waves among these, which can be suitably superposed to form standing waves, which in turn can be freely added to solutions of the Helmholtz equation to yield new solutions, he infers that the physically correct solution is one which can be represented solely as a superposition of outgoing waves. These may be generated by source distributions either throughout space or on lower dimensional manifolds. Using Green's formula and the fundamental solution of the Helmholtz equation, he derives the radiation condition ('Ausstrahlungsbedingung')

$$\lim_{r\to\infty} r^{\frac{n-1}{2}}(u_r - iku) = 0,$$

which he supplements with a condition of finiteness ('Endlichkeitsbedingung')

$$\lim_{r\to\infty} r^{\frac{n-1}{2}} u < \infty.$$

With these two conditions he is able to prove uniqueness for solutions of exterior Helmholtz problems. In 1943, Rellich [92] was able to show uniqueness using only the radiation condition in the weakened form

$$\lim_{R\to\infty} \int_{\Gamma_R} |u_r - iku|^2 \, ds = 0$$

where Γ_R denotes the boundary of a sphere of radius R around the origin. It also turns out that the radiation condition implies the condition of finiteness. A more detailed account of the history of this problem treating also the case of problems with unbounded obstacles can be found in [82].

There is also an interpretation of the radiation condition in terms of the flux of energy cf. [29, Vol. I pp. 645]. To see this, we return to the time dependent wave equation. Let w be a sufficiently smooth solution of $w_{tt} - \Delta w = 0$ on $\Omega \times \mathbb{R}$ where Ω is a regular bounded domain. After multiplying the equation by $\overline{w_t}$, integrating over Ω, applying the divergence theorem, taking real parts and making use of the two identities

$$\frac{1}{2}\frac{\partial}{\partial t}|w_t|^2 = \mathrm{Re}\ \overline{w_t}w_{tt} \quad \text{and} \quad \frac{1}{2}\frac{\partial}{\partial t}|\nabla w|^2 = \mathrm{Re}\ \nabla\overline{w_t}\cdot\nabla w,$$

we obtain the identity

$$\frac{\partial}{\partial t}\int_\Omega \frac{1}{2}(|w_t|^2 + |\nabla w|^2)dx - \mathrm{Re}\int_{\partial\Omega}\overline{w_t}\frac{\partial w}{\partial n}\,ds = 0. \tag{1.16}$$

We now define the quantities

$$\begin{aligned} E_\Omega(w,t) &:= \frac{1}{2}\int_\Omega (|w_t|^2 + |\nabla w|^2)\,dx \\ I_{\partial\Omega}(w,t) &:= -\mathrm{Re}\int_{\partial\Omega}\overline{w_t}\frac{\partial w}{\partial n}\,ds. \end{aligned}$$

The former represents the wave energy contained in Ω at time t while the latter denotes the outward flux of energy through the boundary of Ω at time t. Thus, (1.16) states that

$$\frac{\partial}{\partial t}E_\Omega(w,t) + I_{\partial\Omega}(w,t) = 0,$$

i.e. the increase of energy in the domain is balanced by its outward flux through the boundary. Returning to the time harmonic case $w(x,t) = e^{-ikt}u(x)$ we obtain

$$\begin{aligned} E_\Omega(w,t) \equiv E_\Omega(u) &= \frac{1}{2}\int_\Omega (k^2|u|^2 + |\nabla u|^2)\,dx \\ I_{\partial\Omega}(w,t) \equiv I_{\partial\Omega}(u) &= -\mathrm{Re}\left\{ik\int_{\partial\Omega}\overline{u}\frac{\partial u}{\partial n}\,ds\right\} \end{aligned}$$

i.e. the energy in the domain is constant and hence the flux $I_{\partial\Omega}(u)$ must vanish as well.

We now apply this result to an exterior problem. Let Ω contain a compact set K and denote the set $\Omega \setminus K$ by Ω'. It is shown in [29] that, given any regular domain Ω_0 such that $K \subset \Omega_0 \subset \overline{\Omega}_0 \subset \Omega$, then if u is a solution of the homogeneous Helmholtz equation on Ω', the quantity

$$I(u) := -\mathrm{Re}\ \left\{ ik \int_{\partial\Omega_0} \overline{u} \frac{\partial u}{\partial n}\, ds \right\}$$

is independent of the choice of Ω_0. We shall call $I(u)$ the *energy flux* of u and call the solution u outgoing or incoming depending on whether $I(u) \geq 0$ or $I(u) \leq 0$. The following proposition shows that, if the Sommerfeld radiation condition holds, then the solution is outgoing.

Proposition 1.2.1 *Let u be a solution of the homogeneous Helmholtz equation on $\mathbb{R}^n \setminus K$, K compact and let Γ_R be the boundary of the ball of radius R around the origin. If u also satisfies the Sommerfeld radiation condition, then $I(u) \geq 0$; in particular,*

$$I(u) = k^2 \lim_{R\to\infty} \int_{\Gamma_R} |u|^2\, ds. \tag{1.17}$$

Proof. For R sufficiently large, we obtain

$$I(u) = -\mathrm{Re}\ ik \int_{\Gamma_R} \overline{u} u_r\, ds = -\mathrm{Re}\ \left\{ ik \int_{\Gamma_R} (u_r - iku)\overline{u}\, ds \right\} + k^2 \int_{\Gamma_R} |u|^2\, ds. \tag{1.18}$$

Schwarz's inequality then gives

$$\left| \mathrm{Re}\ ik \int_{\Gamma_R} (u_r - iku)\overline{u}\, ds \right| \leq \left(\int_{\Gamma_R} |u_r - iku|^2\, ds \right)^{\frac{1}{2}} \left(k^2 \int_{\Gamma_R} |u|^2\, ds \right)^{\frac{1}{2}}. \tag{1.19}$$

Applying the triangle inequality to (1.18) and then using (1.19) yields

$$\begin{aligned} k^2 \int_{\Gamma_R} |u|^2\, ds &\leq |I(u)| + \left| \mathrm{Re}\ ik \int_{\Gamma_R} (u_r - iku)\overline{u}\, ds \right| \\ &\leq |I(u)| + \left(\int_{\Gamma_R} |u_r - iku|^2\, ds \right)^{\frac{1}{2}} \left(k^2 \int_{\Gamma_R} |u|^2\, ds \right)^{\frac{1}{2}} \\ &\leq |I(u)| + \int_{\Gamma_R} |u_r - iku|^2\, ds + \frac{1}{4} k^2 \int_{\Gamma_R} |u|^2\, ds \end{aligned}$$

Bringing the common terms to the left hand side gives

$$k^2 \int_{\Gamma_R} |u|^2 \, ds \leq \frac{4}{3} \left(\int_{\Gamma_R} |u_r - iku|^2 \, ds + |I(u)| \right).$$

If we let $R \to \infty$ and use the fact that u satisfies the Sommerfeld condition, the last inequality shows that $k^2 \int_{\Gamma_R} |u|^2 \, ds$ is bounded as $R \to \infty$ so that (1.18) and (1.19) together imply (1.17). $\square$

Hence, imposing the Sommerfeld radiation condition results in a solution consisting of outgoing waves.

The proof that the radiation condition implies uniqueness can be found in Rellich's original paper [92] or e.g. in [26, pp. 79] and [29, Vol. I pp. 651].

1.3 Connections to Acoustics and Electromagnetics

In this section, we briefly indicate how two-dimensional exterior Helmholtz problems of the kind treated in this thesis arise in time-harmonic acoustic and electromagnetic wave scattering problems.

1.3.1 Acoustic Scattering Problems

The simplest equations modelling the propagation of sound assume a homogeneous, isotropic, inviscid fluid and that the disturbances due to the sound waves are of small amplitude. We assume a constant reference state at density ρ_0, pressure p_0 and velocity $\mathbf{u}_0 = 0$. For small disturbances, we have

$$p = p_0 = c^2(\rho - \rho_0), \qquad c^2 = p'(\rho_0). \tag{1.20}$$

The governing equations for density, pressure and velocity as functions of space and time are the momentum and continuity equations

$$\begin{aligned} \rho_0 \mathbf{u}_t &= -\nabla p \\ \rho_t + \rho_0 (\nabla \cdot \mathbf{u}) &= 0. \end{aligned}$$

Assuming the motion to be irrotational allows us to represent $\mathbf{u}$ as the gradient of a scalar potential $\mathbf{u} = \nabla\Psi$. Integrating the momentum equation with respect to time and fixing the necessary constants then gives $\rho_0 \Psi_t = p - p_0$ which, together with (1.20) and the continuity equation result in the linear wave equation

$$\Psi_{tt} - c^2 \Delta \Psi = 0$$

for Ψ. The Helmholtz equation is obtained by assuming Ψ to have the harmonic time dependence

$$\Psi(\mathbf{x}, t) = \operatorname{Re}\left\{e^{-i\omega t}\psi(\mathbf{x})\right\}$$

with angular frequency $\omega > 0$, the substitution of which into the wave equation yields the Helmholtz equation

$$\Delta\psi + k^2\psi = 0, \qquad k = \frac{\omega}{c}$$

for the spatial part ψ of the velocity potential. We also mention that, in case of damped waves, the parameter k^2 becomes complex; in this case k is chosen so that $\operatorname{Im}(k) \geq 0$.

The boundary conditions at an obstacle in the medium are obtained by specifying that at the boundary either the normal velocity vanish (acoustically hard obstacle), the excess pressure vanish (acoustically soft obstacle) or that excess pressure and normal velocity are proportional at the boundary. The acoustically hard case results in a homogeneous Neumann boundary condition for ψ, the acoustically soft case in a homogeneous Dirichlet condition. The third boundary condition, known as an impedance condition, results from the boundary condition

$$\mathbf{n} \cdot \mathbf{u} + \eta(p - p_0) = 0$$

where $\mathbf{u}$ is the unit outward surface normal at the boundary and η is called the normal acoustic impedance of the obstacle. This results in the Robin boundary condition

$$\frac{\partial\psi}{\partial n} + \lambda\psi = 0, \qquad \lambda = i\eta\rho_0\omega.$$

In scattering problems, the spatial part ψ of the wave field is assumed to consist of the sum of a given incident field $\psi^{(i)}$ and the resulting scattered field $\psi^{(s)}$. We will be considering plane waves $\psi^{(i)}(\mathbf{x}) = \exp(ik\mathbf{x}\cdot\mathbf{d})$ propagating in the direction $\mathbf{d}$ as the incident fields, which is the limiting wave field at large distance from the source of the incident field. The condition prescribing the behavior of the scattered field at infinity is the Sommerfeld radiation condition, since the scattered field consists entirely of outgoing waves.

Thus, the acoustic plane wave scattering problem is the exterior Helmholtz problem for the scattered field $\psi^{(s)}$ with boundary conditions obtained by inserting the plane wave as the incident field $\psi^{(i)}$ into whichever of the three boundary conditions introduced above is physically appropriate together with the Sommerfeld radiation condition at infinity. Two dimensional problems are obtained whenever the domain can be idealized as an infinite cylindrical body and the incident field is independent of the axial direction.

1.3.2 Electromagnetic Scattering Problems

The electric and magnetic fields $\mathfrak{E}(\mathbf{x},t)$ and $\mathfrak{H}(\mathbf{x},t)$ at time t in an isotropic, homogeneous and linear medium of electric permittivity ε, magnetic permeability μ and conductivity σ are governed by the Maxwell equations

$$\nabla\times\mathfrak{H} - \varepsilon\mathfrak{E}_t = \sigma\mathfrak{E} \tag{1.21}$$

$$\nabla\times\mathfrak{E} + \mu\mathfrak{H}_t = 0. \tag{1.22}$$

If we assume a harmonic time dependence of the form

$$\mathfrak{E}(\mathbf{x},t) = \mathrm{Re}\left\{\mathbf{E}(\mathbf{x})e^{-i\omega t}\right\}, \qquad \mathfrak{H}(\mathbf{x},t) = \mathrm{Re}\left\{\mathbf{H}(\mathbf{x})e^{-i\omega t}\right\},$$

then the spatial parts of the fields satisfy what are sometimes known as the *reduced Maxwell equations*

$$\nabla\times\mathbf{E} - i\omega\mu\mathbf{H} = 0 \qquad \nabla\times\mathbf{H} - (\sigma - i\omega\varepsilon)\mathbf{E} = 0. \tag{1.23}$$

If we assume that there are no charges present in the medium, then both $\mathbf{E}$ and $\mathbf{H}$ are divergence free, so that taking the curl of (1.23) and then employing the vector identity

$$\nabla\times(\nabla\times\mathbf{V}) = \nabla(\nabla\cdot\mathbf{V}) - \Delta\mathbf{V}$$

which holds for twice continuously differentiable vector valued functions $\mathbf{V}$, shows us that $\mathbf{E}$ and $\mathbf{H}$ satisfy the vector Helmholtz equations

$$\Delta \mathbf{E} + k^2 \mathbf{E} = 0 \qquad \Delta \mathbf{H} + k^2 \mathbf{H} = 0$$

with $k^2 = \mu\omega(i\sigma + \varepsilon\omega)$. The wave number k is again chosen so that $\mathrm{Im}(k) \geq 0$. Note that, if the conductivity σ is nonzero, then the wave is damped. We will consider only undamped waves, i.e. real and positive k, however.

In scattering problems, the total field $\{\mathbf{E} = \mathbf{E}^{(i)} + \mathbf{E}^{(s)}, \mathbf{H} = \mathbf{H}^{(i)} + \mathbf{H}^{(s)}\}$ is taken to be a superposition of a known incident field $\{\mathbf{E}^{(i)}, \mathbf{H}^{(i)}\}$ and an unknown scattered field $\{\mathbf{E}^{(s)}, \mathbf{H}^{(s)}\}$ on the exterior of the scattering obstacle D with smooth boundary Γ. The simplest case is that of a perfectly conducting obstacle, for which the tangential component $\mathbf{n} \times \mathbf{E}$ vanishes on Γ. At points where the surface normal $\mathbf{n}$ fails to exist, additional edge and corner conditions are needed in order for the boundary value problem to have a unique solution.

Two dimensional problems result when the scattering obstacle is an infinite cylinder whose axis is in the z-direction and when the incident field is independent of z. We will consider plane waves whose direction of propagation is perpendicular to the z-axis. It turns out that it is sufficient to consider only two cases: one in which the electric field is aligned with the z-axis, known as the transverse magnetic (TM) case, and the other in which the magnetic field is aligned with the z-axis, known as the transverse electric (TE) case. In the TM case, the boundary condition gives

$$\mathbf{n} \times \mathbf{E} = \begin{bmatrix} n_x \\ n_y \\ n_z \end{bmatrix} \times \begin{bmatrix} 0 \\ 0 \\ E \end{bmatrix} = E \begin{bmatrix} n_y \\ -n_x \\ 0 \end{bmatrix} = 0$$

which implies $E = 0$ on the obstacle boundary. In the TE case, we have $\mathbf{H} = [0\ 0\ H]^T$ and we obtain $\mathbf{E}$ from (1.23) as

$$\mathbf{E} = \frac{1}{\sigma - i\omega\varepsilon} \nabla \times \mathbf{H} = \frac{1}{\sigma - i\omega\varepsilon} \begin{bmatrix} \frac{\partial H}{\partial y} \\ -\frac{\partial H}{\partial x} \\ 0 \end{bmatrix}$$

so that the perfect conductor boundary condition in this case prescribes

$$\mathbf{n} \times \mathbf{E} = -\frac{\partial H}{\partial n} = 0,$$

∂n denoting the derivative in the direction of the normal vector. Thus, the TM case results in an exterior Dirichlet problem for the z-component E of $\mathbf{E}$ while the TE case corresponds to an exterior Neumann problem for the z-component H of $\mathbf{H}$. It is shown in e.g. [18] how the solutions of these two special cases can be combined to solve problems oblique incidence.

1.4 A Model Problem

As a model problem, we consider the exterior problem for the Helmholtz equation with respect to a disk centered at the origin. This problem has the advantage that it can be solved by separation of variables, so that it can serve as a good test for numerical approximations.

The complete problem written in polar coordinates is given by

$$\begin{cases} u_{rr} + \dfrac{1}{r} u_r + \dfrac{1}{r^2} u_{\vartheta\vartheta} + k^2 u = 0, \qquad r > a \\ Bu(a, \vartheta) = g(\vartheta) \\ \dfrac{\partial u}{\partial r}(R, \vartheta) = (M_k u)(R, \vartheta). \end{cases} \tag{1.24}$$

where B is a differential operator in the radial direction of order at most one depending on the boundary condition imposed at $r = a$. The separation Ansatz $u(r, \vartheta) = F(r)G(\vartheta)$ leads to the trigonometric functions

$$G_n(\vartheta) = e^{in\vartheta}, \qquad n \in \mathbb{Z}$$

in the angular variable, which implies that the corresponding functions F_n satisfy

$$F''(r) + \frac{1}{r} F'(r) + \left(k^2 - \frac{n^2}{r^2} \right) F(r) = 0.$$

This is just Bessel's equation of integral order n, of which two linearly independent solutions are the first and second Hankel functions $H_n^{(1)}(kr)$ and $H_n^{(2)}(kr)$ of order n.

Hence the solution is of the form

$$u(r,\vartheta) = \sum_{n\in\mathbb{Z}} [a_n H_n^{(1)}(kr) + b_n H_n^{(2)}(kr)]\, e^{in\vartheta}$$

with coefficients a_n and b_n to be determined by the boundary conditions. The DtN boundary condition at $r = R$ prescribes

$$u_r(R,\vartheta) = k \sum_{n\in\mathbb{Z}} \frac{H_n^{(1)\prime}(kR)}{H_n^{(1)}(kR)} u_n(R) e^{in\vartheta}$$

with Fourier coefficients

$$u_n(R) = \frac{1}{2\pi}\int_0^{2\pi} u(R,\vartheta) e^{-in\vartheta}\, d\vartheta.$$

Equating Fourier coefficients gives,

$$k[a_n H_n^{(1)\prime}(kR) + b_n H_n^{(2)\prime}(kR)] = k\frac{H_n^{(1)\prime}(kR)}{H_n^{(1)}(kR)}[a_n H_n^{(1)}(kr) + b_n H_n^{(2)}(kr)],$$

which implies $b_n = 0$ when making use of the Wronskian relationship

$$H_n^{(1)}(z) H_n^{(2)\prime}(z) - H_n^{(1)\prime}(z) H_n^{(2)}(z) = -\frac{4i}{\pi z}.$$

Hence, the DtN boundary condition rejects the incoming solutions regardless of the boundary condition on the disk, which alone specifies the coefficients a_n.

Since we are mainly interested in plane-wave scattering problems, we now consider boundary data due to an incident plane wave

$$u^{(i)}(r,\vartheta) = e^{ikr\cos\vartheta}$$

propagating in the positive x direction. If the boundary condition on the disk is given by

$$Bu_r^{(tot)} \equiv u_r^{(tot)} + k\eta u^{(tot)} = 0$$

for the total field, this translates into

$$u_r + k\eta u = -u_r^{(i)} - k\eta u^{(i)}, \qquad r = a$$

for the scattered field u. If we now make use of the Jacobi-Anger expansion (cf. [27])

$$e^{ikr\cos\vartheta} = \sum_{n\in\mathbb{Z}} i^n J_n(kr)e^{in\vartheta},$$

J_n denoting the usual Bessel functions, the scattered field comes out as

$$u(r,\vartheta) = -\sum_{n\in\mathbb{Z}} i^n \frac{J_n'(ka) + \eta J_n(ka)}{H_n^{(1)\prime}(ka) + \eta H_n^{(1)}(ka)} H_n^{(1)}(kr)e^{in\vartheta}. \tag{1.25}$$

For the limiting case $\eta \to \infty$ we obtain the solution of the Dirichlet problem

$$u(r,\vartheta) = -\sum_{n\in\mathbb{Z}} i^n \frac{J_n(ka)}{H_n^{(1)}(ka)} H_n^{(1)}(kr)e^{in\vartheta}. \tag{1.26}$$

1.5 Non-reflecting Boundary Conditions

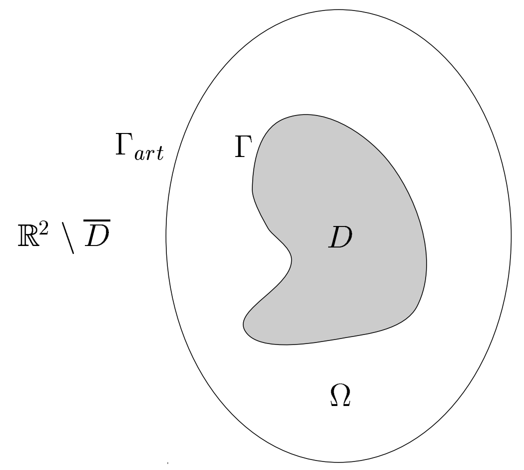

Figure 1.2: A truncated exterior domain

One of the difficulties inherent in solving exterior boundary value problems numerically is dealing with the unbounded domain on which the problem is posed. The usual approach, and the one we will follow here, is to compute a numerical approximation of the solution only on a bounded subdomain Ω of the original domain, which we refer to as the *computational domain*. This truncation of the unbounded domain introduces a new, artificial boundary Γ_{art} (cf. Figure 1.2), and the question of what is the proper boundary condition to impose on this new boundary arises. The most satisfactory answer is, of course, a boundary condition which results in a solution on Ω which is the restriction to Ω of the solution of the original problem. Boundary conditions which achieve this are known as *exact* boundary conditions.

In wave propagation problems, there is an obvious physical interpretation of the boundary condition on the artificial boundary, namely that it should allow waves to pass through the boundary unaffected. In particular, there should be no reflection of outgoing waves back into the domain; for this reason, boundary conditions attempting to achieve this are called *absorbing boundary conditions* (ABC's) or *non-reflecting boundary conditions* (NRBC's).

In this section, we give a short overview of NRBC's and introduce the exact boundary condition which we will use for the fast Helmholtz solver in our imbedding algorithms: the DtN boundary condition. Since the discretization requires an approximation to this boundary condition to be made, we will illustrate the accuracy of this approximation in the case of the model problem of Section 1.4.

1.5.1 Overview

The exact boundary conditions usually have the disadvantage that they are global boundary conditions, i.e. that they specify a coupling of the solution values on the whole artificial boundary by some integral expression. This can lead to difficulties in numerical methods since their discretization leads to dense submatrices which can spoil the sparsity pattern of the discretized differential operator. Also, it may not be straightforward to incorporate these boundary conditions into off-the-shelf finite difference or finite element codes for solving boundary value problems. For this reason, various local approximate boundary conditions have been developed. The most well-known work in this area is that of Engquist and Majda [36, 37], who have derived families of local NRBC's of increasing accuracy and order by replacing the symbol of the nonlocal (pseudo-differential) operator in the boundary condition by a rational approximation.

While Engquist and Majda's approach applies to wave problems of all kinds, there is another approach for obtaining local NRBC's specifically for the Helmholtz equation which is due to Bayliss, Gunzburger and Turkel [8]. This approach uses the asymptotic expansion which solutions of exterior Helmholtz problems satisfy outside of some disk (cf. [7, 110, 111, 66]). By requiring that the approximate solution agree with the exact solution up to the term of the asymptotic expansion with index m on the artificial boundary, Bayliss et al. obtain a sequence of boundary conditions $B_m u = 0$, where B_m is a differential operator of order m. The first two of this sequence are given by

$$\begin{aligned} B_1 u &= u_r - iku + \frac{1}{2r}u \\ B_2 u &= u_{rr} + \left(\frac{3}{r} - 2ik\right) u_r + \left(\frac{3}{4r^2} - \frac{3ik}{r} - k^2\right) u. \end{aligned}$$

As is typical of local NRBC's, the accuracy of the Bayliss, Gunzburger and Turkel (BGT) conditions increases with the order m of the operator B_m as well as with the distance of the artificial boundary from the scattering obstacle.

Finally, we mention another popular boundary condition, which simply sets to zero on the artificial boundary the term appearing in the Sommerfeld radiation condition : $u_r - iku = 0$. This condition is often referred to as the *Sommerfeld-like* condition. We will show some comparisons of the first two BGT conditions as well as the Sommerfeld condition versus the exact DtN condition in Chapter 2.

An extensive survey of existing work on NRBC's can be found in the survey article [46] by Dan Givoli as well as his recent monograph [47].

1.5.2 The DtN Boundary Condition

The DtN boundary condition requires that, on the boundary under consideration, the Dirichlet and Neumann data of the solution of a differential equation be related by the Dirichlet-to-Neumann (DtN) mapping M of the problem at hand : e.g. in our case it requires that on the artificial boundary Γ_{art}

$$\frac{\partial u}{\partial n}(x) = (Mu)(x), \qquad x \in \Gamma_{art}.$$

hold. The DtN map can be computed once one has a suitable representation of the solution. The systematic development of the DtN boundary condition as a tool for solving boundary value problems on truncated domains is due to J.B. Keller and D. Givoli cf. [67, 47, 48] and the references therein.

General Boundaries

For smooth artificial boundaries of general shape, the DtN map is given by an integral operator which, for the Laplace or Helmholtz equations, can be expressed in terms of the classical layer potentials. Given an arbitrary (smooth, say, C^2 or Lyapunov) artificial boundary Γ, the DtN mapping takes the form of an integral operator M_k defined on Γ (cf. [27] p. 48). The operator M_k can be expressed in terms of the four integral operators S, K, K^* and T introduced in Section 1.2.2.

The solution of the exterior Dirichlet problem with respect to Γ with Dirichlet data h can be written as the combined single- and double-layer potential

$$u(x) = \int_\Gamma \left\{ \frac{\partial \Phi(x,y)}{\partial n(y)} - i\eta \Phi(x,y) \right\} \psi(y)\, ds(y), \qquad x \in \Gamma$$

provided the function ψ satisfies the equation

$$(I + K - i\eta S)\psi = 2h$$

on Γ. The latter follows from the standard jump relations for single- and double-layer potentials. The real parameter η is introduced here to avoid the nonuniqueness problem at interior Neumann eigenvalues which one encounters for $\eta = 0$ cf. [27]. We require only that $\eta \mathrm{Re}(k) \geq 0$. The DtN operator giving the Neumann data in terms of the Dirichlet data can now be written as

$$\frac{\partial u}{\partial n} = M_k u := (T - i\eta K' + i\eta I)(I + K - i\eta S)^{-1} u, \qquad \text{on } \Gamma.$$

As is shown in [27], the operator M_k is bounded and bijective from $C^{1,\alpha}(\Gamma) \to C^{0,\alpha}(\Gamma)$, $0 < \alpha < 1$, and has a bounded inverse.

MacCamy and Marin used a similar DtN boundary condition in [77] to solve an interface diffraction problem. Their approach is based on the single-layer potential representation for the solution to the exterior Dirichlet problem, which leads to a first-kind Fredholm integral equation for ψ. It can be obtained by factoring out $i\eta$

from the two operators in the above DtN condition and letting $\eta \to \infty$. The DtN formulation is used there within a finite element framework by solving the first-kind integral equation at the mesh points on Γ. Recently, Kirsch and Monk [72] have used the integral operator representation of the DtN map to obtain the DtN boundary condition for arbitrary smooth artificial boundaries using a Nystrom boundary integral discretization. Other applications of the DtN idea include waveguide problems [54] and underwater acoustics [39].

Circular Artificial Boundaries

When the artificial boundary is a circle, the DtN mapping for the Helmholtz equation can be obtained by using a series expansion of the solution obtained by separation of variables. The solution of the exterior Helmholtz problem outside of a circle Γ_R of radius R with Dirichlet data $u(R,\vartheta) = U(\vartheta)$ is given by

$$u(r,\vartheta) = \sum_{n\in\mathbb{Z}} \frac{H_n^{(1)}(kr)}{H_n^{(1)}(kR)} U_n e^{in\vartheta}, \qquad r > R.$$

with Fourier coefficients U_n. Its normal derivative u_r evaluated on $r = R$ is then given by

$$u_r(R,\vartheta) = k \sum_{n\in\mathbb{Z}} \frac{H_n^{(1)'}(kR)}{H_n^{(1)}(kR)} U_n e^{in\vartheta} \tag{1.27}$$

$$= \frac{k}{2\pi} \sum_{n\in\mathbb{Z}} \frac{H_n^{(1)'}(kR)}{H_n^{(1)}(kR)} \int_0^{2\pi} u(R,\varphi) e^{in(\vartheta-\varphi)}\, d\varphi \tag{1.28}$$

$$=: [M_k u(R,\cdot)](\vartheta) \tag{1.29}$$

where the DtN mapping M_k is seen to be a (pseudo-differential) operator on the space of functions defined on Γ_R or, equivalently, on $[0, 2\pi]$.

Other references which use a separation of variables representation for the DtN mapping include [39, 54, 80].

Exactness of the DtN Boundary Condition

The exactness of the DtN boundary condition, i.e. the fact that imposing it on the artificial boundary of a truncated exterior domain results in a solution which is the restriction of the solution of the exterior problem to the truncated domain, follows from the unique solvability of the exterior problem. The truncated version of the exterior problem (1.1)–(1.3) is given by

$$\Delta u(x) + k^2 u(x) = 0, \qquad x \in \Omega \tag{1.30}$$

$$Bu(x) = g(x), \qquad x \in \Gamma \tag{1.31}$$

$$\frac{\partial u}{\partial n}(x) = (Mu)(x) \quad x \in \Gamma_{art}. \tag{1.32}$$

Given a solution u of (1.30)–(1.32), we can extend it to a solution of the exterior problem u^e of (1.1)–(1.3) by setting

$$u^e(x) = \begin{cases} u(x), & x \in \Omega \cup \Gamma_{art} \\ \hat{u}(x), & x \in \mathrm{ext}(\Gamma_{art}) \end{cases}$$

in which $\hat{u}$ is the solution of the exterior Dirichlet problem with respect to Γ_{art} with Dirichlet data $u|_{\Gamma_{art}}$. By construction, the function u^e is continuous across Γ_{art} along with its normal derivative. Thus, u^e is identical with the unique solution of the original exterior problem (1.1)–(1.3) and u is its restriction to Ω.

Uniqueness of the truncated problem is shown in the same way. A variational existence and uniqueness proof for the truncated problem is given in Chapter 3.

1.5.3 The Truncated DtN Condition for the Model Problem

The DtN operator for a circular artificial boundary is given in (1.27) as an infinite series which must be truncated when using it for numerical computation. We will denote by $M_k^{(N)}$ the DtN operator M_k in (1.27) truncated after the term with index N. Replacing M_k by $M_k^{(N)}$ in the DtN boundary condition raises at least two questions: first, for what values of N does the resulting problem still have a unique solution and, second, how far away is the resulting solution from the solution of the problem with the full DtN condition?

The uniqueness issue is treated e.g. in [58], where lower bounds on N are obtained by considering Dirichlet and Neumann eigenvalues of the Laplacian on annuli enclosing the computational domain.

The accuracy issue has not been treated for general domains to our knowledge. However, for our model problem on the annulus, the analysis can be done using separation of variables. Let $u = u(r, \vartheta)$ be the solution of the exterior Dirichlet problem on the exterior of a disk of radius a with DtN boundary condition at $r = R > a$. Let u^N be the solution of the same problem with M_k replaced by $M_k^{(N)}$. The solutions are given by

$$u(r, \vartheta) = \sum_{n \in \mathbb{Z}} \frac{H_n^{(1)}(kr)}{H_n^{(1)}(ka)} g_n e^{in\vartheta}$$

and

$$\begin{aligned} u^N(r, \vartheta) = & \sum_{n \leq N} \frac{H_n^{(1)}(kr)}{H_n^{(1)}(ka)} g_n e^{in\vartheta} \\ & + \sum_{n > N} \frac{H_n^{(1)'}(kR) H_n^{(2)}(kr) - H_n^{(2)'}(kR) H_n^{(1)}(kr)}{H_n^{(1)'}(kR) H_n^{(2)}(ka) - H_n^{(2)'}(kR) H_n^{(1)}(ka)} g_n e^{in\vartheta} \end{aligned}$$

where the g_n are the Fourier coefficients of the boundary data g. Hence the error $e^N := u - u^N$ is given by

$$e^N(r, \vartheta) = \sum_{n > N} \left\{ \frac{H_n^{(1)}(kr)}{H_n^{(1)}(ka)} - \frac{H_n^{(1)'}(kR) H_n^{(2)}(kr) - H_n^{(2)'}(kR) H_n^{(1)}(kr)}{H_n^{(1)'}(kR) H_n^{(2)}(ka) - H_n^{(2)'}(kR) H_n^{(1)}(ka)} \right\} g_n e^{in\vartheta}.$$

The first term in the curly braces is $\mathcal{O}((a/r)^n)$ as $n \to \infty$ and the second term is bounded for $a \leq r \leq R$ and thus the behavior of the error depends only on the decay rate of the Fourier coefficients g_n which in turn depends only on the smoothness of the data. Thus, for $g \in C^m([0, 2\pi])$, the error decreases as $\mathcal{O}(n^{-m})$ and for analytic data as occurs in plane-wave scattering, the decay is exponential. We conjecture that, at least for smooth enough obstacles, the error behaves in the same way for non-annular domains.

In the discretization methods used in the following, the error of the discrete approximation of the boundary value problem will consist of two contributions: the discretization error of the discretization method and the truncation error of the DtN operator in the boundary condition. We will always use smooth data in our computations and always keep all the terms in the DtN series which the mesh will resolve. Thus the error due to the truncation of the DtN series is always far below that of the discretization method.

Chapter 2

A Finite Difference Capacitance Matrix Method

This chapter describes an imbedding method for the numerical solution of exterior Helmholtz problems. The next chapter will treat finite element discretizations. The finite difference variant has the advantage that it is very simple conceptually and straightforward to implement. One drawback, however, is the difficulty of the convergence analysis, which we were not able to carry out satisfactorily. We thus rely on extensive numerical tests to validate the method.

We wish to solve the exterior problem on the truncated domain Ω, i.e. the boundary value problem to be solved is

$$\begin{cases} -\Delta u - k^2 u = f & \text{in } \Omega \\ Bu = g & \text{on } \Gamma \\ u_r = M_k u & \text{on } \Gamma_R. \end{cases} \tag{2.1}$$

The operator B is again chosen so that a Dirichlet, Neumann or impedance boundary condition results on Γ and M_k is the DtN operator belonging to the wave number k.

2.1 Discretization on an Annulus

It is convenient to work with polar coordinates here, mainly due to the form of the various radiation boundary conditions we will encounter, all of which contain a radial variable. Thus, we seek a twice continuously differentiable function $u = u(r, \vartheta)$ satisfying

$$-\frac{1}{r}(ru_r)_r - \frac{1}{r^2}u_{\vartheta\vartheta} - k^2 u = f. \tag{2.2}$$

The domain of interest will for now be the annulus $\mathcal{A}_{R_0,R}$ centered at the origin with internal and external radii R_0 and R, respectively. We impose a uniform $(m+1) \times n$ grid on $\mathcal{A}_{R_0,R}$ and denote it by

$$\mathcal{A}^h_{R_0,R} := \{(r_i, \vartheta_j) : r_i = R_0 + i\Delta r,\ i = 0, \dots, m \quad \vartheta_j = j\Delta\vartheta,\ j = 1, \dots, n\}.$$

The mesh spacings are given by $\Delta r = (R - R_0)/m$ and $\Delta\vartheta = 2\pi/n$. The usual Taylor series expansion yields the following 5-point difference stencil for the approximate solution values $u_{i,j}$ to $u(r_i, \vartheta_j)$:

$$\begin{aligned} &-\left[\frac{r_{i-1/2}}{r_i}u_{i-1,j} - 2u_{i,j} + \frac{r_{i+1/2}}{r_i}u_{i+1,j}\right] \\ &-\frac{\Delta r^2}{r_i^2\Delta\vartheta^2}\left[u_{i,j-1} - 2u_{i,j} + u_{i,j+1}\right] - (k\Delta r)^2 u_{i,j} = \Delta r^2 f_{i,j}. \end{aligned} \tag{2.3}$$

which has a local truncation error of $\mathcal{O}(\Delta r^2 + \Delta\vartheta^2)$. Here and in the following, the index in the angular direction is taken to be periodic, i.e. $j+1 := 1 + j \mod n$ and $j - 1 := (n + j - 1) \mod n$ for $j = 1, \dots, n$. The quantities $f_{i,j}$ denote the values $f(r_i, \vartheta_j)$ at the grid points. We impose a Dirichlet boundary condition $u(R_0, \vartheta) = g(\vartheta)$ at $r = R_0$ fixing the values $u_{0,j} = g(\vartheta_j)$ as well as a Neumann condition $u_r(R, \vartheta) = h(\vartheta)$ which we approximate with the usual centered difference formula

$$\frac{u_{m+1,j} - u_{m-1,j}}{2\Delta r} = h(\vartheta_j). \tag{2.4}$$

The previous equation gives us an expression for the fictitious points $\{u_{m+1,j}\}_{j=1}^n$ which can be inserted into the difference equation (2.3) in order to eliminate these. Fixing the ordering of the unknowns to be in concentric circles from the inside out beginning with $u_{1,1} \approx u(r_1, \Delta\vartheta)$, the difference equations (2.3) together with the boundary conditions form a linear system of equations

$$B\mathbf{u} = \mathbf{f}.$$

The structure of the matrix B is best written in the notation of Kronecker (tensor) products (cf. [63]), in which B is given as

$$B = (T \otimes I_n) + \frac{\Delta r^2}{\Delta\vartheta^2}(R^{-2} \otimes I_n)(I_m \otimes C) - (\Delta r k)^2 I_{mn}$$

with matrices

$$T = \begin{bmatrix} 2 & -b_1 & & & \\ -a_2 & 2 & -b_2 & & \\ & \ddots & \ddots & \ddots & \\ & & -a_{m-1} & 2 & -b_{m-1} \\ & & & -2 & 2 \end{bmatrix}, \quad a_i = \frac{r_{i-1/2}}{r_i}, b_i = \frac{r_{i+1/2}}{r_i}, \quad i = 1, \dots, m,$$

the diagonal matrix

$$R = \operatorname{diag}(r_1, \dots, r_m),$$

the circulant

$$C = \begin{bmatrix} 2 & -1 & & & -1 \\ -1 & 2 & -1 & & \\ & \ddots & \ddots & \ddots & \\ & & -1 & 2 & -1 \\ -1 & & & -1 & 2 \end{bmatrix},$$

and the identity matrices I_d of $\mathbb{C}^d$. The vectors $\mathbf{u}$ and $\mathbf{f}$ are given by

$$\mathbf{u} = \begin{bmatrix} \mathbf{u}_1 \\ \mathbf{u}_2 \\ \vdots \\ \mathbf{u}_m \end{bmatrix} \text{ and } \mathbf{f} = \begin{bmatrix} \mathbf{f}_1 + a_1\mathbf{g} \\ \mathbf{f}_2 \\ \vdots \\ \mathbf{f}_m + 2\Delta r b_m \mathbf{h} \end{bmatrix} \text{ with } \mathbf{g} = \begin{bmatrix} g(\vartheta_1) \\ g(\vartheta_2) \\ \vdots \\ g(\vartheta_n) \end{bmatrix}, \mathbf{h} = \begin{bmatrix} h(\vartheta_1) \\ h(\vartheta_2) \\ \vdots \\ h(\vartheta_n) \end{bmatrix}$$

as well as

$$\mathbf{u}_i = \begin{bmatrix} u_{i,1} \\ u_{i,2} \\ \vdots \\ u_{i,n} \end{bmatrix} \qquad \text{and} \qquad \mathbf{f}_i = \Delta r^2 \begin{bmatrix} f_{i,1} \\ f_{i,2} \\ \vdots \\ f_{i,n} \end{bmatrix}, \qquad i = 1, \ldots, m.$$

Next, we discretize the DtN boundary condition imposed on the outer circle $r = R$ given by

$$u_r(R, \vartheta_j) = \frac{k}{\pi} \sum_{\nu=0}^{\infty}{}' \frac{H_\nu^{(1)\prime}(kR)}{H_\nu^{(1)}(kR)} \int_0^{2\pi} u(R, \theta') \cos \nu(\vartheta_j - \theta') \, d\theta' = (M_k u)(R, \vartheta_j)$$

at the gridpoints $(R, \vartheta_j), j = 1, \ldots, n$. To this end, we first truncate the infinite series after the term with index $\nu = N$. The value of N should be chosen so as to balance the error incurred by the truncation of the series with the discretization error resulting from the finite difference approximation. Next, we replace the integrals with the trapezoidal rule, which is known to converge exponentially for periodic analytic functions (cf. [74]). This is the case here, since solutions to the Helmholtz equation with smooth data are analytic away from the obstacle and, since we are integrating around a closed curve, the integrand will be a periodic function of ϑ. Thus, the discrete version $M_k^{(N)}$ of the DtN operator is given by

$$M_k^{(N)} u_{m,j} = \frac{k}{\pi} \sum_{\nu=0}^{N}{}' \frac{H_\nu^{(1)\prime}(kR)}{H_\nu^{(1)}(kR)} \Delta\vartheta \sum_{q=1}^{n} u_{m,q} \cos \nu(\vartheta_j - \vartheta_q).$$

If we define the coefficients

$$\alpha_0 = \frac{1}{2} \frac{H_0^{(1)\prime}(kR)}{H_0^{(1)}(kR)}, \quad \alpha_\nu = \frac{H_\nu^{(1)\prime}(kR)}{H_\nu^{(1)}(kR)}, \quad \nu = 1, \ldots, N$$

and the circulant matrices

$$(C_\nu)_{j,q} = \cos \nu(\vartheta_j - \vartheta_q), \quad j, q = 1, \ldots, n, \quad \nu = 0, \ldots, N, \tag{2.5}$$

we can represent the effect of $M_k^{(N)}$ on the elements of the vector $\mathbf{u}_m$ as multiplication of $\mathbf{u}_m$ by the matrix

$$C_{DtN} = \frac{k\Delta\vartheta}{\pi} \sum_{\nu=0}^{N} \alpha_\nu C_\nu,$$

which is also circulant.

Combining the discretization of the Helmholtz operator (2.3) and the DtN boundary condition on $\mathcal{A}_{R_0,R}$ by replacing $h(\vartheta_j)$ in (2.4) by $M_k^{(N)} u_{M,j}$ thus leads to the following form of B:

(2.6)
$$B = (T \otimes I_n) + \frac{\Delta r^2}{\Delta \vartheta^2}(R^{-2} \otimes I_n)(I_m \otimes C) - (\Delta r k)^2 I_{mn} - 2\Delta r\, b_m\, (\mathbf{e}_m \mathbf{e}_m^T \otimes C_{DtN})$$

where $\mathbf{e}_m$ is the coordinate vector $\mathbf{e}_m = [0\ 0 \ldots 0\ 1]^T \in \mathbb{C}^n$.

2.2 A Fast Solver on an Annulus

The linear system (2.6) is amenable to the classical FFT-based fast solver as described e.g. in [61, 22, 102]. A fast Poisson solver on a disk and an annulus based on cyclic reduction can be found in [103]. Generally speaking, the FFT based fast solvers work for linear systems of equations resulting from the discretization of elliptic boundary value problems on separable domains, where the eigenfunctions in one of the variables are trigonometric functions. In our case, since both of the matrices describing angular variations ($I_m \otimes C$ and $\mathbf{e}_m \mathbf{e}_m^T \otimes C_{DtN}$) are block diagonal with circulant blocks (and since the matrix R is diagonal), multiplication of B from the left by $I_m \otimes F_n$ and from the right by $I_m \otimes F_n^H$ will diagonalize these matrices, leaving the remaining matrices unchanged. Here F_n denotes the discrete Fourier transform matrix of order n

$$F_n = \frac{1}{\sqrt{n}} \left\{ e^{-\frac{2\pi i}{n} pq} \right\}_{p,q=0}^{n-1},$$

the multiplication of which by a vector can be accomplished by the fast Fourier transform in $\mathcal{O}(n \log n)$ operations.

Thus, the matrix

$$(I_m \otimes F_n)\, B\, (I_m \otimes F_n^H)$$

is block-tridiagonal with diagonal blocks. Reordering the transformed unknowns $\hat{\mathbf{u}}_i = F_n \mathbf{u}_i, i = 1, \ldots, m$ by grouping the j-th equation of each block into a new j-th block yields n uncoupled tridiagonal sytems of order m

$$T_j \hat{\mathbf{u}}_j = \hat{\mathbf{f}}_j, \qquad j = 1, \ldots, n \tag{2.7}$$

where $\widehat{\mathbf{u}}_j$ denote the transformed and permuted unknown vectors

$$\widehat{\mathbf{u}}_j = [\hat{u}_{1,j} \ \dots \ \hat{u}_{m,j}]^T, \quad j = 1, \dots, n$$

and correspondingly for the permuted and transformed right hand side $\widehat{\mathbf{f}}_j$. The matrices T_j are given by

$$T_j = T + \frac{\Delta r^2}{\Delta \vartheta^2} \lambda_j R^{-2} - (k\Delta r)^2 I_m - 2\Delta r b_m \delta_j \mathbf{e}_m \mathbf{e}_m^T, \qquad j = 0, \dots, n-1$$

where λ_j and δ_j denote the eigenvalues of C and C_{DtN}, respectively. After solving the uncoupled systems (2.7), the solution vector $\mathbf{u}$ is obtained by applying the inverse Fourier transform to the m subvectors of $\widehat{\mathbf{u}}$, each of which are again $\mathcal{O}(n \log n)$-operations. Since the n tridiagonal solves each have a complexity of $\mathcal{O}(m)$, the complete solution algorithm has a complexity of $\mathcal{O}(nm \log n)$.

This algorithm requires the eigenvalues of the circulant matrices C and C_{DtN}, which can be computed using the following

Proposition 2.2.1 *The eigenvalues $\{\delta_j^{(\nu)}\}_{j=0}^{n-1}$ of the matrices $\{C_\nu\}_{\nu=0}^{N}$, $(N < n)$ are given by*

$$\delta_j^{(\nu)} = \frac{n}{2} \left(\delta_{\nu,j} + \delta_{(n-\nu) \mod n,j} \right)$$

in which $\delta_{p,q}$ is the Kronecker symbol and the index j refers to the eigenspace. In other words, for odd n, only C_0 has a single (simple) non-zero eigenvalue $\lambda_0^{(0)} = n$ while the remaining $\{C_\nu\}_{\nu=1}^{N}$ all have one double non-zero eigenvalue $\lambda_\nu^{(\nu)} = \lambda_{n-\nu}^{(\nu)} = \frac{n}{2}$. For even n, the single non-zero eigenvalue occurs also for $C_{\frac{n}{2}}$, which has $\lambda_{\frac{n}{2}} = n$.

Proof. An arbitrary circulant matrix

$$C = \begin{bmatrix} c_0 & c_1 & \cdots & c_{n-1} \\ c_{n-1} & c_0 & \cdots & c_{n-2} \\ \vdots & \vdots & & \vdots \\ c_1 & c_2 & \cdots & c_0 \end{bmatrix}$$

is a linear combination $C = \sum_{k=0}^{n-1} c_k P^k$ of powers, i.e. a polynomial $\psi(P)$, of the 'up-shift' matrix

$$P = \begin{bmatrix} 0 & 1 & 0 & \cdots & 0 \\ & 0 & 1 & \ddots & \\ \vdots & & \ddots & \ddots & 0 \\ 0 & & \cdots & 0 & 1 \\ 1 & 0 & \cdots & & 0 \end{bmatrix}.$$

It is easily verified that the matrix P has the orthogonal system of eigenvectors $\{\mathbf{z}_j\}_{j=0}^{n-1}$, of which the p-th component is given by

$$(\mathbf{z}_j)_p = \omega^{jp}, \qquad p = 0, \ldots, n-1, \qquad \omega = e^{-\frac{2\pi i}{n}}.$$

The eigenvalue belonging to $\mathbf{z}_j$ is ω^j, the j-th root of unity. Thus, for the matrix C, we have

$$C\mathbf{z}_j = \psi(P)\mathbf{z}_j = \sum_{k=0}^{n-1} c_k P^k \mathbf{z}_j = \sum_{k=0}^{n-1} c_k \omega^{jk} \mathbf{z}_j = \psi(\omega^j)\mathbf{z}_j, \qquad j = 0, \ldots, n-1,$$

so that the j-th eigenvalue of C is given by $\psi(\omega^j)$, the value of ψ at the j-th eigenvalue of P. Inserting the entries of C_ν given in (2.5) determines the eigenvalues $\lambda_j^{(\nu)}$ of C_ν to be

$$\text{(2.8)} \qquad \lambda_j^{(\nu)} = \sum_{k=0}^{n-1} c_k^{(\nu)} e^{-\frac{2\pi i}{n} jk} = \sum_{k=0}^{n-1} \cos \nu k \frac{2\pi}{n} \left[\cos \frac{2\pi}{n} jk - i \sin \frac{2\pi}{n} jk \right].$$

We now apply orthogonality relations among discrete sines and cosines, which we briefly derive, to obtain the desired result. We first consider the real part of (2.8), which becomes

$$\text{(2.9)} \quad \begin{aligned} \text{Re } (\lambda_j^{(\nu)}) &= \sum_{k=0}^{n-1} \left(\cos \frac{2\pi}{n} \nu k \ \cos \frac{2\pi}{n} jk \right) = \sum_{k=0}^{n-1} \left(\cosh \frac{2\pi i}{n} \nu k \ \cosh \frac{2\pi i}{n} jk \right) \\ &= \frac{1}{4} \sum_{k=0}^{n-1} \left(\omega^{-k(\nu+j)} + \omega^{-k(\nu-j)} + \omega^{k(\nu-j)} + \omega^{k(\nu+j)} \right), \end{aligned}$$

from which we can see that the value of (2.9) depends on which of the two terms $(\nu + j) \mod n$ and $(\nu - j) \mod n$ vanishes. If both vanish, the value is n, if neither vanishes, the value is 0, and if exactly one of the two vanishes, the value is $n/2$. The same idea applied to the imaginary part shows that it vanishes in all cases. $\square$

The matrices C_ν are circulant and hence share a common system of eigenvectors. Thus, the eigenvalues of their sum C_{DtN} are obtained by summing those of the individual C_ν with the same index. Under the additional assumption that the number of terms in the discrete DtN boundary condition is chosen so that $N \leq n/2$, we have $0 \leq \nu \leq n/2$ for all $\nu = 0, \ldots, N$ and the $N+1$ distinct non-zero eigenvalues of C are

$$\begin{array}{lllll} \delta_0 & = & n\alpha_0 & & \\ \delta_1 & = & \delta_{n-1} & = & \frac{n}{2}\alpha_1 \\ & \vdots & & & \\ \delta_N & = & \delta_{n-N} & = & \frac{n}{2}\alpha_N. \end{array}$$

The assumption concerning N is not restrictive, since there are only n Fourier modes present on a grid with n points subject to periodic boundary conditions. Moreover, due to the cosine terms in the DtN expansion, the $\mathbf{z}_j$ and $\mathbf{z}_{n-j}$ modes have the same coefficient, so that $N = \frac{n}{2}$ covers all the modes.

Using the same idea as in the proof of the proposition, the eigenvalues of C are obtained as

$$\lambda_j = 4\sin^2\frac{j\pi}{n} \quad j = 0, \ldots, n-1.$$

Thus, we have all the pieces in place to solve the exterior Helmholtz problem for a disk with an exact radiation boundary condition in $\mathcal{O}(nm\log n)$ floating point operations.

2.3 A Fast Solver on a Disk

We can also extend this fast Helmholtz solver to the case of the whole disk of radius R, i.e. when $R_0 = 0$ and there is no internal boundary. This occurs in situations where the scattering source is not an obstacle but the rather source term f in the differential equation, or in the context of am imbedding algorithm when the shape of the obstacle suggests including the origin in the computational domain.

In this case one needs a difference formula for the Helmholtz equation at the origin. One such formula is given by (cf. [103])

$$-\frac{4}{n\Delta r^2}\left(\sum_{j=1}^{n} u_{1,j} - n u_{0,0}\right) - k^2 u_{0,0} = f_{0,0},$$

which is obtained by integrating the equation over the disk of radius $\Delta r/2$, applying Green's theorem and approximating the boundary and area integrals with the trapezoidal rule and a one-point quadrature rule, respectively. We can use the 5-point stencil at all other points and we thus arrive at the $(mn+1) \times (mn+1)$ system of equations

$$\begin{bmatrix} \alpha & \mathbf{a}^T \\ \mathbf{b} & B \end{bmatrix} \begin{bmatrix} u_0 \\ \mathbf{u} \end{bmatrix} = \begin{bmatrix} f_0 \\ \mathbf{f} \end{bmatrix}$$

with

$$\alpha = 4 - (k\Delta r)^2, \quad \mathbf{a} = \frac{4}{n}\begin{bmatrix} \mathbf{e} \\ 0 \\ \vdots \\ 0 \end{bmatrix}, \quad \mathbf{b} = -a_1 \begin{bmatrix} \mathbf{e} \\ 0 \\ \vdots \\ 0 \end{bmatrix}, \quad \mathbf{e} = [1 \ \ldots \ 1]^T \in \mathbb{C}^n,$$

each zero denoting the zero vector in $\mathbb{C}^n$ and B and a_1 as before. Solving this system for u_0 leads to

$$u_0 = \frac{f_0 - \mathbf{a}^T B^{-1}\mathbf{f}}{\alpha - \mathbf{a}^T B^{-1}\mathbf{b}}, \tag{2.10}$$

provided the denominator does not vanish, from which $\mathbf{u}$ can be computed as $\mathbf{u} = B^{-1}\mathbf{f} - u_0 B^{-1}\mathbf{b}$. This would entail two fast solves, one for $B^{-1}\mathbf{f}$ and one for $B^{-1}\mathbf{b}$. At closer inspection, however, the computation of the latter is much cheaper. Computing $B^{-1}\mathbf{b}$ using the FFT based fast Helmholtz solver, the first step consists of Fourier transforming the m blocks of $\mathbf{b}$, which yields

$$(I_m \otimes F_n)\mathbf{b} = -\sqrt{n}\, a_1 \begin{bmatrix} \mathbf{e}_1 \\ 0 \\ \vdots \\ 0 \end{bmatrix}.$$

so that, after reordering the transformed system into the n uncoupled tridiagonal systems, only the first has a nonzero right hand side:

$$T_0 \hat{\mathbf{u}}_1 = -\sqrt{n}\, a_1\, \mathbf{e}_1.$$

Thus, after transforming back, we obtain

$$B^{-1}\mathbf{b} = -a_1 \begin{bmatrix} \hat{u}_{1,1}\mathbf{e} \\ \vdots \\ \hat{u}_{1,m}\mathbf{e} \end{bmatrix}, \qquad \hat{\mathbf{u}}_1 = \begin{bmatrix} \hat{u}_{1,1} \\ \vdots \\ \hat{u}_{1,m} \end{bmatrix}.$$

Making use of the structure thus allows computing $B^{-1}\mathbf{b}$ using just one tridiagonal solve. The FFTs, of course, need not be performed. The denominator in (2.10) is then given by

$$\alpha - \mathbf{a}^T B^{-1}\mathbf{b} = 4(1 - a_1 \hat{u}_{1,1}) - (k\Delta r)^2.$$

This quantity can easily be monitored for size. Note also that $B^{-1}\mathbf{b}$ need also be computed only once if many fast solves with different right hand sides are to be computed.

2.4 The Imbedding

In order to extend the applicability of the fast solvers developed in the previous section to exterior problems with general shape, we employ the capacitance matrix method. We wish to solve the exterior problem for an obstacle in the computational domain Ω bounded externally by a circular artificial boundary Γ_R and internally by the scattering obstacle. Thus, it is natural to choose an annulus or a disk as the auxiliary domain $\Omega_0 \supset \Omega$ into which the computational domain is imbedded. We extend the source term f to Ω_0 in an arbitrary way, e.g. by zero, another choice could be to extend it continuously. We will be looking mainly at scattering problems, so the source term will be identically zero anyway. Figure 2.1 shows two typical configurations where a disk and an annulus are used for Ω_0.

We denote by the matrix B the discretization of the Helmholtz operator on Ω_0 with DtN boundary condition imposed on Γ_R as described in the previous sections. In case

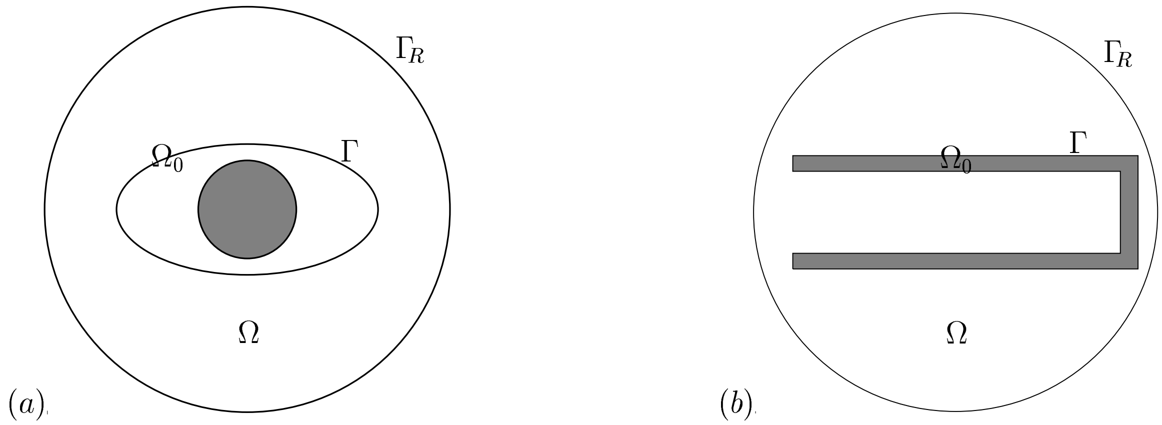

Figure 2.1: Typical configurations for the scattering obstacle, computational domain and auxiliary domain: (a) ellipse: Ω_0 is the annulus between Γ_R and the shaded disk (b) semi-open cavity: Ω_0 is the disk inside Γ_R.

Ω_0 has an internal boundary, we impose a homogeneous Dirichlet boundary condition there. In order to relate the problem on Ω_0 described by the discretization matrix B to the problem which we wish to solve, we first partition the set of gridpoints Ω_0^h which discretizes Ω_0 into three subsets as follows: We denote by Ω^h the set of gridpoints which lie in the interior of Ω or on the artificial boundary Γ_R. The set Γ^h will denote all gridpoints which lie in the interior of Ω such that at least one of its four neighbors in the four coordinate directions lies outside of Ω or on Γ. We will refer to these points as *discrete boundary points.* Finally, Ω_c^h will denote the remaining grid points. i.e. those inside the obstacle or on its boundary Γ. The algorithm will compute solution values here as well, but they are meaningless and can be discarded.

We will show in detail how a Dirichlet boundary condition $u = g$ on Γ is imposed, boundary conditions of Neumann or Robin type are more involved, but can be treated in the same manner.

At all grid points in Γ^h, at least one coordinate line intersects Γ at a distance less that or equal to Δr or $\Delta\vartheta$ in that direction. We denote these distances by Δr_+, Δr_-, $\Delta\vartheta_+$ and $\Delta\vartheta_-$ in the positive and negative r- and θ directions, respectively. We now replace the second-order 5-point stencil used at the interior points to discretize the Helmholtz operator by a first-order accurate stencil involving only points in Ω_h or on

Γ. Such a stencil is given by

(2.11)
$$\begin{aligned}
-(\Delta + k^2)u &= -\frac{1}{r}(ru_r)_r - \frac{1}{r^2}u_{\vartheta\vartheta} - k^2 u \\
&\approx -\frac{1}{r_i}\left[\frac{2r_i + \Delta r_-}{\Delta r_+(\Delta r_+ + \Delta r_-)}u(r_i + \Delta r_+, \vartheta_j)\right. \\
&\qquad + \frac{\Delta r_+ - \Delta r_- - 2r_i}{\Delta r_+ \Delta r_-}u(r_i, \vartheta_j) \\
&\qquad \left. + \frac{2r_i - \Delta r_+}{\Delta r_-(\Delta r_+ + \Delta r_-)}u(r_i - \Delta r_-, \vartheta_j)\right] \\
&\quad - \frac{2}{r_i^2}\left[\frac{u(r_i, \vartheta_j + \Delta\vartheta_+) - u(r_i, \vartheta_j)}{\Delta\vartheta_+(\Delta\vartheta_+ + \Delta\vartheta_-)} - \frac{u(r_i, \vartheta_j) - u(r_i, \vartheta_j - \Delta\vartheta_-)}{\Delta\vartheta_-(\Delta\vartheta_+ + \Delta\vartheta_-)}\right] \\
&\quad - k^2 u(r_i, \vartheta_j).
\end{aligned}$$

This is nothing but the well-known Shortley-Weller formula [40, 56] in polar coordinates. The linear equation at a discrete boundary grid point (r_i, ϑ_j) is obtained by discretizing the Helmholtz operator using the difference formula (2.11) and substituting the Dirichlet data for u at all points in the stencil falling on the boundary. Thus, at the points which lie in Γ^h, an unsymmetric two-sided difference formula is used to discretize the Laplacian. The right hand side of the modified system is obtained by bringing all the known quantities in the modified equations to the right. Thus, the solution $\mathbf{u}$ of the system

$$A\mathbf{u} = \mathbf{f} \tag{2.12}$$

will contain the discrete solution of problem (2.1) in the unknowns belonging to the points in $\Omega^h \cup \Gamma^h$. A consequence of our construction is that the points in $\Omega^h \cup \Gamma^h$ are not coupled to the points of Ω^h_c. Thus, there exists a suitable permutation matrix P such that the reordered matrix has the form

$$PAP^T = \begin{bmatrix} A_{11} & 0 \\ A_{21} & A_{22} \end{bmatrix}.$$

In particular, this means that the solution in $\Omega^h \cup \Gamma^h$ does not depend on the manner in which we have extended the problem to Ω_0.Imbedding methods of this type are known as *upper imbedding methods* cf. [78]..

2.4.1 Imbedding Based on the Woodbury Formula

If we denote by A the matrix resulting after modifying the rows of B as indicated, then A and B differ only in the rows corresponding to the grid points in Γ^h. If there are p such points, then we can write $A = B + UV^T$ with $N \times p$ matrices U and V^T, N being the number of grid points in Ω_0^h. The matrix $U = [\mathbf{e}_{i_1}|\cdots|\mathbf{e}_{i_p}]$ contains in its j-th column the i_j-th unit coordinate vector $\mathbf{e}_{i_j}$, where $\{i_j\}_{j=1}^p$ are the indices of the p discrete boundary points within the complete grid Ω_0^h. The matrices U and U^T can be regarded as extension and restriction operators between Γ^h and Ω_0^h. The matrix $V^T := U^T(A - B)$ is the matrix consisting of the nonzero rows of $A - B$.

The most straightforward approach for solving (2.12) is to use the Sherman-Morrison-Woodbury formula which gives the inverse of a rank-p change of a matrix as

$$A^{-1} = B^{-1} - B^{-1}UC^{-1}V^TB^{-1}$$

where $C = I_p + V^TB^{-1}U$ is the capacitance matrix.

Applying this formula for A^{-1} to the right hand side $\mathbf{f}$ gives the solution

$$\mathbf{u} = B^{-1}\mathbf{f} - B^{-1}UC^{-1}V^TB^{-1}\mathbf{f} = B^{-1}\mathbf{f} + B^{-1}U\boldsymbol{\mu} \tag{2.13}$$

with $\boldsymbol{\mu} \in \mathbb{C}^p$ defined as the solution of the *capacitance matrix equation*

$$C\boldsymbol{\mu} = (I_p + V^TB^{-1}U)\boldsymbol{\mu} = -V^TB^{-1}\mathbf{f}. \tag{2.14}$$

By introducing the intermediate unknown $\boldsymbol{\mu}$, we are actually solving the extended system

$$\begin{bmatrix} B & -U \\ V^T & I \end{bmatrix} \begin{bmatrix} \mathbf{u} \\ \boldsymbol{\mu} \end{bmatrix} = \begin{bmatrix} \mathbf{f} \\ 0 \end{bmatrix}$$

for the vectors $\mathbf{u}$ and $\mathbf{f}$. The capacitance matrix is the Schur complement of this extended system with respect to $\boldsymbol{\mu}$.

The steps for computing $\mathbf{u}$ are summarized in

Algorithm 2.4.1 *(Capacitance Matrix Method)*

1. *Compute* $\mathbf{u}_1 := B^{-1}\mathbf{f}$.

2. *Generate the capacitance matrix* $C = V^T B^{-1} U$ *and use* $\mathbf{u}_1$ *to compute the right hand side* $-V^T \mathbf{u}_1$ *of (2.14).*

3. *Solve the capacitance matrix equation (2.14) for* $\boldsymbol{\mu}$.

4. *Compute* $\mathbf{u} := \mathbf{u}_1 + B^{-1} U \boldsymbol{\mu}$.

Steps 1 and 4 require solving a linear system with coefficient matrix B, which our fast Helmholtz solver performs in $\mathcal{O}(nm \log n)$ operations. Step 2 requires a fast solve applied to every column of U to compute $B^{-1}U$ or, alternatively, since B is complex-symmetric, a fast solve applied to each column of V to compute $V^T B^{-1}$. This amounts to $\mathcal{O}(pmn \log n)$ operations to generate C, but we will show later how symmetries in B^{-1} can be exploited to reduce the number of fast solves. Step 3 requires solving a dense $p \times p$ linear system of equations, i.e. $\mathcal{O}(p^3)$ operations to factorize and $\mathcal{O}(p^2)$ operations for the back-substitution. Thus, in total, Algorithm 2.4.1 requires $\mathcal{O}((p+2)mn \log n + p^3)$ operations to compute a solution to the discretized exterior Helmholtz problem.

A big advantage of this algorithm becomes apparent when the problem is to be solved for several right hand sides, i.e. for different source or boundary data. This occurs in the context of plane wave scattering problems if the problem is to be solved for many angles of incidence. In this case, after the capacitance matrix has been generated and factorized, the operation count for each additional solution is $\mathcal{O}(mn \log n + p^2)$.

The matrix B^{-1} is a discrete approximation of the Green's function $\Phi(x, y)$ for the Helmholtz operator either in all of $\mathbb{R}^2$ (in view of the discrete exact radiation condition) or in the exterior of the inner boundary of Ω_0. In particular, each column of B^{-1} is the discrete solution of the exterior Helmholtz problem with a point source at the grid point belonging to the column number. Thus, the vector $B^{-1}U\boldsymbol{\mu}$ is the solution due to p point sources of strengths $\{\mu_i\}_{i=1}^p$ distributed along the discrete boundary Γ^h. This is the continuous analogue of a single-layer distribution

$$u(x) = \int_\Gamma \Phi(x, y)\mu(y) ds_y, \qquad x \notin \Gamma$$

with density μ.

Similarly, the term $B^{-1}\mathbf{f}$ is the discrete analogue of the space potential term

$$u_{sp}(x) = \int_{\mathrm{ext}(\Gamma)} \Phi(x,y) f(y) dy.$$

In case the source f vanishes, the solution in the the continuous case consists only of the layer potential. In the discrete case, we note that, by our construction, the right hand side of (2.12) is only non-zero at points of Γ^h, so that $\mathbf{f} = U\mathbf{g}$ with some $\mathbf{g} \in \mathbb{C}^p$. Substituting this expression for $\mathbf{f}$ into (2.13) gives

$$\mathbf{u} = B^{-1}U\boldsymbol{\mu}, \qquad \boldsymbol{\mu} = C^{-1}\mathbf{g}$$

with the extended system

$$\begin{bmatrix} B & -U \\ V^T & I \end{bmatrix} \begin{bmatrix} \mathbf{u} \\ \boldsymbol{\mu} \end{bmatrix} = \begin{bmatrix} 0 \\ \mathbf{g} \end{bmatrix}.$$

Thus, in this case, one less fast solve needs to be performed to obtain the solution.

2.4.2 Imbedding Based on Discrete Dipoles

Using the single-layer Ansatz introduced above to solve the exterior Dirichlet problem leads to a first-kind integral equation for the density μ in the continuous case. This is an ill-posed problem, since the operator involved is compact and hence does not possess a bounded inverse. The capacitance matrix, which is a discrete approximation to this operator, should then become more and more ill-conditioned as the mesh is refined. This observation was made by Proskurowski and Widlund in [89] for the potential theoretic case $k = 0$.

We observe this behavior in the following numerical experiment. Using the Woodbury formula approach, we have solved the plane-wave scattering problem for a perfectly conducting ellipse with semi axes $a = 1/2, b = 1/4$, which corresponds to an exterior Dirichlet problem. The problem was solved for four successively halved mesh sizes and wave numbers corresponding to wavelengths $\lambda = a/2$, $\lambda = 2a$ and $\lambda = 128a$. (Wavelength λ and wave number k are related via $k = 2\pi/\lambda$.) We observe that the condition number of the capacitance matrix C does indeed grow with decreasing mesh size and the rate of growth seems to be linear in the mesh size. We also note that, the closer k is to the potential theoretic case, the the higher the proportionality constant seems to be.

$m \times n$	$\kappa(C)$ $(\lambda = a/2)$	$\kappa(C)$ $(\lambda = 2a)$	$\kappa(C)$ $(\lambda = 128a)$
10×60	22.71	9.14	12.42
20×120	12.95	20.97	28.04
40×240	18.24	38.81	51.55
80×480	37.50	83.75	110.4

Table 2.1: Condition numbers $\kappa(C)$ for the Woodbury formula (single-layer) approach to solve the exterior Dirichlet problem for the ellipse with semi-axes $a = 1/2$, $b = 1/4$ for different mesh widths and wavelengths

To remedy this difficulty, it was suggested to mimic what is the proper approach in the continuous case, namely to replace the single- layer Ansatz for the solution with a double-layer Ansatz

$$u(x) = \int_\Gamma \frac{\partial \Phi(x,y)}{\partial n(y)} \mu(y) ds_y, \qquad x \notin \Gamma,$$

which, after applying the jump conditions across Γ, leads to a second-kind Fredholm equation for the density μ.

In the discrete case, we must replace the “single-layer” expression $B^{-1}U\boldsymbol{\mu}$ by a discretization of the double layer distribution. In the term $B^{-1}U\boldsymbol{\mu}$, those columns of the matrix B^{-1}, which is the analog to the Green's function $\Phi(x, y)$, which correspond to unit sources at discrete boundary points, are selected by having a unit coordinate vector in the corresponding column of the matrix U. To obtain a discretization of the double-layer potential, we replace the matrix U with a matrix W of the same dimensions, each column of which contains, instead of a unit vector, the coefficients of a difference formula which linearly combines the columns of B^{-1} to obtain an approximation of the normal derivative of Φ with respect to y. The columns of W are called *discrete dipoles*.

In order to apply the capacitance matrix method in the same way as before, we must impose some restrictions on the difference formulas in the columns of W. We assume the solution to have the form

$$\mathbf{u} = B^{-1}\mathbf{f} + B^{-1}W\boldsymbol{\mu}.$$

For the residual to vanish, we need

$$\begin{aligned} 0 &= A\mathbf{u} - \mathbf{f} \\ &= (B + UV^T)(B^{-1}\mathbf{f} + B^{-1}W\boldsymbol{\mu}) - \mathbf{f} \\ &= W\boldsymbol{\mu} + UV^TB^{-1}W\boldsymbol{\mu} + UV^TB^{-1}\mathbf{f}. \end{aligned} \tag{2.15}$$

The second and third terms after the last equality sign of (2.15) are all zero at grid points belonging to Ω^h. For this to hold also for the remaining term $W\boldsymbol{\mu}$, we need to require that the difference stencils for the discrete dipoles only involve points in $\Gamma^h \cup \Omega^h_c$. If this is assumed, we can multiply (2.15) through by U^T from the left to obtain the capacitance matrix equation

$$(U^TW + V^TB^{-1}W)\boldsymbol{\mu} = -V^TB^{-1}\mathbf{f}. \tag{2.16}$$

Thus, if equation (2.16) holds, then the residual will vanish on $\Omega^h \cup \Gamma^h$, which is where we are interested in the solution. In order to more closely mimic the continuous case, which has an identity operator in the position of U^TW, one could further require that, besides the diagonal element, only points in Ω^h_c be allowed as stencil points and also that the diagonal element be normalized to one. Extensive numerical experiments, however, indicate that these extra restrictions have an adverse effect on the condition number of C. Table 2.2 shows the condition number of the capacitance matrix for the same cases as Table 2.1 except that now the discrete dipole approach has been used.

We observe that the condition numbers remain almost constant across mesh widths. The condition numbers vary somewhat across the different wavelengths, this could be due to interior eigenvalues of the corresponding continuous problems, but we have not investigated this.

$m \times n$	$\kappa(C)$ $(\lambda = a/2)$	$\kappa(C)$ $(\lambda = 2a)$	$\kappa(C)$ $(\lambda = 128a)$
10×60	21.39	31.69	4.11
20×120	25.60	32.67	5.40
40×240	23.04	30.71	4.70
80×480	26.75	33.43	5.04

Table 2.2: Condition numbers $\kappa(C)$ for the discrete dipole approach to solve the exterior Dirichlet problem for the ellipse with semi-axes $a = 1/2$, $b = 1/4$ for different mesh widths and wavelengths

$m \times n$	$\kappa(C)$ $(\lambda = a/2)$	$\kappa(C)$ $(\lambda = 2a)$	$\kappa(C)$ $(\lambda = 128a)$
10×60	12.13	4.24	10.44
20×120	6.31	4.96	12.82
40×240	4.44	5.52	13.28
80×480	3.91	5.68	14.12

Table 2.3: Condition numbers $\kappa(C)$ for the single-layer approach to solve the exterior Neumann problem for the ellipse with semi-axes $a = 1/2$, $b = 1/4$ for different mesh widths and wavelengths

For completeness, we also show the results for the exterior Neumann problem using the single-layer approach in Table 2.3.

In this case, the condition number of the capacitance matrix stays almost constant as the mesh is refined. The relatively large condition number in the coarsest mesh case for $\lambda = a/2$ is due to the insufficient resolution of roughly 6 points per wavelength.

2.4.3 Exploiting Symmetry

In the preceding, computing the capacitance matrix requires applying the fast solver to each column of Uor W, respectively. However, for the $m \times n$ polar mesh we have been using, it turns out that the inverse of B is determined by only m of its mn columns. This is best explained by considering the following fact.

Lemma 2.4.1 *Let M be the block tridiagonal matrix*

$$M = \begin{bmatrix} B_1 & C_1 & & & \\ A_2 & B_2 & C_2 & & \\ & \ddots & \ddots & \ddots & \\ & & A_{m-1} & B_{m-1} & C_{m-1} \\ & & & A_m & B_m \end{bmatrix},$$

in which each block is $n \times n$ and circulant, and let $M\mathbf{x} = \mathbf{y}$. Then $M\tilde{\mathbf{x}} = \tilde{\mathbf{y}}$ holds, for any $\tilde{\mathbf{x}}$ and $\tilde{\mathbf{y}}$ obtained by partitioning $\mathbf{x}$ and $\mathbf{y}$ conformingly with M and then shifting down each block by one, placing the last entry first.

Proof. With the appropriate modifications for the first and last equations, each block equation of $M\mathbf{x} = \mathbf{y}$ is given by

$$A_i\mathbf{x}_{i-1} + B_i\mathbf{x}_i + C_i\mathbf{x}_{i+1} = \mathbf{y}_i$$

and those of $M\tilde{\mathbf{x}} = \tilde{\mathbf{y}}$ by

$$A_iE\mathbf{x}_{i-1} + B_iE\mathbf{x}_i + C_iE\mathbf{x}_{i+1} = E\mathbf{y}_i$$

with the downshift matrix

$$E = \begin{bmatrix} 0 & 1 & & & \\ & 0 & 1 & & \\ & & \ddots & \ddots & \\ & & & 0 & 1 \\ 1 & 0 & \cdots & & 0 \end{bmatrix}.$$

The lemma now follows by noting that E is circulant as well and that circulant matrices commute, since they have a common unitary diagonalizing matrix. □

The matrix B has the form described in the lemma, the sub- and superdiagonal blocks being multiples of the identity. Thus, B^{-1} is determined e.g. by the solutions of the m equations $B\mathbf{x}_i = \mathbf{e}_{j_i}, i = 1, \ldots, m$, where the indices $\{j_i\}_{i=1}^m$ correspond any set of grid points containing a point on each grid circle $\{r = r_i\}_{i=1}^m$.

In particular, when forming the capacitance matrix $C = I_p + V^T B^{-1} W$ or $C = I_p + V^T B^{-1} U$, respectively, one needs only those columns of B^{-1} for which the corresponding blocks in any column of W or U contain non-zero elements. Thus, the number of fast solves needed to construct the capacitance matrix can be reduced from p to $\hat{p}$, where $\hat{p}$ is roughly the number of circular gridlines containing discrete boundary points.

2.5 Numerical Results

2.5.1 Problems posed on an Annulus

In this section, we apply the fast Helmholtz solver to the model problem described in Section 1.4. The domain is the annulus with inner boundary at $R_0 = 0.5$ and outer boundary at $R = 1$. For this domain, one application of the fast Helmholtz solver suffices to solve the discrete problem.

Convergence of the Finite Difference/DtN Discretization

To test the convergence rate of the discretization, we solve the plane wave scattering problem for the infinite cylinder of radius R_0 for the wave numbers $k = 2\pi$, $k = 8\pi$ and $k = 32\pi$. Each problem is solved for three different boundary conditions specified at $r = R$: the Dirichlet condition $u^{tot} = 0$, the Neumann condition $u_r^{tot} = 0$ and the impedance (Robin) condition $u_r^{tot} + ku^{tot} = 0$. We then solve each of the nine resulting boundary value problems on a sequence of meshes beginning with a 10×60 grid which is successively refined by a factor of two until the finest mesh of size 160×960 is reached. We compare each solution to one of the series solutions (1.25) or (1.26) which are summed until new terms no longer contribute to the result. Figure 2.2 shows a loglog plot of the radial mesh width Δr against the difference between the computed solution u and the series solution u^{ex} across different meshes and wave numbers for the Dirichlet and Neumann problems. Figure 2.3 shows the same results for the impedance boundary value problem. In each plot, the solid line represents the case $k = 2\pi$, the dashed line $k = 8\pi$ and the dash-dotted line the case $k = 32\pi$. For

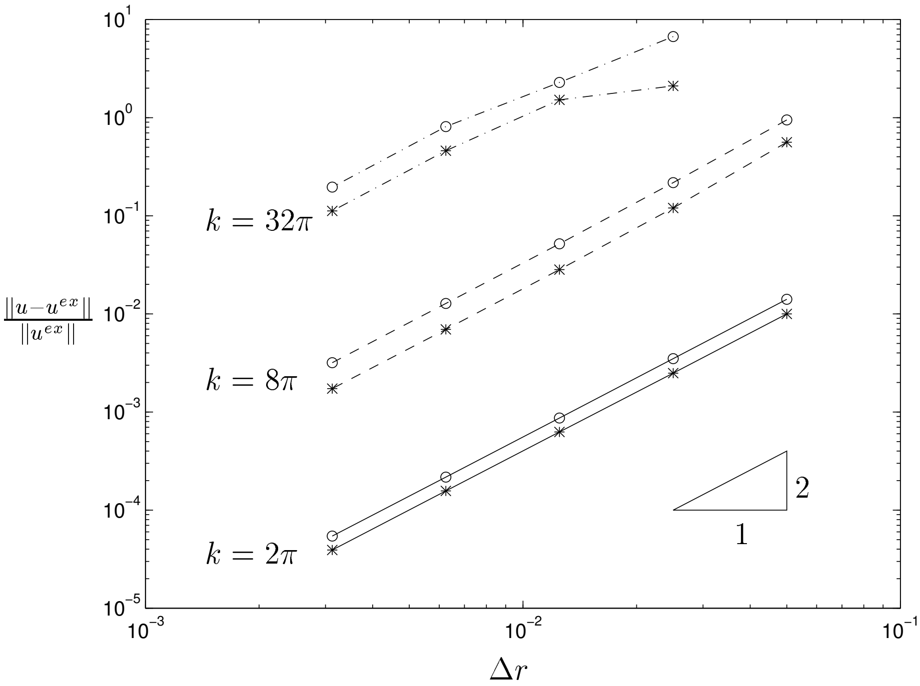

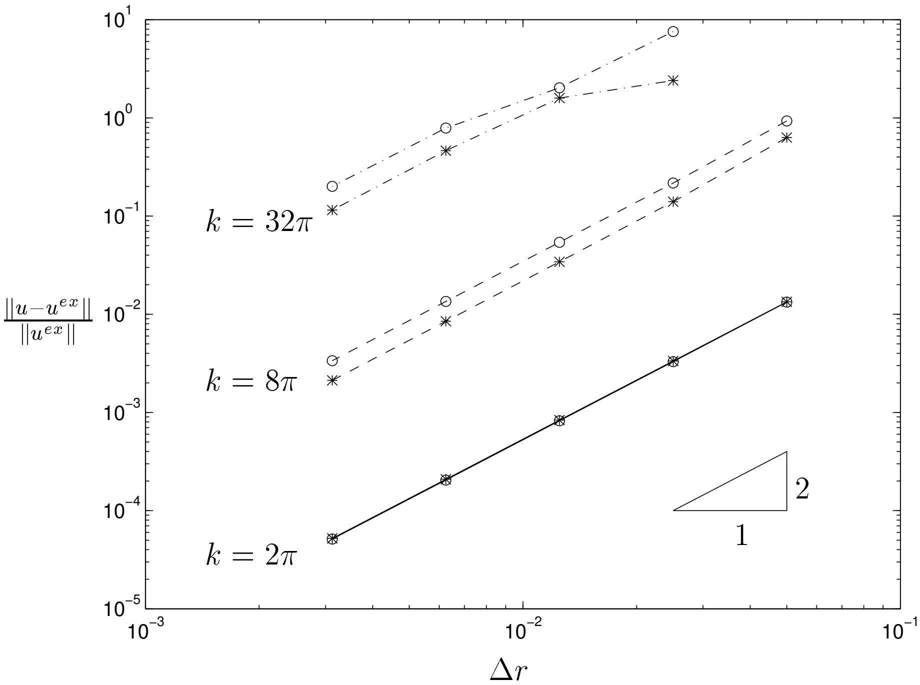

Figure 2.2: Convergence rate of the finite difference/DtN discretization of the plane wave scattering problem on the exterior of the disk. (Upper plot : Dirichlet Problem, lower plot:Neumann Problem)

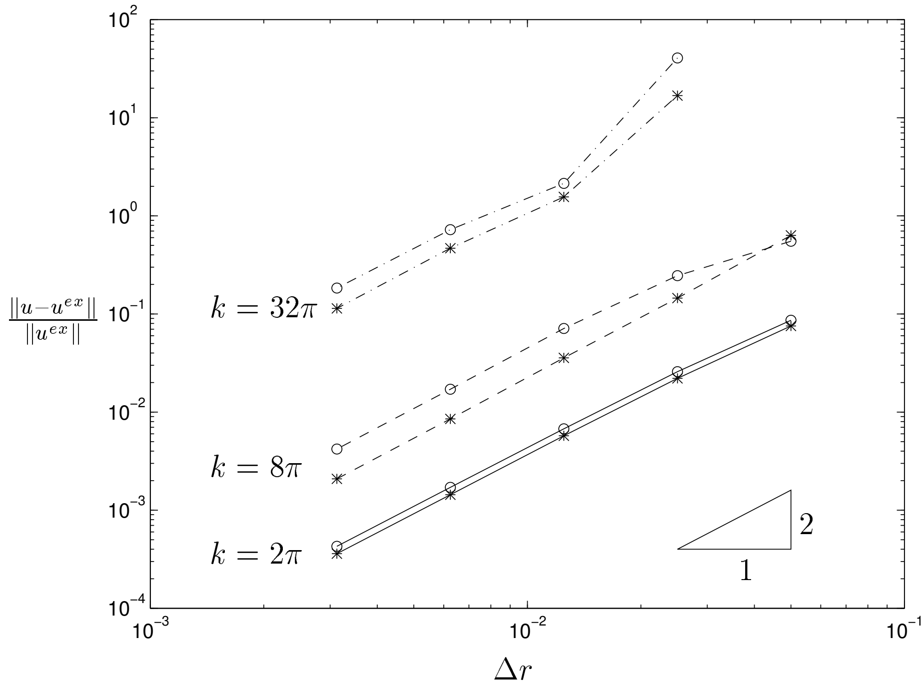

Figure 2.3: Convergence rate of the finite difference/DtN discretization of the plane wave scattering problem on the exterior of the disk. (Impedance Problem)

each case, the relative error $\|u - u^{ex}\|/\|u^{ex}\|$ is plotted in both the maximum norm and the discrete L^2 norm, the latter being the lower of the two curves in all cases. The angular mesh width $\Delta\vartheta$ was always $\Delta\vartheta = \Delta r/6$.

We observe second order convergence with respect to Δr in all cases. The wave resolution in the radial direction corresponds to 20, 40, 80, 160 and 320 points per wavelength for $k = 2\pi$; 5, 10, 20, 40 and 80 points per wavelength for $k = 8\pi$ and 2.5, 5, 10 and 20 points per wavelength for $k = 32\pi$. (For $k = 32$ the coarsest mesh was 20×120.) We also note that a resolution of roughly ten points per wavelength is needed for the asymptotic convergence rate to set in.

Table XX shows the cpu times for computing the finite difference solutions. The computations were done in MATLAB 4.2 on a Sun Sparc10 as well as in FORTRAN on an IBM RS/6000 model 370.

Comparison with Approximate Radiation Boundary Conditions

To compare the performance of the (exact) DtN boundary condition with other popular numerical radiation boundary conditions which are local and based based on asymptotic properties of the exact solution, we repeat some of the computations of the last section using the the Sommerfeld-like boundary condition

$$B_0 u \equiv u_r - iku = 0 \text{ on } \Gamma_R$$

as well as the first two Bayliss-Gunzburger and Turkel (BGT) boundary conditions

$$\begin{aligned} B_1 u &\equiv u_r - iku + \frac{1}{2r}u \\ B_2 u &\equiv u_{rr} + \left(\frac{3}{r} - 2ik\right) u_r + \left(\frac{3}{4r^2} - \frac{3ik}{r} - k^2\right) u. \end{aligned}$$

cf. Section??. The test problem is again the plane-wave scattering problem for the disk of radius 0.5 centered at the origin with the artificial boundary located at $R = 1$. The mesh size begins at 10×60 and is successively doubled.

Figure 2.4 shows the error curves for the wave numbers $k = 2\pi$ and $k = 8\pi$. We observe that the DtN boundary condition performs best in all cases, followed by BGT2, BGT1 and the Sommerfeld-like boundary condition. The accuracy of the solutions computed using the approximate radiation conditions is limited by the accuracy of the radiation boundary condition. Refining the mesh decreases the discretization error up to the point where the error in the boundary condition dominates. This can be observed in Figure 2.4, where the error curve of each of the approximate boundary conditions levels off at a given accuracy and then no longer improves as the mesh is refined. The error in the DtN-solution is essentially due only to the (finite difference) discretization error and so it decreases at the corresponding rate as the mesh is refined. The best possible accuracy of the approximate boundary conditions also appears to decrease slightly as k increases. The error due to the boundary condition can only be decreased by moving the artificial boundary further away from the scatterer, thus enlarging the computational domain and making the computation more expensive.

Despite this difficulty, one should note that a significant departure of the DtN error from the BGT2 error doesn't occur until the mesh has grown to the relatively high resolution of 40 mesh points per wavelength in the radial direction. Better use of the accuracy of the DtN boundary condition will thus be made when higher order discretization methods are used in the interior.

2.5.2 Applications of the Imbedding Algorithm

In this section we apply the imbedding algorithm to three test cases taken from the suite of test problems posed at the Workshop on the Numerical Solutions of Maxwell's Equations held in October 1993 cf. [91].

Ellipse

The first problems we consider are the exterior Dirichlet and Neumann problem with respect to the ellipse with semi-axes $a = 1/2$ and $b = 1/4$ located symmetric with respect to the coordinate axes. We place the artificial boundary at $R = 0.7$ and imbed the resulting computational domain into the annulus with interior radius $R_0 = 0.2$ and exterior radius $R = 0.7$. We solve the problem with wave number $k = 8\pi$, which corresponds to the wavelength $\lambda = a/2$, i.e. four waves along the long axis of the ellipse. The incident wave is propagating in the direction of the positive x-axis. The exact solution of this problem involves summing series of Mathieu functions, so instead we use the numerical solution on a very fine mesh of size 320×1920 (160 points/λ) as a reference solution to compute approximations to the discretization error at various coarser meshes.

Figure 2.5 shows a contour plot of the solution of the Neumann problem, which corresponds to the scattered field. Figure 2.6 displays the error curves with respect to the maximum and discrete L^2 norms. We observe second-order convergence for the Dirichlet problem and a slightly reduced rate of convergence for the Neumann problem. We expect this reduction to be due to the implementation of the Neumann boundary condition on the scattering boundary, which uses unsymmetric one-sided differences.

NACA0012 Airfoil

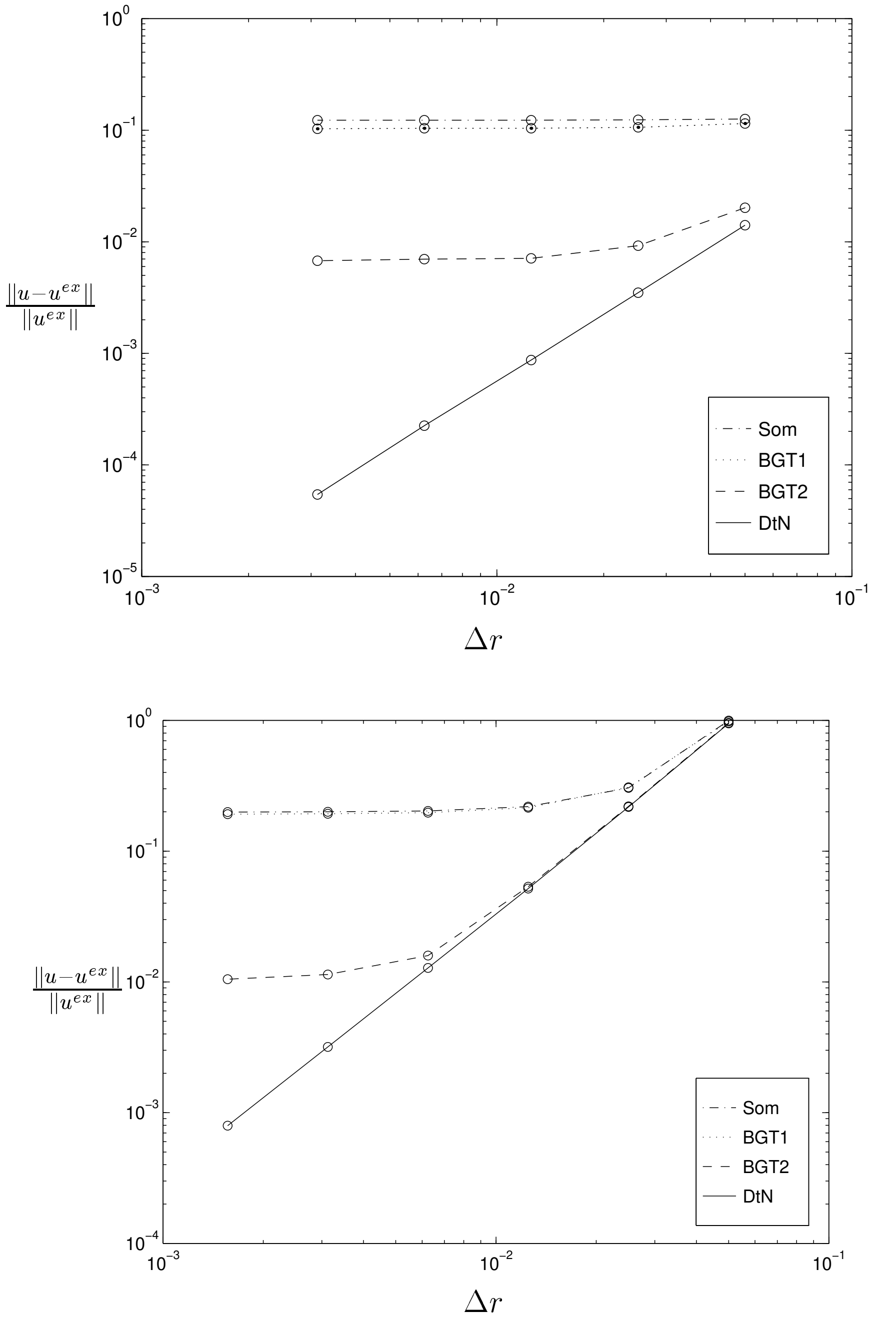

Figure 2.4: Error curves of DtN vs. several approximate radiation boundary conditions; upper plot : $k = 2\pi$, lower plot : $k = 75\pi$.

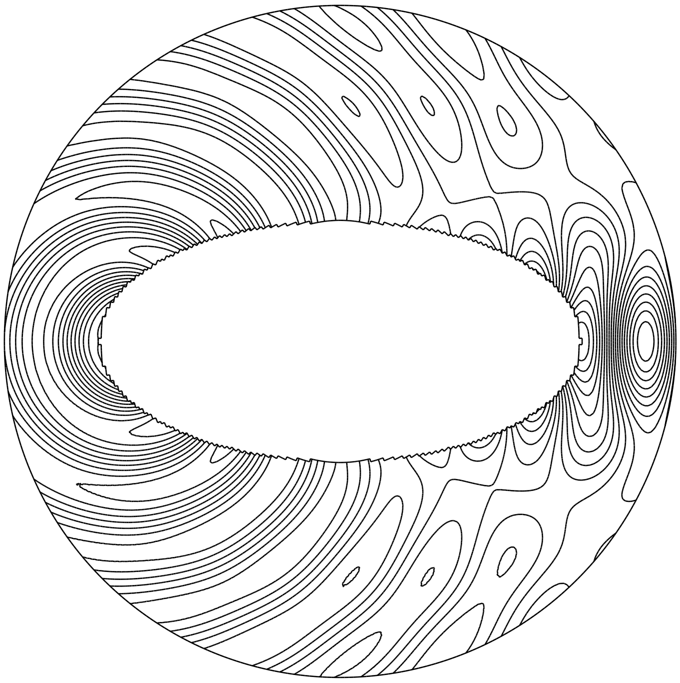

Figure 2.5: Solution of the Neumann problem for the Ellipse

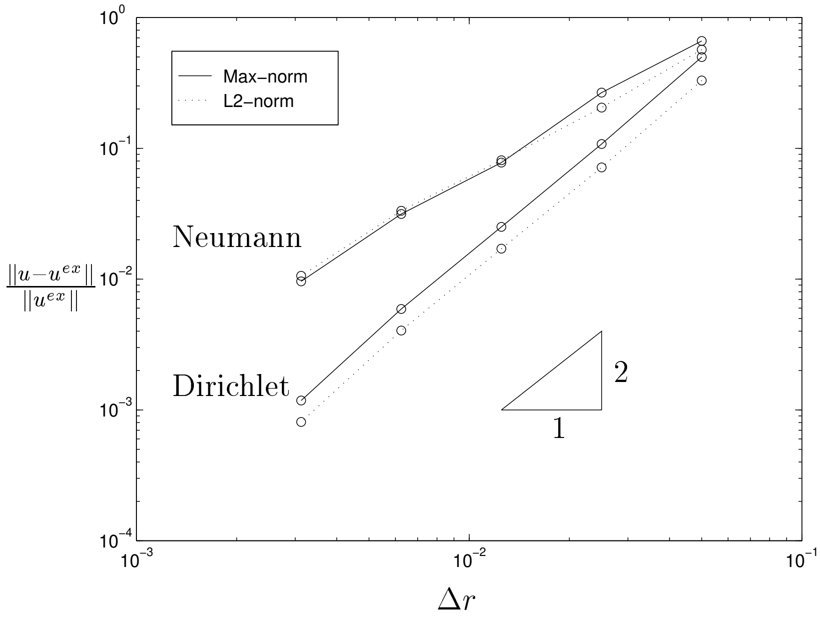

Figure 2.6: Error curves for Dirichlet and Neumann Problems for the ellipse.

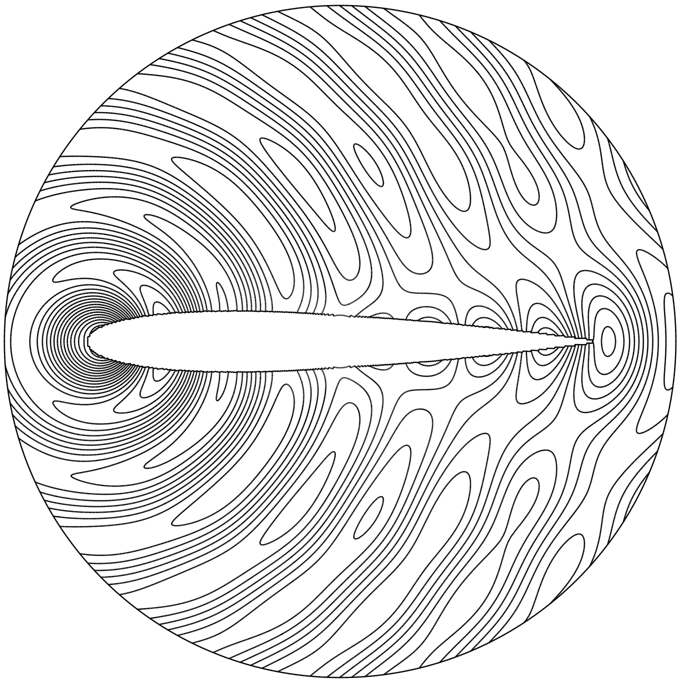

Figure 2.7: Solution of the Neumann problem for the airfoil

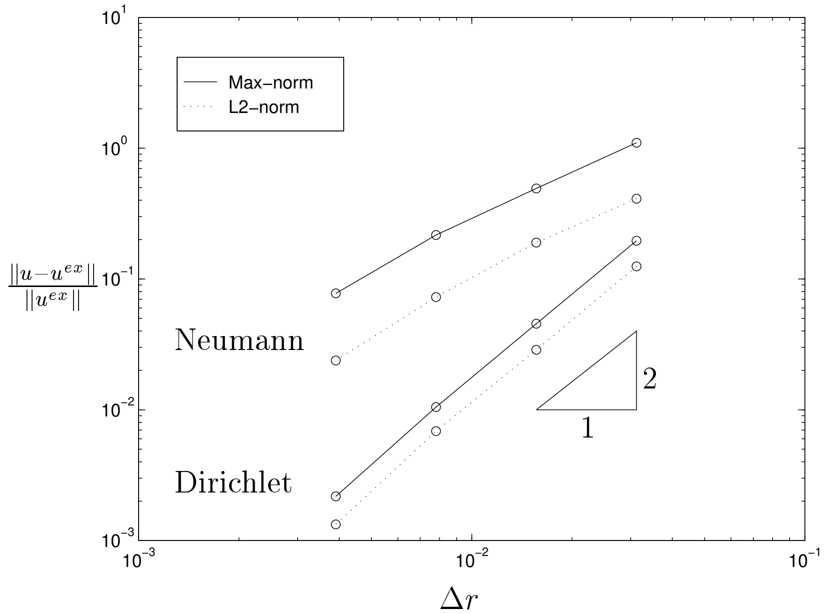

Figure 2.8: Error curves for Dirichlet and Neumann problems for the NACA0012 airfoil.

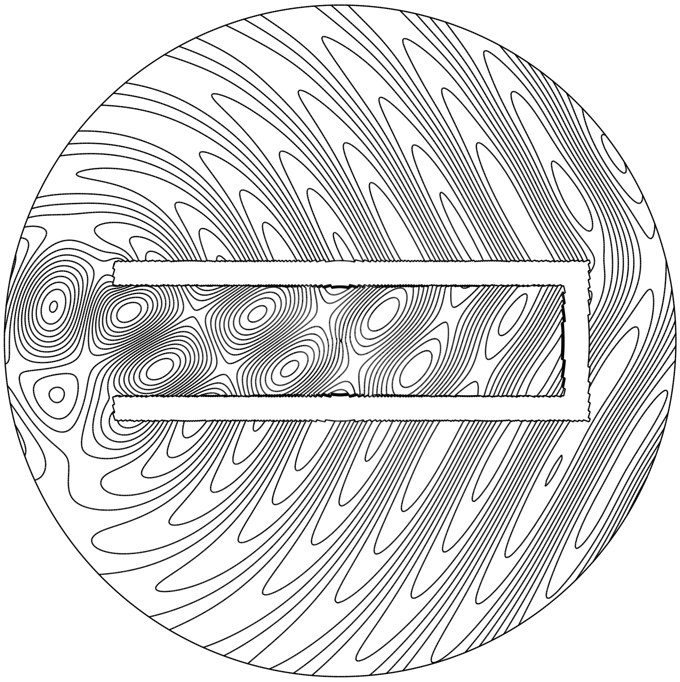

Figure 2.9: Solution of the Dirichlet problem for the Semi-open Cavity

The next obstacle is a NACA 0012 airfoil (*cf.*[93]) with chord length $c = 1$. Figure 2.8 shows convergence curves For the Dirichlet and Neumann problems and Figure 2.7 shows a contour plot of the scattered field at 0^o degrees incidence. We observe second-order convergence for the Dirichlet problem and a somewhat lower convergence order for the Neumann problem. The solutions were again compared to a reference solution on a very fine mesh.

Semi-open Cavity

Finally, we attempt a more difficult geometry, the semi-open cavity seen in Figure 2.9. This obstacle has a much larger boundary than the previous two examples and thus leads to more discrete boundary points and larger capacitance matrices. Figure 2.10 shows the convergence curves. Again we observe second-order convergence for the Dirichlet problem and a slightly slower rate for the Neumann problem.

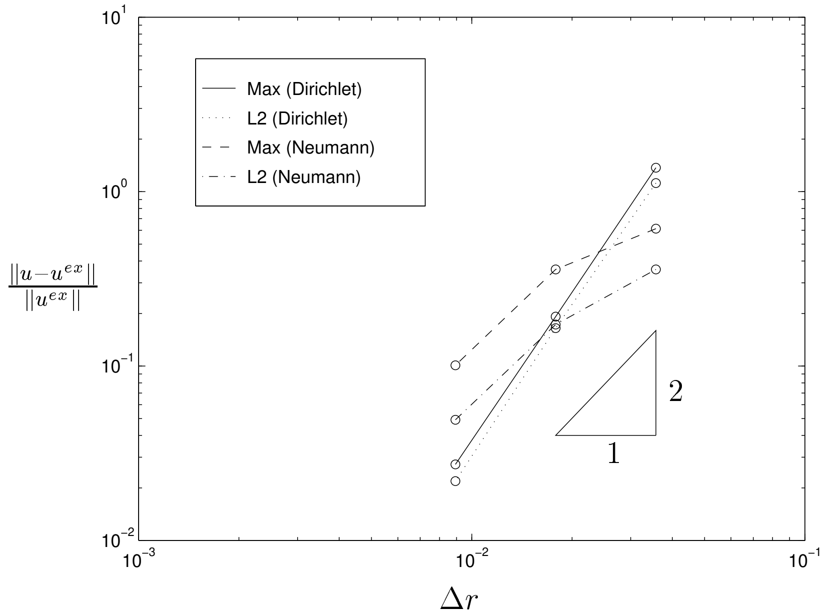

Figure 2.10: Error curves for Dirichlet and Neumann problems for the cavity.

2.5.3 Computing the Scattering Cross Section

As a measure of the amount of radiation scattered back by an obstacle, the (bistatic) *scattering cross section* σ is defined as the limit

$$\sigma(\vartheta) = \lim_{r\to\infty} 2\pi r \frac{|u^s|^2}{|u^i|^2}.$$

Here r is the distance from the scattering surface, ϑ is the backscatter angle, $u_s = u$ is the scattered field and u_i is the incident field, which in the case of a plane wave has unit modulus (cf. [73]).

Once our imbedding algorithm has been used to compute an approximate solution of the scattering problem, the solution is available on that portion of the radial mesh lying outside the scatterer. We will use the computed values of the numerical solution $\{u_{m,j}\}_{j=1}^n$ on the artificial boundary Γ_R to compute an approximation of the scattering cross section using quantities which were already computed when setting up the DtN boundary condition. Using the solution values on the artificial boundary $\{r = R\}$ as Dirichlet data, the solution of the exterior Dirichlet problem on the *exterior* of Γ_R is given by

$$u(r,\vartheta) = \sum_{\nu\in\mathbb{Z}} \frac{H_\nu^{(1)}(kr)}{H_\nu^{(1)}(kR)}\, u_\nu(R)\, e^{i\nu\vartheta}$$

with Fourier coefficients

$$u_\nu(R) = \frac{1}{2\pi}\int_0^{2\pi} u(R,\vartheta)\, e^{-i\nu\vartheta}\, d\vartheta.$$

Using the asymptotic formula

$$H_\nu^{(1)}(z) = \sqrt{\frac{2}{\pi z}} e^{i(z-\frac{\nu\pi}{2}-\frac{\pi}{4})}\left(1 + O(|z|^{-1})\right)$$

for the first-kind Hankel function (cf. [76]), we find that

$$\sqrt{2\pi r}|H_\nu^{(1)}(kr)| = \left|\sqrt{\frac{4}{k}} e^{i(kr-\frac{\nu\pi}{2}-\frac{\pi}{4})}\left\{1 + O\left(\frac{1}{kr}\right)\right\}\right|$$

giving

$$\sqrt{2\pi r}|u(r,\vartheta)| = \left|\sqrt{\frac{4}{k}} e^{i(kr-\frac{\pi}{4})} \sum_{\nu\in\mathbb{Z}} \frac{u_\nu(R)}{H_\nu^{(1)}(kR)} e^{-\frac{i\nu\pi}{2}} e^{i\nu\vartheta}\left\{1 + O\left(\frac{1}{kr}\right)\right\}\right|$$

which results in an expression for the scattering cross section

$$\sigma(\vartheta) = \frac{4}{k}\left|\sum_{\nu\in\mathbb{Z}} \frac{(-i)^\nu u_\nu(R)}{H_\nu^{(1)}(kR)}\, e^{i\nu\vartheta}\right|^2 .$$

The values of the Hankel functions are also needed in the DtN boundary condition and can thus be reused. As in the DtN boundary condition, we obtain an approximation of σ by truncating the series and computing the Fourier coefficients $u_\nu(R)$ using the trapezoidal rule to integrate over the artificial boundary. This computation can be done very efficiently by again using the FFT.

Scattering Cross Section for the Model Problem

Using the formula derived above, the scattering cross section for the disk with Dirichlet boundary condition becomes

$$\sigma^{Dir}(\vartheta) = \frac{4}{k}\left|\sum_{\nu\in\mathbb{Z}} \frac{J_\nu(ka)}{H_\nu^{(1)}(ka)}\, e^{i\nu\vartheta}\right|^2$$

and

$$\sigma^{Imp}(\vartheta) = \frac{4}{k}\left|\sum_{\nu\in\mathbb{Z}} \frac{J_\nu'(ka) + \eta J_\nu(ka)}{H_\nu^{(1)'}(ka) + \eta H_\nu^{(1)}(ka)}\, e^{i\nu\vartheta}\right|^2$$

for the impedance problem which reduces to the Neumann problem for $\eta = 0$. Figure 2.11 shows the resulting error curves for the scattering cross section computations based on the solution values coming from the finite-difference/DtN discretization compared to the series expression for the true scattering cross section. We again observe second-order convergence as expected. Figure 2.12 shows the scattering cross section for the $k = 32\pi$ Neumann problem for the disk using the 160×960 grid (20 points/wavelength). Except for a few dips which are lower than in the series solution, the two curves are indistinguishable to plotting accuracy. Here and in the following, when plotting the scattering cross section as a function of angle, we plot the quantity

$$\hat{\sigma} = 10 \log_{10} \frac{\sigma}{\lambda}$$

rather than σ, as is common in the Engineering literature.

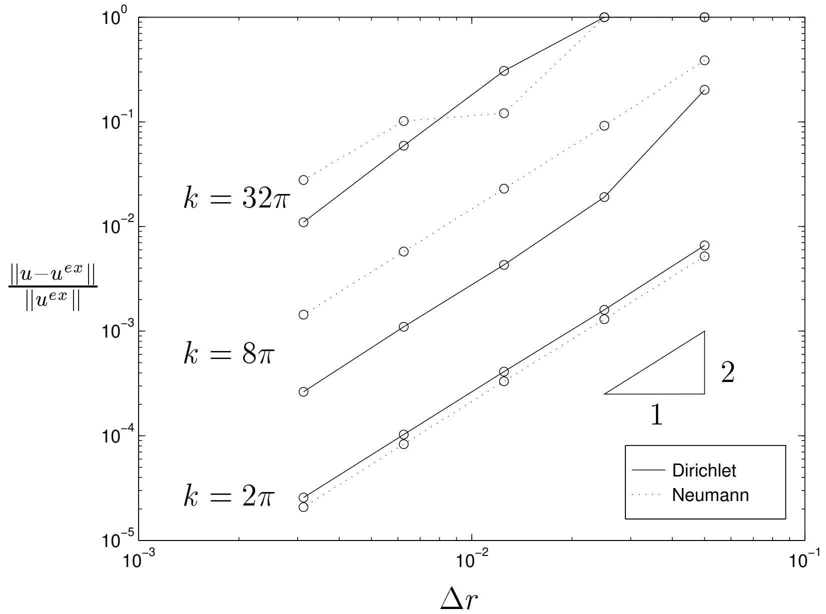

Figure 2.11: Error curves for Scattering Cross Section for the disk

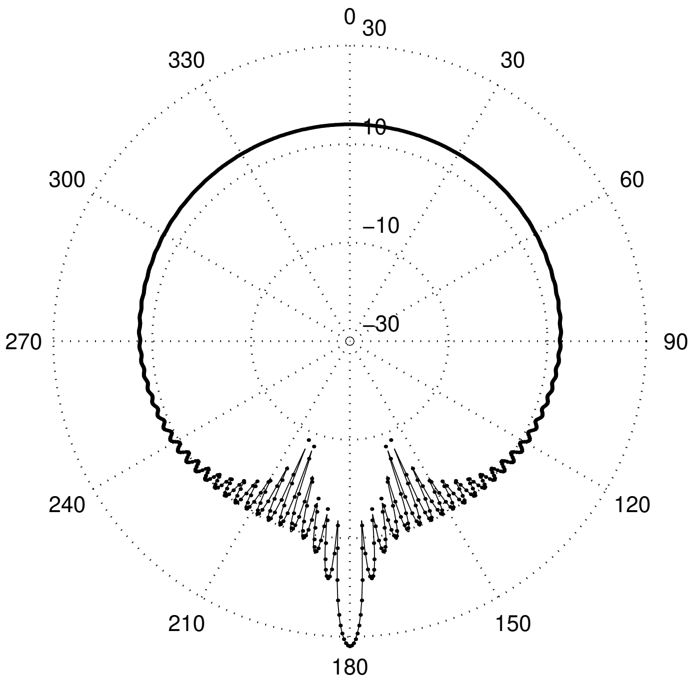

Figure 2.12: Scattering cross sections for the disk with Neumann boundary condition for $k = 32\pi$. Solid line: series solution, dotted line: using fast solver solution.

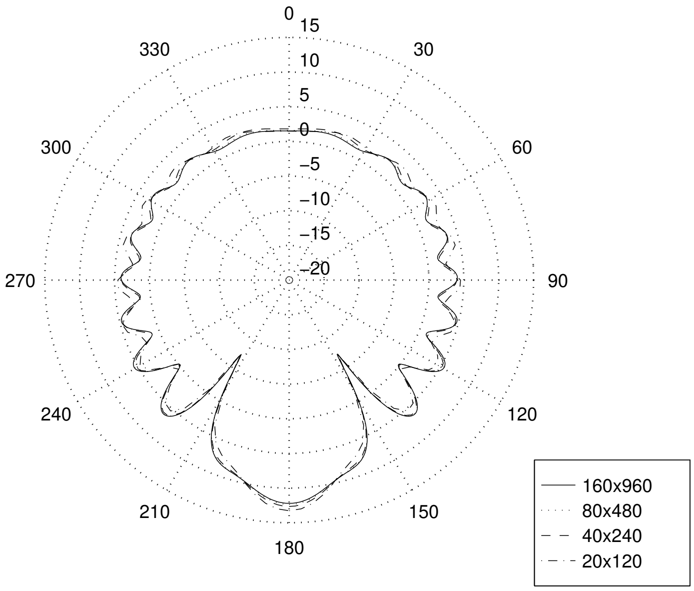

Figure 2.13: Scattering cross sections for the ellipse with Neumann boundary condition at 0^o incidence on various meshes.

Scattering Cross Sections from the Imbedding Algorithm

In this section, we show the results of computing the scattering cross section from the data supplied by the finite difference imbedding algorithm for the ellipse, the airfoil and the cavity test cases.

Figure 2.13 shows scattering cross sections computed from the solution data on the artificial boundary on grids of resolutions 10×60, 20×120 and 160×960. For resolutions higher than the 20×120 grid, the scattering cross section plot could be distinguished from that resulting from the solution on the 160×960 grid.

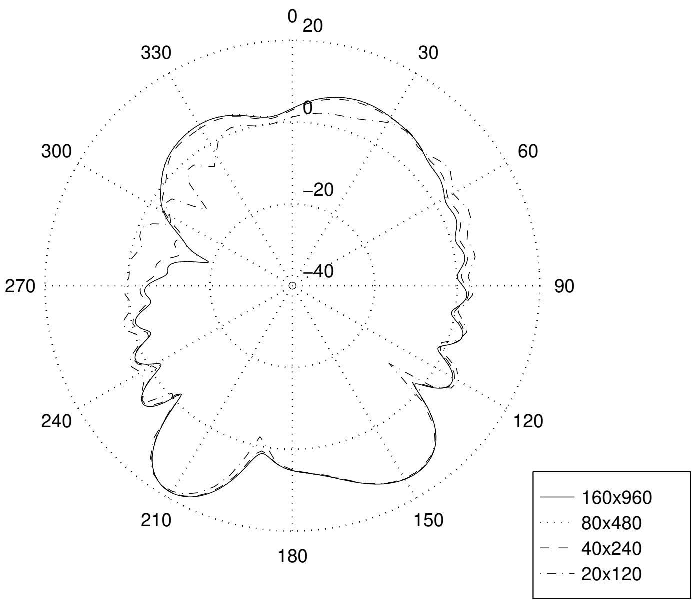

Figure 2.14: Scattering cross sections for the cavity with Dirichlet boundary condition at 30^o incidence on various meshes.

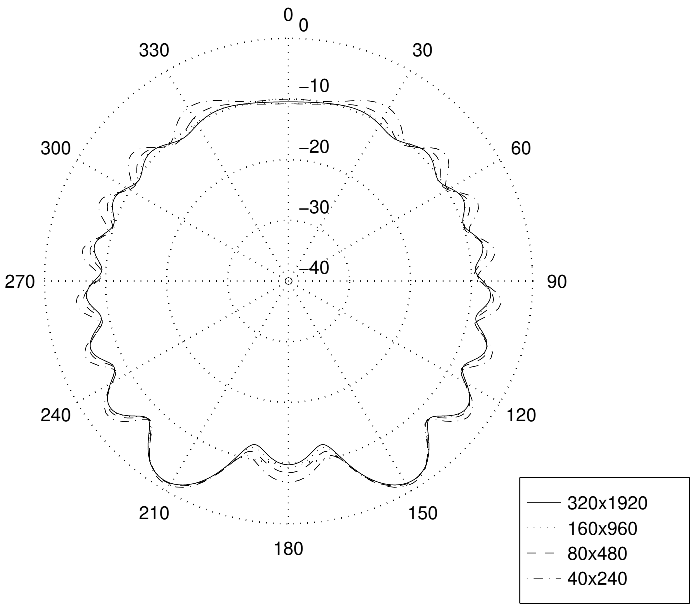

Figure 2.15: Scattering cross sections for the airfoil with Neumann boundary condition at 0^o incidence on various meshes.

Chapter 3

A Finite-Element Capacitance Matrix Method

3.1 Introduction

In this chapter we develop an imbedding method for exterior Helmholtz problems based on a finite element discretization. The finite element discretization has the advantage of being based on a variational principle for the continuous problem which carries over to the discrete formulation. This allows us to carry out the convergence analysis for the discretization method, which we were unable to do for the finite-difference algorithm in Chapter 2. The linear system of equations arising from the discretization is again solved efficiently by using an imbedding method based on an FFT-based fast Helmholtz solver on a disk/annulus. This time, however, we solve the capacitance matrix equation iteratively and show why the number of iterations needed to solve the equation up to a given accuracy is independent of the mesh size.

Other methods using coupled finite-element and integral equation methods in a similar way are Masmoudi [80], from which the idea for the convergence proof is taken, Kirsch and Monk [71, 72] and Hsiao and Wendland [64], which uses boundary integral operators to develop domain decomposition algorithms.

There is a large amount of literature on using finite elements to solve exterior Helmholtz problems and other exterior problems. Early work includes Giroire and

Nedelec [45] and Nedelec and Planchard [84] as well as an important paper concerning stability by A. Schatz [94]. C. Goldstein has written as series of papers on this subject, a partial list being [51, 53, 52, 50]. T. Hughes and his students have recently done work on using stabilized finite elements [58, 59] and adaptive mesh refinement strategies [100, 99] for solving exterior Helmholtz problems. See also the recent survey paper [60].

This chapter is organized as follows : in Section 3.2 we introduce the variational formulation of Problem (3.1) stated below and, after proving some properties of the DtN operator, show existence and uniqueness for the variational problem in a way that is seen in Section 3.3 to also work for the corresponding discrete problem. Section 3.4 introduces the finite element discretization on the annulus using bilinear quadrilaterals in the variables r and ϑ along with the discrete DtN boundary condition; it is seen that an FFT-based fast solver can again be used to solve the resulting linear system. Then in Section 3.5 we introduce an iterative imbedding algorithm to accommodate obstacles of arbitrary shape upon which numerical experiments follow in Section 3.6.

We focus on the exterior Dirichlet problem in the following, but note here that the same approach can be applied to the Neumann- and Impedance boundary value problems with minor modifications.

We seek a solution of the exterior Dirichlet problem (cf. Figure 3.1)

$$\left\{\begin{aligned} \Delta u + k^2 u = 0 \quad & \text{in } \Omega \\ u = g \quad & \text{on } \Gamma \\ \frac{\partial u}{\partial r} = M_k u \ & \text{on } \Gamma_R \end{aligned}\right. \tag{3.1}$$

on the computational domain Ω bounded internally by the obstacle boundary Γ and externally by the circular artificial boundary Γ_R on which the DtN boundary condition is imposed.

3.2 The Variational Formulation

In order to apply the finite element method to solve Problem (3.1) we reformulate it as a variational problem. To this end, we multiply the Helmholtz equation with a

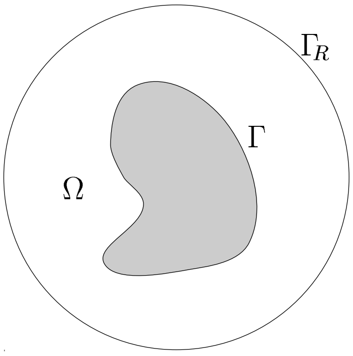

Figure 3.1: The computational domain Ω bounded externally by the circle Γ_R and internally by the obstacle boundary Γ

smooth function v and integrate by parts to obtain

$$\int_\Omega (\nabla u \cdot \nabla \bar{v} - k^2 u \bar{v}) dx - \int_{\Gamma_R - \Gamma} \bar{v} \frac{\partial u}{\partial n} ds = 0. \tag{3.2}$$

We introduce the space of trial functions $\mathscr{S}$ and the space of weighting functions $\mathscr{V}$ as

$$\begin{aligned} \mathscr{S} &:= \{u \in H^1(\Omega) \ : \ u_{|\Gamma} = g\} \\ \mathscr{V} &:= \{v \in H^1(\Omega) \ : \ v_{|\Gamma} = 0\}, \end{aligned}$$

where $H^1(\Omega)$ is the usual Sobolev space and the restriction of functions to boundaries is to be understood in the sense of the trace operator. We require that $v \in \mathscr{V}$ in (3.2) so that the integral over Γ vanishes. Also, since the solution u is required to satisfy the DtN boundary condition on Γ_R, we can replace its normal derivative there with $M_k u$. The image of a function $\varphi \in H^{\frac{1}{2}}(\Gamma_R)$ under the DtN operator M_k for the case where Γ_R is a circle of radius R around the origin can be written as the the Fourier series

$$(M_k\varphi)(\vartheta) = k \sum_{n\in\mathbb{Z}} \frac{H_n^{(1)\prime}(kR)}{H_n^{(1)}(kR)} \varphi_n e^{in\vartheta}, \qquad \varphi \in H^{\frac{1}{2}}(\Gamma_R)$$

with Fourier coefficients

$$\varphi_n = \frac{1}{2\pi} \int_0^{2\pi} \varphi(\vartheta) e^{-in\vartheta}\, d\vartheta, \qquad n \in \mathbb{Z}.$$

A variational formulation of problem (3.1) is thus to

$$\text{(3.3)} \qquad \textit{Find } u \in \mathscr{S} \textit{ such that} \quad a(u,v) = 0 \quad \forall v \in \mathscr{V}.$$

The bilinear form $a(\cdot,\cdot) : H^1(\Omega) \times H^1(\Omega) \to \mathbb{C}$ is defined as

$$a(u,v) := \int_\Omega (\nabla u \cdot \nabla \overline{v} - k^2 u \bar{v}) dx - \int_{\Gamma_R} \overline{v} M_k u \, ds.$$

We note that, while the first term in the bilinear form is self-adjoint, the boundary integral term is only 'symmetric'. More precisely, if $\langle \cdot,\cdot \rangle_{\Gamma_R}$ denotes the duality pairing between $H^{-\frac{1}{2}}(\Gamma_R)$ and $H^{\frac{1}{2}}(\Gamma_R)$ considered as an extension of the (complex) L^2-inner product on Γ_R, we have

$$\begin{aligned}
\langle M_k \varphi, \psi \rangle_{\Gamma_R} &= \int_{\Gamma_R} \overline{\psi} M_k \varphi \, ds \\
&= R \int_0^{2\pi} \left(k \sum_n \frac{H_n^{(1)\prime}(kR)}{H_n^{(1)}(kR)} \varphi_n e^{in\vartheta} \right) \overline{\psi(\vartheta)} \, d\vartheta \\
&= R \int_0^{2\pi} \left(k \sum_n \frac{H_n^{(1)\prime}(kR)}{H_n^{(1)}(kR)} \overline{\psi_n} e^{-in\vartheta'} \right) \varphi(\vartheta) \, d\vartheta' \\
&= \langle M_k \overline{\psi}, \overline{\varphi} \rangle_{\Gamma_R}.
\end{aligned}$$

Because of this, the discretization matrices we will obtain later by restricting u and v to finite dimensional subspaces of $H^1(\Omega)$ will be complex-symmetric.

We now investigate some important properties of the DtN operator. In the proof of the next theorem, we will need a characterization of the dual space $H^{-p}(\Gamma_R)$ of $H^p(\Gamma_R)$ for $p \geq 0$. Since the artificial boundary Γ_R is a circle, we can write each $g \in L^2(\Gamma_R)$ as a Fourier series

$$g(\vartheta) = \sum_{n \in \mathbb{Z}} g_n e^{in\vartheta}$$

with Fourier coefficients g_n. The $H^p(\Gamma_R)$-norm of g is then given by

$$\|g\|_{p,\Gamma_R} = \left\{ \sum_{n \in \mathbb{Z}} (1+n^2)^p |g_n|^2 \right\}^{1/2}.$$

A functional G on $H^p(\Gamma_R)$ then belongs to the dual $H^{-p}(\Gamma_R)$ if and only if its norm

$$\|G\|_{-p,\Gamma_R} = \left\{ \sum_{n\in\mathbb{Z}} (1+n^2)^{-p} |G_n|^2 \right\}^{1/2}$$

is finite. Here G_n is the value of the functional G applied to the trigonometric monomial $\mu_n(\vartheta) := \exp(in\vartheta)$. Conversely, for every sequence of complex numbers $\{F_n\}_{n\in\mathbb{Z}}$ satisfying $\sum(1+n^2)^{-p}\||F_n|^2 < \infty$, there exists an $F \in H^{-p}(\Gamma_R)$ with $F(\mu_n) = F_n,\ n \in \mathbb{Z}$.

Theorem 3.2.1 *For all non-negative integers p, the DtN operator M_k is a bounded linear operator from $H^{p+\frac{1}{2}}(\Gamma_R)$ to $H^{p-\frac{1}{2}}(\Gamma_R)$, i.e.*

$$M_k \in \mathscr{L}(H^{p+\frac{1}{2}}(\Gamma_R), H^{p-\frac{1}{2}}(\Gamma_R)).$$

Proof. We first consider the case $p = 0$. Given $g \in H^{\frac{1}{2}}(\Gamma_R)$, we must show that its image $G := M_k g$ lies in $H^{-\frac{1}{2}}(\Gamma_R)$. By the definition of M_k,

$$G(\vartheta) = k \sum_{n\in\mathbb{Z}} g_n \frac{H_n^{(1)'}(kR)}{H_n^{(1)}(kR)} e^{in\vartheta}.$$

Since

$$G_n = G(e^{in\vartheta}) = k g_n \frac{H_n^{(1)'}(kR)}{H_n^{(1)}(kR)},$$

we have

$$\begin{aligned}
\|M_k g\|^2_{\frac{1}{2},\Gamma_R} = \|G\|^2_{\frac{1}{2},\Gamma_R} &= \sum_n \frac{|G_n|^2}{(1+n^2)^{\frac{1}{2}}} \\
&= |k|^2 \sum_n \left| \frac{H_n^{(1)'}(kR)}{H_n^{(1)}(kR)} \right|^2 \frac{|g_n|^2}{(1+n^2)^{\frac{1}{2}}} \\
&= |k|^2 \sum_n |g_n|^2 (1+n^2)^{\frac{1}{2}} \left| \frac{H_n^{(1)'}(kR)}{H_n^{(1)}(kR)} \right|^2 \frac{1}{1+n^2} \\
&\le C_M^2 |k|^2 \|g\|^2_{\frac{1}{2},\Gamma_R}
\end{aligned}$$

provided we can show that there exists C_M such that

$$\left| \frac{H_n^{(1)'}(kR)}{H_n^{(1)}(kR)} \right|^2 \frac{1}{1+n^2} \le C_M^2 \qquad \text{for all } n \in \mathbb{Z}.$$

To this end, we make use of the following asymptotic formula for $H^{(1)}$ for large index cf. [18]:

$$H_n^{(1)}(z) = -i\sqrt{\frac{2}{n\pi}}\left(\frac{2n}{ez}\right)^n \left\{1 + \mathcal{O}\left(\frac{1}{n}\right)\right\} \text{ as } n \to \infty \tag{3.4}$$

as well as the recursion formula cf. [76]

$$H_n^{(1)'}(z) = \frac{1}{2}\left(H_{n-1}^{(1)}(z) - H_{n+1}^{(1)}(z)\right), \qquad n \geq 1. \tag{3.5}$$

By (3.5), the expression we wish to bound becomes

$$\frac{H_n^{(1)'}(kR)}{H_n^{(1)}(kR)} = \frac{1}{2}\left(\frac{H_{n-1}^{(1)}(kR)}{H_n^{(1)}(kR)} - \frac{H_{n+1}^{(1)}(kR)}{H_n^{(1)}(kR)}\right).$$

For the first term, we obtain

$$\frac{H_{n-1}^{(1)}(kR)}{H_n^{(1)}(kR)} = \left(\frac{n}{n-1}\right)^{\frac{1}{2}}\left(1 - \frac{1}{n}\right)^{n-1}\left(\frac{ekr}{2n}\right)\left\{1 + \mathcal{O}\left(\frac{1}{n}\right)\right\} \to 0 \text{ as } n \to \infty$$

since all terms are bounded and the third term in parentheses tends to zero. The second term yields

$$\frac{H_{n+1}^{(1)}(kR)}{H_n^{(1)}(kR)} = \left(\frac{n}{n+1}\right)^{\frac{1}{2}}\left(1 + \frac{1}{n}\right)^{n}\left(\frac{2(n+1)}{ekr}\right)\left\{1 + \mathcal{O}\left(\frac{1}{n}\right)\right\} = \mathcal{O}(n) \text{ as } n \to \infty$$

since, in this case, all terms are bounded except for the third term in parentheses which is $\mathcal{O}(n)$. Thus, we have

$$\left|\frac{H_n^{(1)'}(kR)}{H_n^{(1)}(kR)}\right|^2 \frac{1}{1+n^2} = \mathcal{O}(n^2) \cdot \frac{1}{1+n^2} = \mathcal{O}(1) \text{ as } n \to \infty$$

which insures the existence of the desired bound C_M. The same proof works also for arbitrary $m \in \mathbb{N}$. $\square$

Theorem 3.2.1 implies continuity of the bilinear form:

Corollary 3.2.1 *There exists a constant $C_b > 0$ such that*

$$|a(u,v)| \leq C_b \|u\|_{1,\Omega}\, \|v\|_{1,\Omega} \qquad \forall u, v \in H^1(\Omega).$$

Proof. The Cauchy-Schwarz inequality, the boundedness of M_k and the trace theorem give, successively,

$$\begin{aligned} |a(u,v)| &\leq (1+k^2)\|u\|_{1,\Omega}\,\|v\|_{1,\Omega} + \|M_k u\|_{-\frac{1}{2},\Gamma_R}\,\|v\|_{\frac{1}{2},\Gamma_R} \\ &\leq (1+k^2+C_M C_{\text{trace}})\,\|u\|_{1,\Omega}\,\|v\|_{1,\Omega} \qquad \forall u,v \in H^1(\Omega). \end{aligned}$$

□

Theorem 3.2.2 *The DtN operator belonging to the purely imaginary wave number $k = i$ is negative definite on $H^{\frac{1}{2}}(\Gamma_R)$, i.e.*

$$\langle -M_i\psi, \psi\rangle_{\Gamma_R} \geq 0 \qquad \forall \psi \in H^{\frac{1}{2}}(\Gamma_R).$$

Proof. For any $\psi \in H^{\frac{1}{2}}(\Gamma_R)$ we have

$$\langle -M_i\psi, \psi\rangle_{\Gamma_R} = -i\sum_n |\psi|^2 \frac{H_n^{(1')}(iR)}{H_n^{(1)}(iR)} = -\sum_n |\psi|^2 \frac{K_n'(R)}{K_n(R)} \geq 0.$$

The first identity follows from the identity

$$H_n^{(1)}(iz) = \frac{2}{\pi i} e^{\frac{n\pi i}{2}} K_n(z)$$

valid for $-\pi < \arg(z) < \frac{\pi}{2}$, where K_n is the modified Bessel function of the third kind of order n (cf. [76]). The inequality follows from the fact that $K_n(R) > 0,\ \ K_n'(R) < 0$ for $R > 0$, which can be inferred from the integral representation

$$K_n(z) = \int_0^\infty e^{-z\cosh t} \cosh nt\; dt$$

valid for $\mathrm{Re}(z) > 0$. □

This implies, in particular, that the bilinear form $a_i(\cdot,\cdot)$ belonging to $k = i$ is $H^1(\Omega)$-coercive:

$$a_i(u,u) = \int_\Omega (|\nabla u|^2 + |u|^2)\; dx - \langle M_i u, u\rangle_{\Gamma_R} \geq \|u\|_{1,\Omega}^2 .$$

Theorem 3.2.3 *For two wave numbers k_1 and k_2 with non-negative imaginary part there holds*

$$(M_{k_1} - M_{k_2})\psi \in H^{\frac{3}{2}}(\Gamma_R) \qquad \forall \psi \in H^{\frac{1}{2}}(\Gamma_R)$$

and there exists a constant $C > 0$ such that

$$\|(M_{k_1} - M_{k_2})\psi\|_{\frac{3}{2},\Gamma_R} \leq C\|\psi\|_{\frac{1}{2},\Gamma_R}$$

Proof. By definition, we have

$$\begin{aligned}
\|M_{k_1}\psi - M_{k_2}\psi\|^2_{\frac{3}{2},\Gamma_R} &= \sum_n \left| k_1 \frac{H_n^{(1)'}(k_1R)}{H_n^{(1)}(k_1R)} - k_2 \frac{H_n^{(1')}(k_2R)}{H_n^{(1)}(k_2R)} \right|^2 \psi_n|^2(1+n)^{\frac{3}{2}} \\
&\leq C^2 \sum_n |\psi_n|^2(1+n^2)^{\frac{1}{2}} \\
&= C^2\|\psi\|_{\frac{1}{2},\Gamma_R}
\end{aligned}$$

if we can establish that

$$H(n) := \left| k_1 \frac{H_n^{(1)'}(k_1R)}{H_n^{(1)}(k_1R)} - k_2 \frac{H_n^{(1)'}(k_2R)}{H_n^{(1)}(k_2R)} \right| \leq C \qquad \text{for all } n$$

for some suitable C. By the recursion formula (3.5),

$$H(n) = \frac{1}{2}\left\{ \left(k_1 \frac{H_{n-1}^{(1)}(k_1R)}{H_n^{(1)}(k_1R)} - k_2 \frac{H_{n-1}^{(1)}(k_2R)}{H_n^{(1)}(k_2R)} \right) - \left(k_1 \frac{H_{n+1}^{(1)}(k_1R)}{H_n^{(1)}(k_1R)} - k_2 \frac{H_{n+1}^{(1)}(k_2R)}{H_n^{(1)}(k_2R)} \right) \right\}.$$

As in the proof of Theorem , the first term in parentheses is $\mathcal{O}(1/n)$. Applying the asymptotic formula (3.4) to the second term yields

$$\begin{aligned}
&k_1 \frac{H_{n+1}^{(1)}(k_1R)}{H_n^{(1)}(k_1R)} - k_2 \frac{H_{n+1}^{(1)}(k_2R)}{H_n^{(1)}(k_2R)} \\
&\qquad = \left(\frac{n}{n+1}\right)^{\frac{1}{2}} \left(1 + \frac{1}{n}\right)^n \left(k_1 \frac{2(n+1)}{ek_1R} - k_2 \frac{2(n+1)}{ek_2R} \right) \left\{ 1 + \mathcal{O}\left(\frac{1}{n}\right) \right\} = 0
\end{aligned}$$

Thus,

$$|H(n)|^2 \cdot (1+n^2) = \mathcal{O}\left(\frac{1+n^2}{n^2}\right) = \mathcal{O}(1).$$

□

Given a function $\lambda \in H^{\frac{1}{2}}(\Gamma_R)$, consider the problem (P_λ) given by

$$(P_\lambda) \quad \begin{cases} \Delta u + k^2 u = f \text{ in } \Omega \\ u = g \text{ on } \Gamma \\ \dfrac{\partial u}{\partial r} - M_k u = \lambda \text{ on } \Gamma_R. \end{cases}$$

Theorem 3.2.4 *Problem (P_λ) has a unique solution. If Γ is sufficiently regular (e.g. C^1) and if in addition the data satisfies $f \in L^2(\Omega)$, $g \in H^{\frac{3}{2}}(\Gamma)$ and $\lambda \in H^{\frac{1}{2}}(\Gamma_R)$, then $u \in H^2(\Omega)$ and satisfies*

$$\|u\|_{2,\Omega} \leq \beta \left(\|f\|_{0,\Omega} + \|g\|_{\frac{3}{2},\Gamma} + \|\lambda\|_{\frac{1}{2},\Gamma_R} \right)$$

for some $\beta > 0$.

Proof. The proof proceeds in three steps. We begin by finding a function $u_1 \in H^2(\Omega)$ which satisfies $\Delta u_1 + k^2 u_1 = f$ in Ω. No boundary conditions are imposed so that u_1 can be found e.g. by using the Fourier transform. We set

$$\lambda_1 := \frac{\partial u_1}{\partial r} - M_k u_1 \in H^{\frac{1}{2}}(\Gamma_R)$$

and define $\tilde{u}_2$ to be the solution of the problem

$$(3.6) \qquad \begin{cases} \Delta \tilde{u}_2 + k^2 \tilde{u}_2 = 0 & \text{in } \mathbb{R}^2 \setminus \Gamma_R \\ \left[\dfrac{\partial \tilde{u}_2}{\partial r} \right]_{\Gamma_R} = \lambda - \lambda_1 \end{cases}$$

where $[v]_{\Gamma_R}$ denotes the jump $v^- - v^+$ of a function v across Γ_R as one moves from the inside to the outside. This problem can be solved using the layer potentials summarized in Sections 1.2.2 and 1.2.4. We can express $\tilde{u}_2$ as the single-layer potential

$$\tilde{u}_2(x) = \widetilde{S}(\lambda - \lambda_1)(x) = 2 \int_{\Gamma_R} [\lambda(y) - \lambda_1(y)] \Phi(x, y) \, ds(y)$$

with density $\lambda - \lambda_1$. The mapping properties of $\widetilde{S}$ assure that $\tilde{u}_2$ lies in $H^2(\mathrm{int}(\Gamma_R))$ and in $H^2_{loc}(\mathrm{ext}(\Gamma_R))$, respectively, and the jump conditions imply that $\tilde{u}_2$ solves the problem (3.6).

We now set $u_2 := \tilde{u}_2|_\Omega$ and verify that

$$\frac{\partial u_2}{\partial r} - M_k u_2 = \lambda - \lambda_1 \qquad \text{on } \Gamma_R.$$

To see this, note that the DtN map M_k maps $u_2|_{\Gamma_R}$ to the normal derivative on Γ_R of the solution of the exterior Dirichlet problem with data $u_2|_{\Gamma_R}$. This normal derivative is just $\partial \tilde{u}_2^+/\partial r$, giving

$$\frac{\partial u_2}{\partial r} - M_k u_2 = \frac{\partial \tilde{u}_2^-}{\partial r} - \frac{\partial \tilde{u}_2^+}{\partial r} = \lambda - \lambda_1.$$

We now define u_3 to be the solution of

$$\begin{cases} \Delta u_3 + k^2 u_3 = 0 & \text{in } \Omega \\ u_3 = g - u_1|_\Gamma - u_2|_\Gamma & \text{on } \Gamma \\ \dfrac{\partial u_3}{\partial r} - M_k u_3 = 0 & \text{on } \Gamma_R. \end{cases} \tag{3.7}$$

The regularity properties of solutions of the exterior problem (3.7) (cf. Theorem 1.2.4) give $u_3 \in H^2(\Omega)$ and, setting $u := u_1 + u_2 + u_3$, we obtain a solution of problem (P_λ). The continuity with respect to the data follows from standard regularity theorems or from the fact that all the operators involved are bounded. Uniqueness results from the fact that the solution of the homogeneous counterpart of (P_λ) can be extended to a solution of the homogeneous exterior Dirichlet problem, implying that it must vanish identically. $\square$

We now define the following mapping :

$$\begin{aligned} \mathscr{A} : \mathscr{V} &\rightarrow \mathscr{V} \\ u &\mapsto v = \mathscr{A} u \\ \text{such that } a_i(v, \varphi) &= a(u, \varphi) \quad \forall \varphi \in \mathscr{V}. \end{aligned}$$

We note that this mapping is well defined since the bilinear form $a_i(\cdot, \cdot)$ is coercive and $a(u, \cdot)$ is a continuous linear form on $H^1(\Omega)$.

Theorem 3.2.5 *The mapping $\mathscr{A}$ has the following properties:*

1. *$\mathscr{A}$ is an automorphism of $\mathscr{V}$*

2. $(\mathscr{A} - I)u \in H^2(\Omega) \quad \forall v \in \mathscr{V}$

3. $\exists \beta > 0 : \|(\mathscr{A} - I)u\|_{2,\Omega} \leq \beta \|u\|_{1,\Omega}\,,$ *i.e.* $\mathscr{A} - I \in \mathscr{L}(\mathscr{V}, H^2(\Omega))$.

Proof. We first show that $\mathscr{A}$ is injective and surjective:
Injectivity: $\mathscr{A}u = 0$ for $u \in \mathscr{V}$ means that, for all $\varphi \in \mathscr{V}$, we have $0 = a_i(\mathscr{A}u, \varphi) = a(u, \varphi)$. But this means that u is a solution of the weak homogeneous exterior Dirichlet problem which implies that $u = 0$.

Surjectivity: given $v \in \mathscr{V}$ we need to find $u \in \mathscr{V}$ such that $\mathscr{A}u = v$. Setting $w := u - v$, we have

$$\begin{aligned} v = \mathscr{A}u \Leftrightarrow a_i(v, \varphi) &= a(u, \varphi) & \forall \varphi \in V \\ \Leftrightarrow a(w, \varphi) &= a_i(v, \varphi) - a(v, \varphi) & \forall \varphi \in V. \end{aligned}$$

The last equality, written out, says that

$$a(w, \varphi) = (1 + k^2)(v, \varphi)_{0,\Omega} + \langle (M_k - M_i)v, \varphi \rangle_{\Gamma_R} \quad \forall \varphi \in \mathscr{V},$$

the angle brackets denoting the duality pairing between $H^{-\frac{1}{2}}(\Gamma_R)$ and $H^{\frac{1}{2}}(\Gamma_R)$. But this is a weak formulation of the following problem

$$\begin{cases} (\Delta + k^2)w = (1 + k^2)v & \text{in } \Omega \\ w = 0 & \text{on } \Gamma \\ \dfrac{\partial w}{\partial r} - M_k w = (M_k - M_i)v & \text{on } \Gamma_R. \end{cases}$$

This is a problem of the type (P_λ) studied previously with $\lambda = (M_k - M_i)v \in H^{\frac{3}{2}}(\Gamma_R)$. For this problem, Theorem 3.2.4 assures the existence of a unique solution w. In this case the homogeneous Dirichlet boundary condition implies $w \in \mathscr{V}$ so that $u := v + w \in \mathscr{V}$ is the desired function satisfying $\mathscr{A}u = v$ and surjectivity is shown.

By the preceding, $(I - \mathscr{A})u = u - v = w$ is the solution of (P_λ). Since $v \in \mathscr{V} \subset H^1(\Omega)$, we have $v|_{\Gamma_R} \in H^{\frac{3}{2}}(\Gamma_R)$ and thus

$$\|(M_k - M_i)v|_{\Gamma_R}\|_{\frac{3}{2},\Gamma_R} \leq C\|v\|_{\frac{1}{2},\Gamma_R} \leq \widetilde{C}\|v\|_{1,\Omega}\,.$$

The regularity result for w now gives

$$\|w\|_{2,\Omega} \leq \beta\left((1+k^2)\|v\|_{0,\Omega} + \tilde{C}\|v\|_{1,\Omega}\right)$$

implying $w = (\mathscr{A} - I)u \in H^2(\Omega)$.

By the estimate above, we have

$$\|(\mathscr{A} - I)u\|_{2,\Omega} = \|w\|_{2,\Omega} \leq \tilde{\beta}\|v\|_{1,\Omega}$$

which proves the last assertion. □

Since $\mathscr{A}$ is bounded and surjective and maps the closed subspace $\mathscr{V}$ of $H^1(\Omega)$ onto itself, $\mathscr{A}$ is open by the open mapping theorem and thus $\mathscr{A}^{-1}$ is bounded, which means that there exists an $\alpha > 0$ such that

$$\|\mathscr{A}u\|_{1,\Omega} \geq \alpha\|u\|_{1,\Omega} \quad \forall u \in \mathscr{V}.$$

In addition, we have

Corollary 3.2.2 $\forall u \in \mathscr{V}\ \exists v \in \mathscr{V}, v \neq 0 : a(u,v) \geq \alpha\|u\|_{1,\Omega}\|v\|_{1,\Omega}$.

Proof. Choose $v := \mathscr{A}u$. Then

$$a(u,v) = a_i(v,v) \geq \|v\|_{1,\Omega}^2 = \|v\|_{1,\Omega}\|\mathscr{A}u\|_{1,\Omega} \geq \alpha\|u\|_{1,\Omega}\|v\|_{1,\Omega}.$$

□

This corollary also implies uniqueness of the solution to the variational problem, since if $a(u_1,v) = a(u_2,v) = 0 \quad \forall v \in H^1(\Omega)$, it supplies the existence of $v_0 \neq 0$ such that $0 = a(u_1 - u_2, v_0) \geq \alpha\|u_1 - u_2\|_{1,\Omega}\,\|v_0\|_{1,\Omega} \geq 0$, implying $u_1 = u_2$.

3.3 The Discrete Variational Problem

We now consider the finite dimensional counterpart of the variational problem. To this end, we impose a triangulation on the domain Ω into triangles $\{e_j\}_{j=1}^N$ of which the longest side has length h. We define the finite dimensional subspaces $\mathscr{S}^h \subset \mathscr{S}$ and $\mathscr{V}^h \subset \mathscr{V}$ as spaces of continuous functions which are linear on each triangle e_j.

The discrete variational problem is obtained by restricting the trial and weighting functions to $\mathscr{S}^h$ and $\mathscr{V}^h$:

$$\text{(3.8)} \qquad \textit{Find } u_h \in \mathscr{S}^h \textit{ such that } \quad a(u_h, v_h) = 0 \quad \forall v_h \in \mathscr{V}^h.$$

Existence, uniqueness and the best approximation property of the discrete solution u_h of (3.8) rests on establishing the following discrete analogue of Corollary 3.2.2:

Lemma 3.3.1 *There exist $h_0 > 0$ and $\tilde{\alpha} > 0$ such that if $h \in (0, h_0]$ there exists for every $v_h \in \mathscr{V}^h$ a function $\varphi_h \in \mathscr{V}^h$ satisfying*

$$a(v_h, \varphi_h) \geq \tilde{\alpha} \|v_h\|_{1,\Omega} \, \|\varphi_h\|_{1,\Omega} \, .$$

Before proceeding with the proof of Lemma 3.3.1, we show

Lemma 3.3.2 *Given $v_h \in \mathscr{V}^h$, define $w := \mathscr{A} v_h$ and $w_h := v_h + I_h(w - v_h)$, where $I_h : \mathscr{V} \to \mathscr{V}^h$ is the interpolation operator mapping a function in $\mathscr{V}$ to its nodal interpolant in $\mathscr{V}^h$. Then*

$$\|w - w^h\|_{1,\Omega} \leq Kh \|w\|_{1,\Omega}$$

for some constant K.

Proof. We have from Theorem 3.2.5

$$\begin{aligned}
\|w - w_h\|_{1,\Omega} &= \|w - v_h - I_h(w - v_h)\|_{1,\Omega} \\
&= \|(\mathscr{A} - I)v_h - I_h((\mathscr{A} - I)v_h)\|_{1,\Omega} \\
&\leq \beta h \|(\mathscr{A} - I)v_h\|_{2,\Omega} \\
&\leq \beta C h \|v_h\|_{1,\Omega}
\end{aligned}$$

where the last inequality comes from the fact that $\mathscr{A} - I \in \mathscr{L}(\mathscr{V}, H^2(\Omega))$. Also, since $\mathscr{A}$ has a bounded inverse,

$$\|w\|_{1,\Omega} = \|\mathscr{A} v_h\|_{1,\Omega} \geq \alpha \|v^h\|_{1,\Omega}$$

so that

$$\|v_h\|_{1,\Omega} \leq \frac{1}{\alpha} \|w\|_{1,\Omega} \, .$$

Combining these two inequalities yields

$$\|w - w^h\|_{1,\Omega} \leq \frac{\beta C}{\alpha} h \|w\|_{1,\Omega}\,,$$

which is the assertion with $K = \beta C/\alpha$. $\square$

We now turn to the proof of Lemma 3.3.1.

Proof. Given $v_h \in \mathscr{V}^h$, we have already shown that, by choosing $w = \mathscr{A} v_h$, there holds

$$a(v_h, w) \geq \alpha \|v_h\|_{1,\Omega}\, \|w\|_{1,\Omega}$$

and that we can find w_h satisfying

$$\|w - w_h\|_{1,\Omega} \leq hK\|w\|_{1,\Omega}\,.$$

Thus,

$$\begin{aligned} a(v_h, w_h) &= a(v_h, w) - a(v_h, w_h - w) \\ &\geq \alpha\|v_h\|_{1,\Omega}\, \|w\|_{1,\Omega} - C_b\|v_h\|_{1,\Omega} \cdot Kh\|w\|_{1,\Omega} \\ &= (\alpha - C_b Kh)\|v_h\|_{1,\Omega}\, \|w\|_{1,\Omega}\,. \end{aligned}$$

Also, from

$$\|w\|_{1,\Omega} = \|w_h - (w_h - w)\|_{1,\Omega} \geq \|w_h\|_{1,\Omega} - hK\|w\|_{1,\Omega}$$

we obtain

$$\|w\|_{1,\Omega} \geq \frac{1}{1 + hK}\|w_h\|_{1,\Omega}\,.$$

Thus,

$$a(v_h, w_h) \geq \frac{\alpha - C_b hK}{1 + hK}\|v_h\|_{1,\Omega}\, \|w_h\|_{1,\Omega}$$

This proves the assertion with $\tilde{\alpha} = (\alpha - C_b hK)/(1 + hK)$ which is positive for h sufficiently small. $\square$

Lemma 3.3.1 yields uniqueness of the discrete solution in the same manner as in the continuous case. This also implies existence, since we are now dealing with finite dimensional spaces. The best approximation property can now be established as follows. Let $u_h \in \mathscr{S}^h$ be a solution of the discrete problem. This implies

$$a(u_h - u, \varphi_h) = 0 \quad \forall \varphi_h \in \mathscr{V}^h.$$

For arbitrary $w_h \in \mathscr{S}^h$, we then have

$$a(u_h - w_h, \varphi_h) = a(u_h - u, \varphi_h) + a(u - w_h, \varphi_h) \leq 0 + C_b \|u - w_h\|_{1,\Omega} \, \|\varphi_h\|_{1,\Omega} \, .$$

Also, to $u_h - w_h \in \mathscr{V}^h$, there exists $v_h \in \mathscr{V}^h$ with

$$a(u_h - w_h, v_h) \geq \tilde{\alpha} \|u_h - w_h\|_{1,\Omega} \, \|v_h\|_{1,\Omega} \, .$$

Thus,

$$\begin{aligned} \|u - u_h\|_{1,\Omega} &= \|u - w_h\|_{1,\Omega} + \|w_h - u_h\|_{1,\Omega} \\ &\leq \|u - w_h\|_{1,\Omega} + \frac{a(u_h - w_h, v_h)}{\tilde{\alpha}\|v_h\|_{1,\Omega}} \\ &\leq \|u - w_h\|_{1,\Omega} + \frac{C_b}{\tilde{\alpha}} \|u - w_h\|_{1,\Omega} \\ &\leq (1 + \frac{C_b}{\tilde{\alpha}}) \|u - w_h\|_{1,\Omega} \, . \end{aligned}$$

Since w_h was arbitrary in $\mathscr{S}^h$, this implies

$$\|u - u_h\|_{1,\Omega} \leq \left(1 + \frac{C_b}{\tilde{\alpha}}\right) \inf_{w_h \in \mathscr{S}^h} \|u - w_h\|_{1,\Omega} \, .$$

Together with the interpolation estimate, this means that our finite element approximation converges with order h in the $H^1(\Omega)$-norm.

3.4 Finite Element Discretizations of the Annulus

In this section, we introduce simple finite-element spaces on an annulus in polar coordinates, i.e. our trial and test functions will be piecewise polynomials in the r and ϑ variables. We give the local and global mass and stiffness matrices for bilinear rectangles below, linear triangles are treated in the appendix.

3.4.1 Bilinear Rectangles

We impose a uniform rectangular grid on the the rectangle $[R_0, R] \times [0, 2\pi)$ in the $r - \vartheta$ plane consisting of rectangles of width Δr and height $\Delta\vartheta$ and sides parallel to the coordinate axes. The four Lagrangian nodal basis functions on the rectangle with corners (r_i, ϑ_j), (r_{i+1}, ϑ_j), $(r_{+1}i, \vartheta_{j+1})$ and (r_i, ϑ_{j+1}) are then given by

$$\varphi_1(r, \vartheta) = \left(1 - \frac{r - r_i}{\Delta r}\right)\left(1 - \frac{\vartheta - \vartheta_j}{\Delta\vartheta}\right) \tag{3.9}$$

$$\varphi_2(r, \vartheta) = \frac{r - r_i}{\Delta r}\left(1 - \frac{\vartheta - \vartheta_j}{\Delta\vartheta}\right) \tag{3.10}$$

$$\varphi_3(r, \vartheta) = \frac{r - r_i}{\Delta r}\frac{\vartheta - \vartheta_j}{\Delta\vartheta} \tag{3.11}$$

$$\varphi_4(r, \vartheta) = \left(1 - \frac{r - r_i}{\Delta r}\right)\frac{\vartheta - \vartheta_j}{\Delta\vartheta}. \tag{3.12}$$

Figure 3.2 shows a typical interior node in the mesh and the four elements to which it belongs.

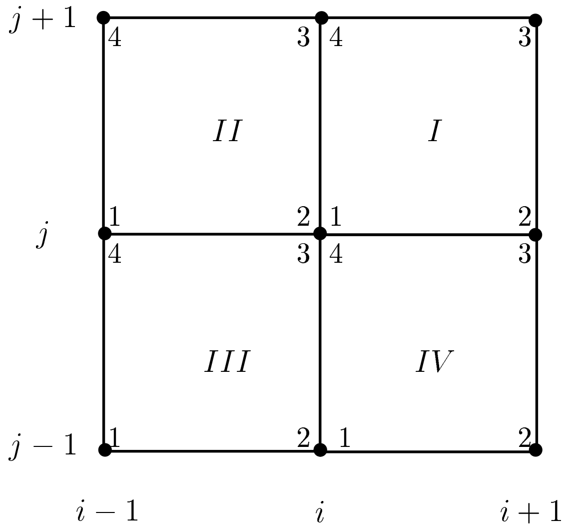

Figure 3.2: Node i, j in the rectangular grid and its neighboring elements along with the local node numbering in each element.

The element stiffness matrices K^e of the inner products

$$\int_{\Omega^e} \nabla\varphi_i \cdot \nabla\varphi_j \; dxdy = \int_{\Omega^e} \left((\varphi_i)_r(\varphi_j)_r + \frac{1}{r^2}(\varphi_i)_\vartheta(\varphi_j)_\vartheta \right) r dr d\vartheta \quad i,j = 1,2,3,4$$

for a rectangular element Ω^e are given by

$$K^e = \frac{\Delta\vartheta}{6\Delta r} r_{i+1/2} \begin{pmatrix} 2 & -2 & -1 & 1 \\ * & 2 & 1 & -1 \\ * & * & 2 & -2 \\ * & * & * & 2 \end{pmatrix} + \frac{\log \frac{r_{i+1}}{r_i}}{\Delta r^2 \Delta\vartheta} \begin{pmatrix} r_{i+1}^2 & -r_i r_{i+1} & r_i r_{i+1} & -r_{i+1}^2 \\ * & r_i^2 & -r_i^2 & r_i r_{i+1} \\ * & * & r_i^2 & -r_i r_{i+1} \\ * & * & * & r_{i+1}^2 \end{pmatrix}$$
$$+ \frac{1}{2\Delta r \Delta\vartheta} \begin{pmatrix} r_i - 3r_{i+1} & r_i + r_{i+1} & -r_i - r_{i+1} & -r_i + 3r_{i+1} \\ * & -3r_i + r_{i+1} & 3r_i - r_{i+1} & -r_i - r_{i+1} \\ * & * & -3r_i + r_{i+1} & r_i + r_{i+1} \\ * & * & * & r_i - 3r_{i+1} \end{pmatrix}.$$

The corresponding element mass matrices M^e of the inner products

$$\int_{\Omega^e} \varphi_i\varphi_j \; dxdy = \int_{\Omega^e} \varphi_i\varphi_j \; r dr d\vartheta \quad i,j = 1,2,3,4$$

are given by

$$M^e = \frac{\Delta r \Delta\vartheta}{72} \begin{pmatrix} 8r_i + 2\Delta r & 4r_{i+1} - 2\Delta r & 2r_{i+1} - \Delta r & 4r_i + \Delta r \\ * & 8r_{i+1} - 2\Delta r & 4r_{i+1} - \Delta r & 2r_{i+1} - \Delta r \\ * & * & 8r_{i+1} - 2\Delta r & 4r_{i+1} - 2\Delta r \\ * & * & * & 8r_i + 2\Delta r \end{pmatrix}$$

After assembly, the global stiffness matrix K for bilinear rectangles is given by

$$K = \frac{1}{\Delta\vartheta} T_1 \otimes C_1 + \frac{\Delta\vartheta}{6} T_2 \otimes C_2$$

with $n \times n$ circulant matrices

$$C_1 = \begin{bmatrix} 2 & -1 & & & -1 \\ -1 & 2 & -1 & & \\ & \ddots & \ddots & \ddots & \\ & & -1 & 2 & -1 \\ -1 & & & -1 & 2 \end{bmatrix} \text{ and } C_2 = \begin{bmatrix} 4 & 1 & & & 1 \\ 1 & 4 & 1 & & \\ & \ddots & \ddots & \ddots & \\ & & 1 & 4 & 1 \\ 1 & & & 1 & 4 \end{bmatrix}$$

and tridiagonal $m \times m$ matrices

$$T_1 = \text{ tridiag}(\nu_{i-1/2}, \mu_i, \nu_{i+1/2}), \qquad i = 1, \ldots, m$$

with

$$\nu_i = \frac{r_i}{\Delta r} - \frac{r_{i-1/2} r_{i+1/2}}{\Delta r} \log \frac{r_{i+1/2}}{r_{i-1/2}}$$
$$\mu_i = -\frac{2r_i}{\Delta r} + \frac{r_{i+1}^2}{\Delta r^2} \log \frac{r_{i+1}}{r_i} + \frac{r_{i-1}^2}{\Delta r^2} \log \frac{r_i}{r_{i-1}}$$

and

$$T_2 = \text{ tridiag}(\frac{-r_{i-1/2}}{\Delta r}, \frac{2r_i}{\Delta r}, \frac{-r_{i+1/2}}{\Delta r}), \qquad i = 1, \ldots, m.$$

The global mass matrix M is given by

$$M = \frac{\Delta r \Delta \vartheta}{36} T_3 \otimes C_2$$

with

$$T_3 = \text{ tridiag}(r_{i-1/2}, 4r_i, r_{i+1/2}) \qquad i = 1, \ldots, m.$$

The matrices above correspond to Dirichlet boundary data imposed at r_0 and r_{m+1}. Imposing a Neumann condition at the outer boundary $r = r_m$ results in modification of the m-th diagonal blocks in K and M due to a change in the (m, m) element of the tridiagonal matrices T_1,T_2 and T_3 as follows:

$$T_1 : \mu_m \to \frac{r_{m-1}^2}{\Delta r^2} \log \frac{r_m}{r_{m-1}} - \frac{r_{m-3/2}}{\Delta r}$$
$$T_2 : \frac{2r_m}{\Delta r} \to \frac{r_{m-1/2}}{\Delta r}$$
$$T_3 : 4r_m \to 2r_m - \frac{\Delta r}{2}$$

A similar adjustment occurs in the case of a Neumann boundary condition at $r = r_1$.

3.4.2 The Discrete DtN Operator

The Dirichlet to Neumann (DtN) map for the Helmholtz operator on a circle of radius R centered at the origin is given by

$$u(R, \vartheta) \mapsto u_r(R, \vartheta) =: (M_k u)(R, \vartheta)$$

where

$$(M_k g)(\vartheta) = \frac{k}{\pi} {\sum_{\nu=0}^{\infty}}' \frac{H_\nu^{(1)'}(kr)}{H_\nu^{(1)}(kR)} \int_0^{2\pi} g(\vartheta') \cos\nu(\vartheta - \vartheta')\, d\vartheta'$$

For any $g \in L^2(0, 2\pi)$. Here, $H_\nu^{(1)}$ is the first-kind Hankel function of order ν and the prime after the summation symbol indicates that the first term is halved. The contribution of the DtN boundary condition to the bilinear form of the variational formulation is thus

$$\begin{aligned}\langle M_k u, v\rangle_{\Gamma_R} &= \int_0^{2\pi} v(R,\vartheta)(Mu(R,\vartheta)Rd\vartheta \\ &= \frac{kR}{\pi} {\sum_{\nu=0}^{\infty}}' a_\nu \int_0^{2\pi}\int_0^{2\pi} v(R,\vartheta)u(R,\vartheta')\cos(\nu(\vartheta-\vartheta'))d\vartheta' d\vartheta\end{aligned}$$

where we have set $a_\nu := H_\nu^{(1)'}(kR)/H_\nu^{(1)}(kR)$. Only those nodal basis functions whose node lies on the exterior boundary will contribute to the DtN term. If those nodes are ordered last, the DtN term will result in a dense $n \times n$ block being added to the (m, m) block of the discretization matrix. If we denote by $\varphi_{i,j}$ the nodal basis function belonging to the node (r_i, ϑ_j), then the (p, q) entry in this block matrix is given by

$$\begin{aligned}\langle M\varphi_{m,p}, \varphi_{m,q}\rangle_{\Gamma_R} &= \frac{kR}{\pi} {\sum_{\nu=0}^{\infty}}' a_\nu \int_{\vartheta_{p-1}}^{\vartheta_{p+1}}\int_{\vartheta_{q-1}}^{\vartheta_{q+1}} \varphi_{p,m}(R,\vartheta)\varphi_{m,q}(R,\vartheta')\cos(\nu(\vartheta-\vartheta'))d\vartheta' d\vartheta \\ &= \frac{kR}{\pi} {\sum_{\nu=0}^{\infty}}' a_\nu \frac{4(1-\cos\nu\Delta\vartheta)^2}{\Delta\vartheta^2\nu^4}\cos(\nu(\vartheta_p - \vartheta_q)).\end{aligned}$$

For $\nu = 0$, the expression in the summation symbol is obtained by taking the limit as $\nu \to 0$ which is $a_0\Delta\vartheta^2$.

3.5 A Domain Imbedding Method

Our approach is based on the work of Max Dryja and Olof Widlund in the context of interior boundary value problems for self-adjoint positive operators. We first indicate how their 'Dirichlet-Neumann algorithm', which was developed by Bjørstadt and Widlund in [109, 11, 12], can be used to obtain an imbedding algorithm for the model problem on the disk and then generalize the idea to general domains.

3.5.1 The Dirichlet Neumann Algorithm for the Model Problem

We consider the exterior Helmholtz problem for a disk of radius a about the origin. We introduce an artificial boundary Γ_R at $r = R$ resulting in the computational domain $\{a < r < R\}$. We imbed this domain in the larger annulus $\{R_0 < r < R\}$ with some $0 < R_0 < a$ and wish to relate how an algorithm for solving the exterior problem on the larger domain can be used to recover the solution of the problem on the smaller domain. To this end, we define

$$\Omega := \{(r, \vartheta) : R_0 < r < R\}$$

$$\Omega_1 := \{(r, \vartheta) : R_0 < r < a\}$$

$$\Omega_2 := \{(r, \vartheta) : a < r < R\}$$

and the interface $\Gamma = \{(r, \vartheta) : r = a\}$, so that $\Omega = \Omega_1 \cup \Gamma \cup \Omega_2$. As Ω is a rectangle in the r, ϑ plane, we can introduce a grid

$$\mathcal{G} = \mathcal{G}_{m,n} = \{(r_i, \vartheta_j) : 0 \leq i \leq m, \quad 0 \leq j \leq n-1\},$$

where $r_i = R_0 + i\Delta r, \vartheta_j = j\Delta\vartheta$ and $\Delta r = (R - R_0)/m, \Delta\vartheta = 2\pi/n$. By adjusting the inner radius R_0, we can arrange for Γ to coincide with a grid line (circle) $i = m_\Gamma$. This arrangement is depicted in Figure 3.3. The two bilinear forms

$$\begin{aligned} a_1(u, v) &= \int_{\Omega_1} (u_r v_r + \frac{u_\vartheta v_\vartheta}{r^2} - k^2 uv)\, r dr d\vartheta \\ a_2(u, v) &= \int_{\Omega_2} (u_r v_r + \frac{u_\vartheta v_\vartheta}{r^2} - k^2 uv)\, r dr d\vartheta - \int_{\Gamma_R} v M_k u \, ds \end{aligned}$$

on appropriate function spaces correspond to the variational form of the following two boundary value problems:

$$(P_1) \begin{cases} \Delta u_1 + k^2 u_1 = 0 \text{ on } \Omega_1 \\ u_1 = 0 \text{ at } r = R_0 \\ \dfrac{\partial u_1}{\partial n} = 0 \text{ on } \Gamma \end{cases} \tag{3.13}$$

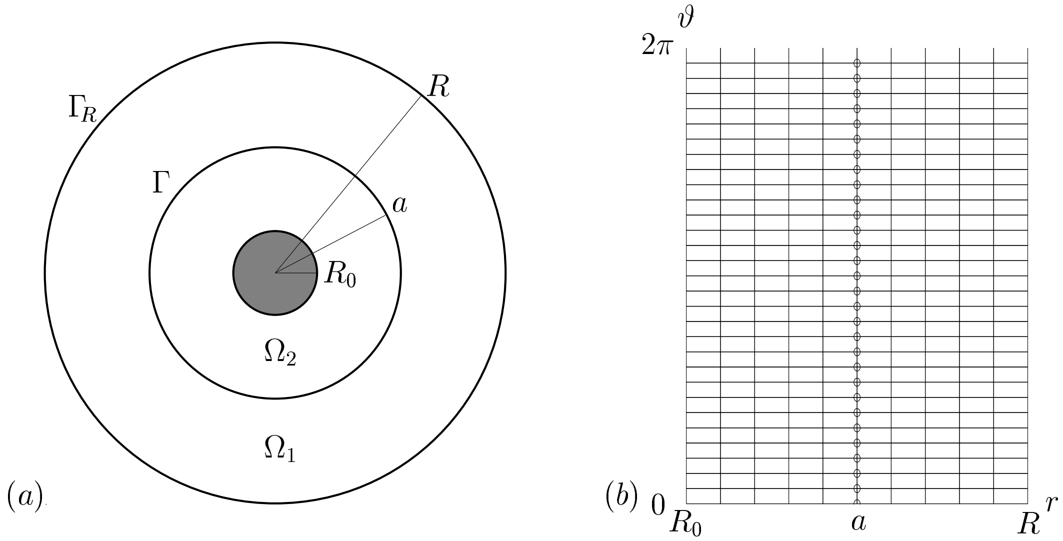

Figure 3.3: (a) the annulus Ω_1 imbedded into the larger annulus $\Omega = \Omega_1 \cup \Gamma \cup \Omega_2$ (b) the corresponding uniform finite element mesh in the r,ϑ plane

$$(P_2) \begin{cases} \Delta u_2 + k^2 u_2 = 0 \text{ on } \Omega_2 \\ u_2 = g \text{ on } \Gamma \\ \dfrac{\partial u_2}{\partial r} - M_k u_2 = 0 \text{ on } \Gamma_R. \end{cases} \tag{3.14}$$

The sum $a(\cdot,\cdot) := a_1(\cdot,\cdot) + a_2(\cdot,\cdot)$ then corresponds to the problem on the large domain Ω:

$$(P) \begin{cases} \Delta u + k^2 u = 0 \text{ on } \Omega \\ u = 0 \text{ at } r = R_0 \\ \dfrac{\partial u}{\partial n} - M_k u = 0 \text{ on } \Gamma_R. \end{cases} \tag{3.15}$$

We discretize problem (P) using bilinear quadrilateral elements and obtain the discretization matrix in the block form

$$B = \begin{bmatrix} A_{11} & 0 & A_{13} \\ 0 & A_{22} & A_{23} \\ A_{13}^T & A_{23}^T & A_{33} \end{bmatrix}. \tag{3.16}$$

with respect to the usual Lagrangian nodal basis. The partition is such that unknowns corresponding to nodes lying in Ω_1, Ω_2 and Γ have been grouped together into the first, second and third block vectors. We also define the matrices $A_{33}^{(1)}$ and $A_{33}^{(2)}$ as those contributions of A_{33} coming only from elements on the interior and exterior of Γ, respectively, so that $A_{33} = A_{33}^{(1)} + A_{33}^{(2)}$. In terms of these matrices, we can write the discretization of problems (P_1) and (P_2) as

$$\begin{bmatrix} A_{11} & A_{13} \\ A_{13}^T & A_{33}^{(1)} \end{bmatrix} \begin{bmatrix} \mathbf{u}_1 \\ \mathbf{u}_3 \end{bmatrix} = \begin{bmatrix} 0 \\ \mathbf{h} \end{bmatrix} \quad \text{and} \quad \begin{bmatrix} A_{22} & A_{23} \\ 0 & I \end{bmatrix} \begin{bmatrix} \mathbf{u}_2 \\ \mathbf{u}_3 \end{bmatrix} = \begin{bmatrix} 0 \\ \mathbf{g} \end{bmatrix},$$

where the vectors $\mathbf{g}, \mathbf{h} \in \mathbb{C}^n$ contain the Dirichlet- and Neumann data prescribed on Γ in each case. We also note that we can recover the discrete solution of (P_2) from the solution of the combined problem

$$Au := \begin{bmatrix} A_{11} & 0 & A_{13} \\ 0 & A_{22} & A_{23} \\ A_{13}^T & 0 & A_{33}^{(1)} \end{bmatrix} \begin{bmatrix} \mathbf{u}_1 \\ \mathbf{u}_2 \\ \mathbf{u}_3 \end{bmatrix} = \begin{bmatrix} 0 \\ -A_{23}\mathbf{g} \\ 0 \end{bmatrix} =: \mathbf{f} \tag{3.17}$$

as long as the matrix

$$\begin{bmatrix} A_{11} & A_{13} \\ A_{13}^T & A_{33}^{(1)} \end{bmatrix}$$

is non-singular, which is the case for a sufficiently fine mesh when k^2 is not an eigenvalue of the Laplacian on Ω_1 with Dirichlet data on the inner circle and Neumann data on Γ.

Following the approach introduced by Dryja, we seek the solution of (3.17) in the form $\mathbf{u} = B^{-1}\mathbf{f} + B^{-1}E\mathbf{w}$ where the vector $\mathbf{w} \in \mathbb{C}^n$ is a grid function on Γ^h and $E = [0\ 0\ I_n]^T \in \mathbb{C}^{nm \times n}$ is the discrete extension operator mapping grid functions defined on Γ_h to grid functions defined on the whole grid Ω^h vanishing outside of Γ^h. This is a solution of (3.17) provided that

$$\begin{aligned} 0 = A\mathbf{u} - \mathbf{f} &= A(B^{-1}\mathbf{f} + B^{-1}E\mathbf{w}) - \mathbf{f} \\ &= (B + A - B)B^{-1}\mathbf{f} + AB^{-1}E\mathbf{w} - \mathbf{f} \\ &= AB^{-1}E\mathbf{w} + (A - B)B^{-1}\mathbf{f}, \end{aligned}$$

i.e. if

$$AB^{-1}E\mathbf{w} = -(A-B)B^{-1}\mathbf{f} \tag{3.18}$$

holds. Since the matrices A and B agree in the first two block rows, the matrix AB^{-1} has the structure

$$AB^{-1} = \begin{bmatrix} I & 0 & 0 \\ 0 & I & 0 \\ * & * & * \end{bmatrix} \tag{3.19}$$

so that the first two blocks of (3.18) are zero. We therefore obtain an equivalent system by multiplying both sides by E^T yielding

$$C\mathbf{w} := E^T AB^{-1}E\mathbf{w} = -E^T(A-B)B^{-1}\mathbf{f}. \tag{3.20}$$

The matrix C is the capacitance matrix and we will refer to (3.20) as the capacitance matrix equation. Rather than solve the (dense) system (3.20) directly, we will employ an iterative method. The most powerful and versatile iterative linear system solvers are the family of algorithms known as *Krylov subspace methods*, of which the most well known is the Conjugate Gradients method. At the n-th step of the iteration, $n = 1, 2, \dots,$ these methods choose an approximation to the solution of the linear system with coefficient matrix C from the Krylov space

$$K_n(\mathbf{x}_0, C) := \operatorname{span}\{\mathbf{x}_0, C\mathbf{x}_0, \dots, C^{n-1}\mathbf{x}_0\}$$

where $\mathbf{x}_0$ is an initial guess. Since the capacitance matrix C is non-Hermitian, we shall use the QMR algorithm of Freund and Nachtigal [41, 42], a very robust and efficient generalization of the CG algorithm to non-Hermitian systems which possesses many desirable mathematical properties.

In terms of computation, Krylov subspace methods require the coefficient matrix only in order to form a matrix-vector product at every step of the iteration. In case of the QMR algorithm in the implementation we use, a product with the transpose of the coefficient matrix is also necessary. Multiplication of a vector $\mathbf{w} \in \mathbb{C}^n$ by C consists of multiplying the vector $E\mathbf{w}$ by B^{-1}, an operation which can be performed by the fast Helmholtz solver, followed by multiplication with the (sparse) matrix A and, finally, multiplication of the result by the restriction matrix E^T. Due to the efficiency of the fast solver, these matrix-vector products are inexpensive to compute. Multiplication with C^T is also inexpensive, since the matrix B is (complex) symmetric and thus the fast solver can be used here as well. Multiplication with E and E^T are simply indexing operations. We also note that, even though the matrix A contains the dense $n \times n$ block due to the DtN boundary condition, multiplication by this block can be achieved efficiently using the FFT.

The convergence rate of Krylov subspace methods is governed among other things by the degree to which the spectrum of the coefficient matrix is clustered around a non-zero point in the complex plane. In the following, we will show that the spectrum of C exhibits such a clustering by showing that it is the discretization of an operator with a clustered spectrum.

To this end, we introduce the matrices

$$Q = A_{33} - A_{13}^T A_{11}^{-1} A_{13} - A_{23}^T A_{22}^{-1} A_{23} \tag{3.21}$$

$$Q^{(1)} = A_{33}^{(1)} - A_{13}^T A_{11}^{-1} A_{13} \tag{3.22}$$

$$Q^{(2)} = A_{33}^{(2)} - A_{23}^T A_{22}^{-1} A_{23} \tag{3.23}$$

which are the Schur complements of the matrix A and the two matrices

$$\begin{bmatrix} A_{11} & A_{13} \\ A_{13}^T & A_{33}^{(1)} \end{bmatrix} \text{ and } \begin{bmatrix} A_{22} & A_{23} \\ A_{23}^T & A_{33}^{(2)} \end{bmatrix},$$

respectively, with regard to the unknowns on Γ^h. We note that $Q = Q^{(1)} + Q^{(2)}$. One easily verifies the following relation:

$$\begin{bmatrix} A_{11} & A_{13} \\ A_{13}^T & A_{33}^{(1)} \end{bmatrix} \begin{bmatrix} A_{11} & A_{13} \\ 0 & I \end{bmatrix}^{-1} \begin{bmatrix} 0 \\ \mathbf{g} \end{bmatrix} = \begin{bmatrix} 0 \\ Q^{(1)}\mathbf{g} \end{bmatrix}. \tag{3.24}$$

The matrix on the left is the discrete analog of the operator belonging to the interior problem with a Neumann condition on Γ. The second matrix in (3.24) is the inverse of the discretization matrix of the same problem with Dirichlet data imposed on Γ. Thus, equation (3.24) states that the matrix $Q^{(1)}$ maps the Dirichlet data $\mathbf{g}$ into the

Neumann data $Q^{(1)}\mathbf{g}$ for the interior problem. The corresponding relation for $Q^{(2)}$ and the exterior problem is

$$\begin{bmatrix} A_{22} & A_{23} \\ A_{23}^T & A_{33}^{(2)} \end{bmatrix} \begin{bmatrix} A_{22} & A_{23} \\ 0 & I \end{bmatrix}^{-1} \begin{bmatrix} 0 \\ \mathbf{g} \end{bmatrix} = \begin{bmatrix} 0 \\ Q^{(2)}\mathbf{g} \end{bmatrix}. \tag{3.25}$$

In this case, however, the Neumann data is given by $-Q^{(2)}\mathbf{g}$ since the normal vector then points in the opposite direction . We now relate the matrices $Q^{(1)}$ and $Q^{(2)}$ to the capacitance matrix C.

Lemma 3.5.1 *The capacitance matrix $C = E^T AB^{-1}E$ has the representation*

$$C = Q^{(1)}Q^{-1} = (I + Q^{(2)}(Q^{(1)})^{-1})^{-1}.$$

Proof. If $\mathbf{w} \in \mathbb{C}^n$ is an arbitrary vector, then $E\mathbf{w} = [0\ 0\ \mathbf{w}]^T \in \mathbb{C}^{mn}$. Letting $\mathbf{x} := B^{-1}E\mathbf{w}$ for $\mathbf{x} = [\mathbf{x}_1\ \mathbf{x}_2\ \mathbf{x}_3]^T$ gives $B\mathbf{x} = E\mathbf{w}$ which, written out, yields the block equations

$$\begin{aligned} A_{11}\mathbf{x}_1 \qquad\quad + A_{13}\mathbf{x}_3 &= 0 \\ A_{22}\mathbf{x}_2 + A_{23}\mathbf{x}_3 &= 0 \\ A_{13}^T\mathbf{x}_1 + A_{23}^T\mathbf{x}_2 + A_{33}\mathbf{x}_3 &= \mathbf{w}. \end{aligned} \tag{3.26}$$

Since the diagonal blocks are non-singular, we obtain by block elimination $Q\mathbf{x}_3 = \mathbf{w}$ as well as $\mathbf{x}_2 = -A_{22}^{-1}A_{23}\mathbf{x}_3$ and hence

$$AB^{-1}E\mathbf{w} = A\mathbf{x} = \begin{bmatrix} A_{11} & 0 & A_{13} \\ 0 & A_{22} & A_{23} \\ A_{13}^T & 0 & A_{33}^{(1)} \end{bmatrix} \begin{bmatrix} \mathbf{x}_1 \\ \mathbf{x}_2 \\ \mathbf{x}_3 \end{bmatrix} = \begin{bmatrix} A_{11}\mathbf{x}_1 + A_{13}\mathbf{x}_3 \\ A_{22}\mathbf{x}_2 + A_{23}\mathbf{x}_3 \\ A_{13}^T\mathbf{x}_1 + A_{33}^{(1)}\mathbf{x}_3 \end{bmatrix}.$$

The first two blocks vanish by (3.19) and for the third block we obtain

$$\begin{aligned} A_{13}^T\mathbf{x}_1 + A_{33}^{(1)}\mathbf{x}_3 &= A_{13}^T\mathbf{x}_1 + A_{23}^T\mathbf{x}_2 + A_{33}\mathbf{x}_3 - A_{23}^T\mathbf{x}_2 - A_{33}^{(2)}\mathbf{x}_3 \\ &= \mathbf{w} - A_{33}^{(2)}\mathbf{x}_3 - A_{23}^T(-A_{22}^{-1}A_{23}\mathbf{x}_3) \\ &= \mathbf{w} - Q^{(2)}\mathbf{x}_3 \\ &= \mathbf{w} - Q^{(2)}Q^{-1}\mathbf{w} \\ &= (I - Q^{(2)}Q^{-1})\mathbf{w} = Q^{(1)}Q^{-1}\mathbf{w}. \end{aligned}$$

The last identity follows by factoring out Q^{-1} and using $Q = Q^{(1)} + Q^{(2)}$. $\square$

The continuous counterparts of the operators $Q^{(1)}$ and $Q^{(2)}$ turn out to be the Dirichlet-to-Neumann (DtN) maps associated with the problems (P_1) and (P_2). We can obtain a representation for these maps with the help of the classical integral operators S, K, K^* and T from the method of integral equations cf. Section 1.2.2 for solving the Helmholtz equation.

For simplicity we set the internal radius R_0 of the imbedding annulus to zero, so that the domain Ω_1 becomes the disk of radius a about the origin. When $R_0 > 0$, as it will be for or numerical computations which make use of the fast Helmholtz solver on an annulus, the function Φ in kernels of the integral operators is replaced by the modified Green's function $\widehat{\Phi}$ introduced in Section 1.2.3. As shown there, the exterior boundary value problems with respect to Γ are uniquely solvable in terms of layer potentials resulting from the modified kernels. The modified operators also remain compact.

The solution of the interior Dirichlet problem with data g on Γ can be obtained as the double-layer potential

$$u_1(x) = (\widetilde{K}\varphi)(x) = \int_\Gamma \frac{\partial \Phi(x,y)}{\partial n(y)} \varphi(y)\, ds_y, \quad x \in \Omega_1$$

provided the density φ satisfies the integral equation $(I - K)\varphi = -2g$ on Γ. We also assume for the following that k^2 is not an eigenvalue of the Laplacian for either the interior Dirichlet or Neumann problems. The interior DtN map is obtained by computing the normal derivative of u_1 on Γ, which gives

$$\frac{\partial u_1}{\partial n} = \frac{1}{2}(T\varphi)(x) = -T(I-K)^{-1} g,$$

i.e. the interior DtN map, which we denote by $Q^{(-)}$, has the representation $Q^{(-)} = -T(I-K)^{-1}$. Another representation of the interior DtN map is obtained by evaluating the solution of the interior Neumann problem on Γ. The interior Neumann problem can be found as the single layer potential

$$v_1(x) = (\widetilde{S}\psi)(x) = \int_\Gamma \Phi(x,y)\psi(y)\, ds_y, \quad x \in \Gamma$$

subject to $(I + K^*)\psi = 2h$ on Γ. Thus, we have on Γ

$$v_1(x) = \int_\Gamma \Phi(x,y)\psi(y) ds_y = \frac{1}{2} S\psi(x) = S(I+K^*)^{-1} h.$$

Thus, inverting gives $Q^{(-)} = (I + K^*)S^{-1}$.

Two further representations of the interior DtN map are obtained using the representation theorem 1.2.3 for solutions u of the interior Dirichlet and Neumann problems on Ω_1, which states that

$$\int_\Gamma \left\{ u(y)\frac{\partial\Phi(x,y)}{\partial n(y)} - \frac{\partial u}{\partial n(y)}\Phi(x,y) \right\} \, ds_y = \begin{cases} -u(x) & x \in \Omega_1 \\ 0 & x \in \mathbb{R}^2 \backslash \overline{\Omega}_1 \end{cases}$$

Taking the limits of the values and normal derivative of this identity on Γ and using the jump relations leads to two more integral equations on Γ for the value and normal derivative of the solution:

$$(-I + K)u - S\frac{\partial u}{\partial n} = -2u \tag{3.27}$$

$$Tu - (I + K^*)\frac{\partial u}{\partial n} = -2\frac{\partial u}{\partial n}. \tag{3.28}$$

Solving each of these for the normal derivative gives

$$Q^- = S^{-1}(I - K) = (-I + K^*)T.$$

In a completely analogous way, one finds the corresponding four representations of the *exterior* DtN mapping Q^+ to be

$$Q^+ = (K^* - I)S^{-1} = T(K + I)^{-1} = S^{-1}(K - I) = (K^* + I)^{-1}T.$$

In summary, $Q^{(1)}$ is the discrete analog of Q^- and $Q^{(2)}$ that of $-Q^+$. We now choose two convenient representations for the interior and exterior DtN mappings out of the four previously derived:

$$Q^+ = (-I + K^*)S^{-1}, \qquad Q^- = (I + K^*)S^{-1},$$

yielding a continuous analog of $C = (I + Q^{(2)}(Q^{(1)})^{-1})^{-1}$ to be

$$\begin{aligned} (I - Q^+(Q^-)^{-1})^{-1} &= \left[I - (-I + K^*)(I + K^*)^{-1}\right]^{-1} \\ &= \left[(I + K^* + I - K^*)(I + K^*)^{-1}\right]^{-1} \\ &= \frac{1}{2}(I + K^*). \end{aligned}$$

The operator K^* is compact for smooth curves and data and hence its spectrum is clustered about the origin. Therefore, that of $\frac{1}{2}(I + K^*)$ will lie clustered about $\frac{1}{2}$ in the complex pane. Since C is a discrete analog of this operator, we expect its eigenvalues to approach this distribution as the discretization is refined. This indicates that Krylov subspace methods will converge quickly when used to solve the capacitance matrix equation.

We have carried out some numerical calculations which seem to verify these considerations.

3.5.2 The Inexact Dirichlet-Neumann Algorithm for General Domains

For a non-circular obstacle, we select an annulus $\{R_0 < r < R\}$ which contains the boundary curve Γ of the problem domain and impose a uniform rectangular grid on this annulus in the r, ϑ plane. We choose the inner radius R_0 to be positive since we then need not discretize the origin, resulting in a faster fast Helmholtz solver than had we discretized the whole disk $\{r < R\}$. Next, we modify the rectangular grid locally near Γ so that vertices in the vicinity of the Γ are moved onto Γ. The rectangles containing moved vertices are then split into two triangles along the shorter diagonal. This results in a mesh consisting mostly of uniform rectangles and a few triangles in the vicinity of Γ. Also, since nodes were only moved, there remains a one to one correspondence between the nodes of the original, uniform mesh and those of the modified mesh.

The algorithm we use to generate the locally fitted mesh from the initial uniform mesh is due to Bespalov et al. [10] and proceeds as follows :

Algorithm 3.5.1 *1. Trace the boundary curve Γ and successively collect each edge and node crossed by Γ in an edge/node list.*

2. Traverse the edge/node list and select from it a sequence of boundary nodes to be modified later. If we assume that the j-th edge/node of the list has been processed, we consider the $j+1$-st edge/node. If this is a node, then it is

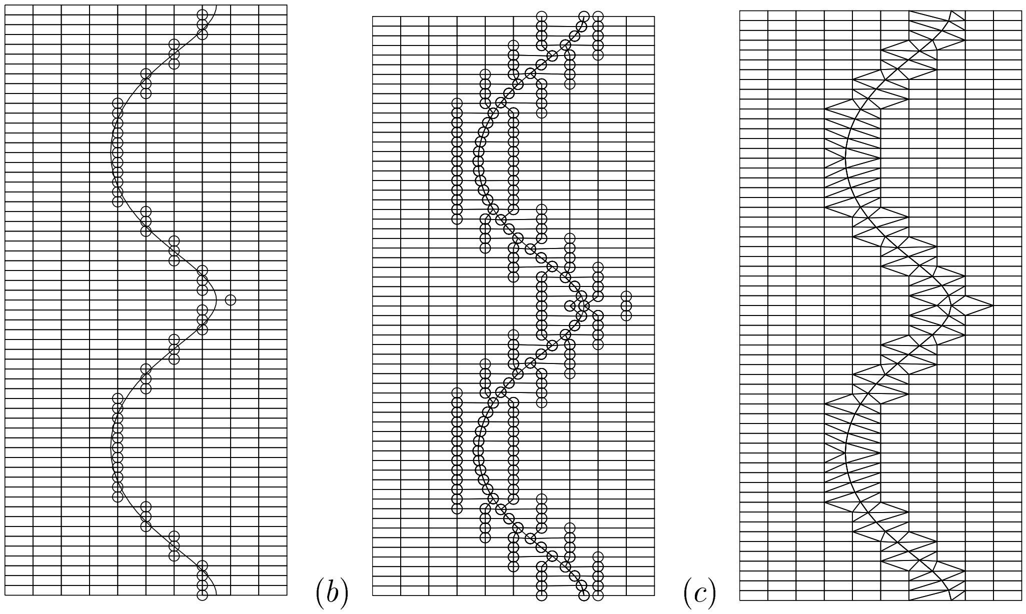

(a) (b) (c)

Figure 3.4: The grid modification algorithm in the r,ϑ plane for an ellipse: (a) : identification of the nodes to be moved (b) : the grid with the moved boundary nodes and the nodes whose equations are affected by the grid modification (c) : the modified grid.

inserted into the sequence of boundary nodes unless it has already been inserted previously. In case of an edge, then whichever of its two end points is closer to Γ and is not already contained in the sequence is inserted unless either of its two endpoints are equal to the last inserted node. In that case no nodes are inserted for this edge.

3. *Traverse the sequence of boundary nodes and move each one to the closest point on Γ. The sequence of moved points now approximates the discrete boundary Γ^h.*

4. *Split each rectangle of the uniform mesh of which at least one node has moved into two triangles. If one of the diagonals of the modified rectangle belongs to the boundary Γ^h, then we divide along this diagonal, otherwise along the shorter diagonal.*

The various stages of the algorithm for the case of an ellipse are depicted in Figure 3.4. The curve winding through the grid is the boundary of the ellipse in polar coordinates. Figure 3.5 shows the resulting modified grid in the x,y plane.

When we split the unknowns into exterior, interior and boundary unknowns as in the case of the two annuli, then the resulting matrices A and B still have the same block structure as in (3.16) and (3.17), but now the matrix B is the discrete operator belonging to the annulus based on the modified mesh and hence systems with coefficient matrix B can no longer be solved with the fast Helmholtz solver. If we compare the matrix B with the matrix $\tilde{B}$ belonging to the regular mesh, however, we note that B and $\tilde{B}$ differ only in a few rows. More precisely, let us denote by $\mathcal{G}_1$ the set of interior nodes contained only in rectangles which were unaffected by the grid modification and by $\mathcal{G}_{1'}$ the remaining interior nodes. Similarly, we partition the exterior nodes into $\mathcal{G}_2$ and $\mathcal{G}_{2'}$. Denoting the set of boundary nodes by $\mathcal{G}_3$, the complete modified grid is the union of these five sets and the matrices A, B and $\tilde{B}$

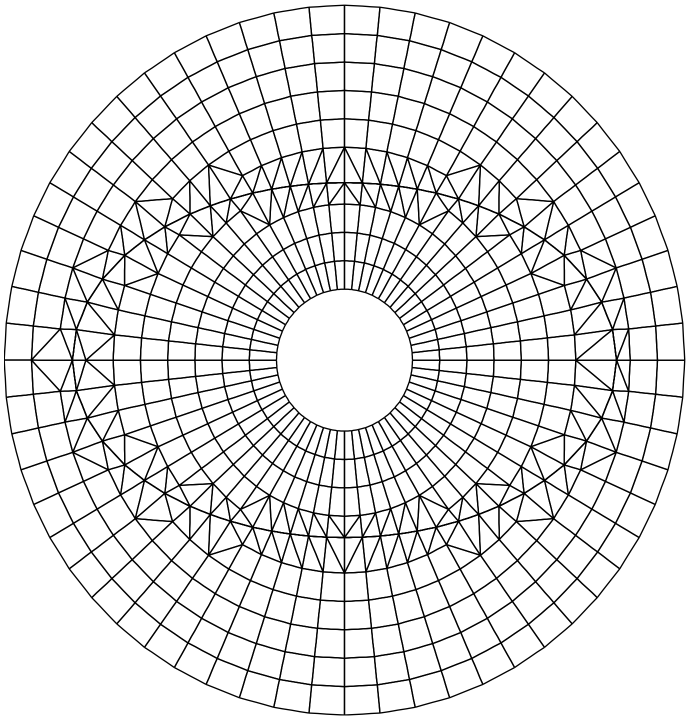

Figure 3.5: The modified grid in the x,y plane

have the block forms

$$A = \begin{bmatrix} A_{11} & A_{11'} & 0 & 0 & 0 \\ A_{11'}^T & A_{1'1'} & 0 & 0 & A_{1'3} \\ 0 & 0 & A_{2'2'} & A_{2'2} & A_{2'3} \\ 0 & 0 & A_{2'2}^T & A_{22} & 0 \\ 0 & A_{1'3}^T & 0 & 0 & A_{33}^{(1)} \end{bmatrix},$$

$$B = \begin{bmatrix} A_{11} & A_{11'} & 0 & 0 & 0 \\ A_{11'}^T & A_{1'1'} & 0 & 0 & A_{1'3} \\ 0 & 0 & A_{2'2'} & A_{2'2} & A_{2'3} \\ 0 & 0 & A_{2'2}^T & A_{22} & 0 \\ 0 & A_{1'3}^T & A_{2'3}^T & 0 & A_{33} \end{bmatrix}$$

and

$$\tilde{B} = \begin{bmatrix} A_{11} & A_{11'} & 0 & 0 & 0 \\ A_{11'}^T & \tilde{A}_{1'1'} & 0 & 0 & \tilde{A}_{1'3} \\ 0 & 0 & \tilde{A}_{2'2'} & A_{2'2} & \tilde{A}_{2'3} \\ 0 & 0 & A_{2'2}^T & A_{22} & 0 \\ 0 & \tilde{A}_{1'3}^T & \tilde{A}_{2'3} & 0 & \tilde{A}_{33} \end{bmatrix}.$$

We see that B and $\tilde{B}$ differ in the block rows corresponding to $\mathcal{G}_1'$, $\mathcal{G}_2'$ and $\mathcal{G}_3$. If we look for a solution $\mathbf{u}$ of the combined problem $A\mathbf{u} = \mathbf{f}$ in the form

$$\mathbf{u} = \tilde{B}^{-1}\mathbf{f} + \tilde{B}^{-1}\tilde{E}\mathbf{w}$$

with

$$\mathbf{f} = \begin{bmatrix} 0 \\ 0 \\ -A_{2'3}\mathbf{g} \\ 0 \\ 0 \end{bmatrix} \qquad \text{and} \qquad \tilde{E} = \begin{bmatrix} 0 \\ I \\ I \\ 0 \\ I \end{bmatrix} \in \mathbb{C}^{mn\times\tilde{n}}, \quad \tilde{n} = |\mathcal{G}_{1'} \cup \mathcal{G}_{2'} \cup \mathcal{G}_3|,$$

each I denoting the identity matrix of its block, then, as in the case of the two annuli, $\mathbf{u}$ solves the system $A\mathbf{u} = \mathbf{f}$ provided $\mathbf{w}$ solves the capacitance matrix equation

$$\tilde{C}\mathbf{w} := \tilde{E}^T A\tilde{B}^{-1}\tilde{E} = -(A - \tilde{B})\tilde{B}^{-1}\mathbf{f}. \tag{3.29}$$

Now the multiplication of a vector by the capacitance matrix equation can once again be performed using the fast Helmholtz solver. The dimension of the capacitance matrix remains proportional to the number of unknowns on the boundary Γ.

3.6 Numerical Results

3.6.1 Computations with the Model Problem

We first apply the imbedding algorithm to the model problem, i.e. the exterior problem for a disk. We imbed the annular computational domain $\{a < r < R\}$ into

1/8 wave ($k = \pi/2$)			1 wave ($k = 4\pi$)			8 waves ($k = 32\pi$)		
grid size	$\Delta r/\lambda$	it's	grid size	$\Delta r/\lambda$	it's	grid size	$\Delta r/\lambda$	it's
15×90	1/80	5	15×90	1/10	12			
30×180	1/160	5	30×180	1/20	12			
60×360	1/320	5	60×360	1/40	12	60×360	1/5	63
			120×720	1/80	12	120×720	1/10	60
			240×1440	1/160	12	240×1440	1/20	57

Table 3.1: Iteration counts for the iterative imbedding method applied to the two annular domains

the larger annulus $\{R_0 < r < R\}$ for an $R_0 < a$. Table 3.1 shows the iteration counts for the Dirichlet problem with plane wave data. We have set $R_0 = 0.25$, $a = 0.5$, $R = 1$ and have chosen k so that there are 1/8, 1 and 8 wavelengths between a and R. In all cases the angular resolution was chosen to be six times that of the radial direction. The stopping criterion for the iteration was a reduction of the initial residual by 10^{-8}. We observe that, as soon as the waves are resolved, which occurs for roughly five to ten grid points per wavelength, the iteration count does indeed remain constant. In the case of eight waves it actually decreases somewhat.

Figure 3.6 shows the residual curves for the previous three test problems. We see that they are virtually identical for the different grids. Finally, Figure 3.7 shows the distance of the eigenvalues of the capacitance matrix C from the point 1/2 in the complex plane for three different grid sizes and wave number $k = 4\pi$. We see that the clustering persists across the three grids.

3.6.2 Computations for other geometries

We have also applied the iterative imbedding algorithm to some of the test geometries of Chapter 2: an ellipse with semi-axes $a = 0.8$ and $b = 0.5$, a slender ellipse with semi axes $a = 0.9$ and $b = 0.09$ and the NACA0012 airfoil. Figures 3.8, 3.9 and 3.10 show examples of the locally modified grids used with the portion of the grid inside the obstacle removed for better visibility.

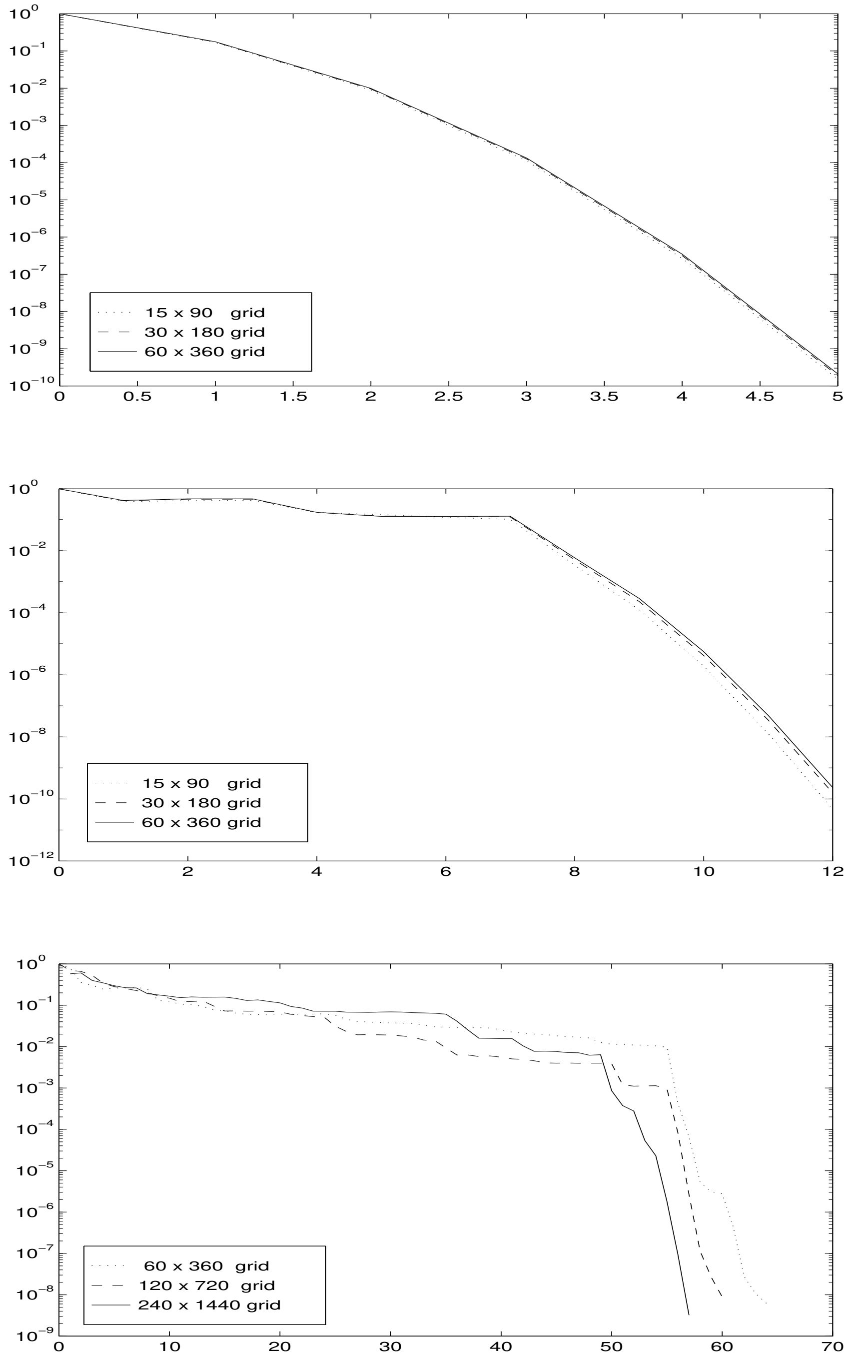

Figure 3.6: Residual norm vs. iteration number for the iterative imbedding algorithm for the two annuli.

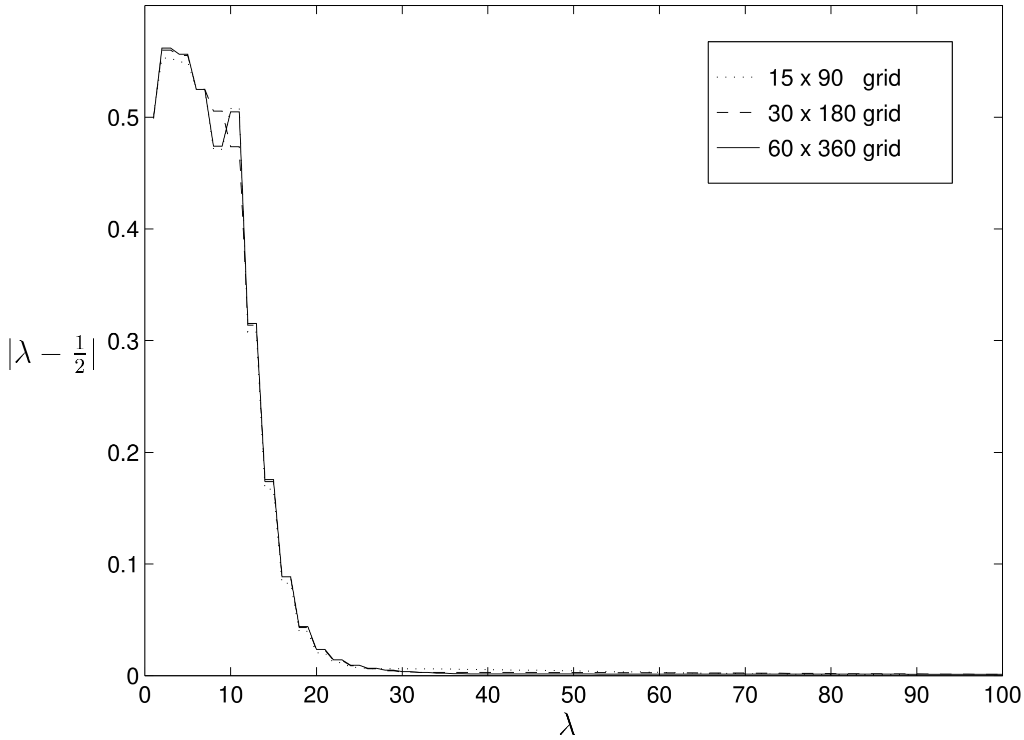

Figure 3.7: The clustering of the eigenvalues of the capacitance matrix C for $k = 4\pi$ in the case of the two annuli.

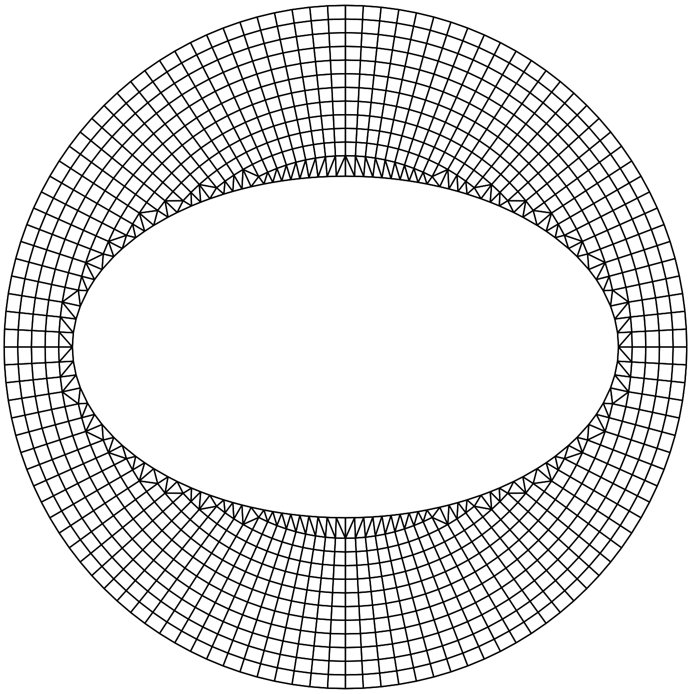

Figure 3.8: Locally modified grid for the ellipse

ellipse: $a = 0.8$, $b = 0.5$, $R_0 = 0.2$, $R = 1$				
$\vartheta_{inc} = 0^o$				
grid size	$k = 2\pi$	$k = 4\pi$	$k = 8\pi$	$k = 16\pi$
10×60	25	27	43	159
20×120	25	28	42	66
40×240	26	29	44	63
80×480	25	29	45	61
160×960	26	29	45	62
$\vartheta_{inc} = 45^o$				
grid size	$k = 2\pi$	$k = 4\pi$	$k = 8\pi$	$k = 16\pi$
10×60	31	39	64	-
20×120	31	45	62	118
40×240	32	46	65	107
80×480	34	49	67	102
160×960	32	50	69	110

Table 3.2: Iteration counts for the ellipse geometry

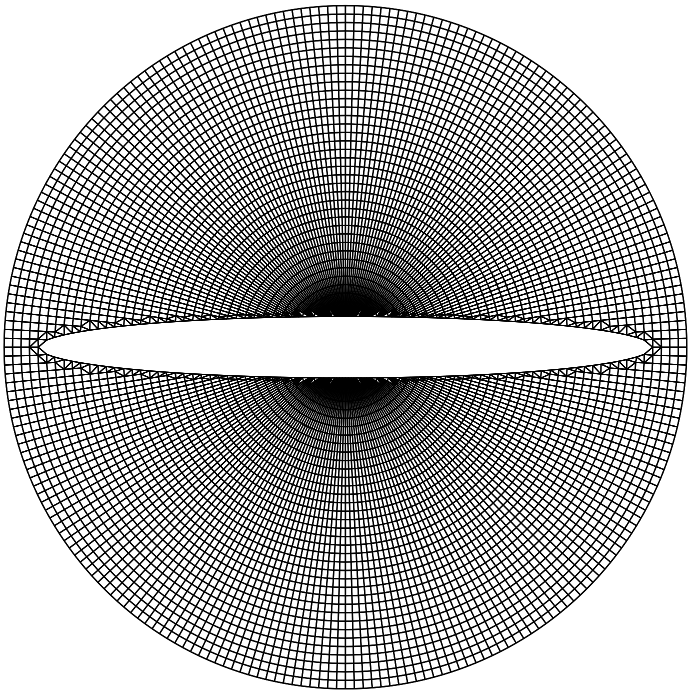

Figure 3.9: Locally modified grid for the slender ellipse

slender ellipse: $a = 0.9$, $b = 0.09$, $R_0 = 0.01$, $R = 1$				
$\vartheta_{inc} = 0^o$				
grid size	$k = 2\pi$	$k = 4\pi$	$k = 8\pi$	$k = 16\pi$
20×120	48	51	79	125
40×240	51	56	85	131
80×480	60	64	98	143
$\vartheta_{inc} = 45^o$				
grid size	$k = 2\pi$	$k = 4\pi$	$k = 8\pi$	$k = 16\pi$
20×120	50	59	79	125
40×240	53	63	85	131
80×480	62	74	98	143

Table 3.3: Iteration counts for the slender ellipse geometry

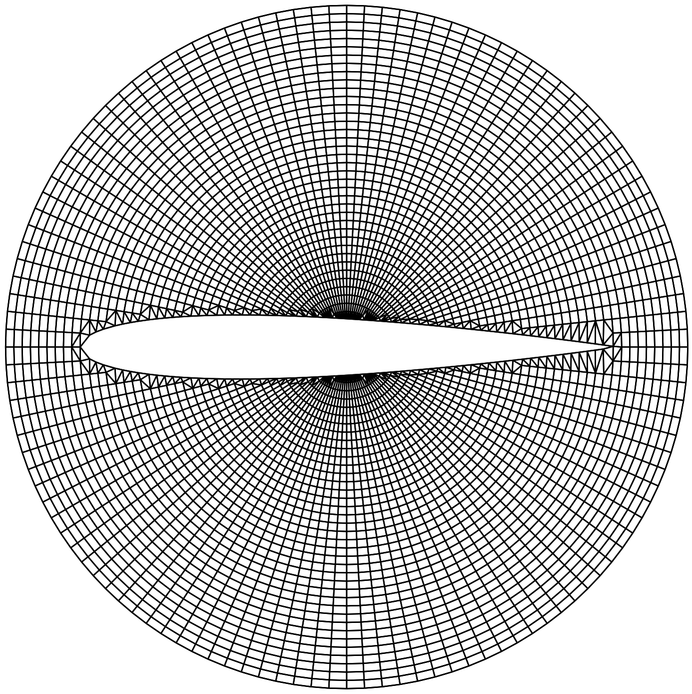

Figure 3.10: Locally modified grid for NACA0012 airfoil

NACA 0012: c=1, $R_0 = 0.02$, $R = 0.64$				
$\vartheta_{inc} = 0^o$				
grid size	$k = 2\pi$	$k = 4\pi$	$k = 8\pi$	$k = 16\pi$
20×120	66	70	80	107
40×240	69	74	86	120
80×480	73	78	87	145
160×960	71	74	89	146
$\vartheta_{inc} = 45^o$				
grid size	$k = 2\pi$	$k = 4\pi$	$k = 8\pi$	$k = 16\pi$
20×120	67	71	81	107
40×240	68	72	88	122
80×480	71	73	89	145
160×960	67	69	90	142

Table 3.4: Iteration counts for the NACA 0012 geometry

Chapter 4

Implementation and Performance Issues

In this chapter, we describe the implementation of the imbedding algorithms introduced in the previous chapters on a workstation and a distributed-memory parallel computer: the IBM 9076 SP1. We also examine performance issues and attempt to demonstrate that our imbedding algorithms are a powerful tool for efficiently solving exterior Helmholtz problems.

The numerical results were all obtained on an IBM SP1, the serial results were obtained using one node of the SP1, which is comparable in performance to an IBM RS/6000 Model 370 workstation rated at about 125 Mflops peak performance.

4.1 Serial Versions

Both the finite difference and the finite element algorithm were initially developed in MATLAB and later ported to FORTRAN 77 in order to obtain a realistic idea of their performance. This section describes the implementation of the two algorithms and gives timings for several test geometries.

grid	# unknowns	cpu time [s]	cpu time/$mn \log n$
10×60	600	.004	3.75e-6
20×120	2,400	.014	2.81e-6
40×240	9,600	.060	2.63e-6
80×480	38,400	.290	2.82e-6
160×960	153,600	1.31	2.86e-6
320×1920	614,400	6.15	3.05e-6

Table 4.1: Execution times for the fast Helmholtz solver

4.1.1 Fast Solver

In all our computations, we have used an FFT-based fast Helmholtz solver to solve problems posed on an annulus. For a grid with m radial and n angular grid points, the algorithm consists three stages:

Algorithm 4.1.1 *(FFT based Fast Helmholtz Solver)*

1. *Perform m FFTs of order n on the m blocks of the right hand side, each corresponding to data on one circular grid line.*

2. *Regroup the transformed data into n subvectors corresponding to radial mesh lines and solve a tridiagonal linear system with each of these as the right hand side.*

3. *Reorder back into the original ordering and perform the inverse FFT on each of the circular grid lines.*

Since the m FFTs each require $\mathcal{O}(n \log n)$ floating point operations and the n tridiagonal solves each $\mathcal{O}(m)$, the complexity of our fast Helmholtz solver is $\mathcal{O}(mn \log n)$. Table 4.1 shows cpu times for the fast Helmholtz solver on a sequence of grids. We observe that even fairly large problems can be solved in a matter of seconds. As the fourth column shows, where the cpu time is normalized by $nm \log n$, the complexity indeed behaves as $mn \log n$. The timings in Table 4.1 are for the finite difference code, the timings for the finite element fast Helmholtz solver on the annulus are similar.

In all our computations, the FFTs were computed using the routines from P. Swarztrauber's FFTPACK package available from NETLIB in the form rewritten for complex double-precision data by P. Bjørstadt. The tridiagonal solves were done using LAPACK's tridiagonal solver which uses partial pivoting and is thus very stable. The Hankel functions were computed using W.J. Cody's Bessel function suite which is also available from NETLIB.

4.1.2 The Finite Difference Imbedding Algorithm

The direct imbedding algorithm consists of four stages. First, in a grid generation stage, the grid on the annulus or disk used as the imbedding domain is partitioned into interior, exterior and boundary points. A data structure is maintained containing the distance to the boundary in each coordinate direction in which there is an intersection with Γ as well as the normal vectors at these intersections. In the second phase, the equations at the discrete boundary points are replaced by non-uniform stencils such as the Shortley-Weller formula (*cf.* [56]). Boundary data from any of the intersections with Γ of the grid lines emanating from a boundary point with Γ is moved to the right hand side as data. In this way, Dirichlet, Neumann or Impedance boundary conditions are imposed at the discrete boundary points, resulting in the matrix $A = B + UV^T$. In the third and most expensive stage, the capacitance matrix $C = I_p V^T B^{-1} U$ or $C = I_p V^T B^{-1} W$, respectively, are computed by performing a fast solve once for each unit vector in the columns of U, making use of the symmetry described in Chapter 3. The capacitance matrix is then factored using *Lapack*'s `zgsv` dense general linear system LU factorization routine. Once the factorization is available, each additional right hand side can be treated with one or two fast solves in addition to a back-solve with the factored capacitance matrix.

The matrices A and B are of course never computed, all the information necessary for the solution algorithm resides in the (sparse) matrix V. The matrix B occurs in the formulation only as its inverse, thus, B enters only implicitly through the fast Helmholtz solver on the annulus/disk.

The direct imbedding algorithm becomes most useful when a given problem with

grid size	generate	factorize & solve	1 fast solve	add. rhs	total/rhs
40×240	1.9	1.02	.06	.086	0.11
80×480	16.5	7.8	0.30	0.39	0.59
160×960	139	61	1.4	1.78	3.45
320×1920	1257	589	6.35	13.11	28.34

Table 4.2: Execution times in seconds for the imbedding algorithm with multiple right hand sides applied to the ellipse.

grid size	generate	factorize & solve	1 fast solve	add. rhs	total/rhs
40×240	2.52	1.62	.07	.091	0.13
80×480	21.8	12.6	0.29	0.41	0.69
160×960	189	102	1.31	1.91	4.31
320×1920	1707	1008	6.23	14.9	37.28

Table 4.3: Execution times in seconds for the imbedding algorithm with multiple right hand sides applied to the airfoil.

one wavenumber k is to be solved for several right hand sides, since then the factored capacitance matrix can be reused and each new solution can be computed at essentially the expense of one or two fast solves. A case where this occurs naturally is when the plane-wave scattering problem needs to be solved for many angles of incidence, e.g. for the calculation of the *monostatic* scattering cross section. The Table 4.1.2 shows the execution times for different stages of the imbedding algorithm with 120 additional right hand sides. The first column gives the time needed to generate the capacitance matrix C using the fast generation algorithm outlined in Section 2.4.3. The second column shows the time needed to factorize the capacitance matrix and to obtain the first solution. Column 3 shows the time needed for one application of the fast solver, column 4 shows the time needed for each additional right hand side and the last column shows the time per right hand side when the computation and factorization of C are taken into account. We see that, after the first solution has been computed, additional solutions are almost as cheap as one fast solve. For 120 right hand sides, which is a low number for scattering cross section calculations, the

grid size	generate	factorize & solve	1 fast solve	add. rhs	total/rhs
20×120	0.46	0.91	0.01	0.033	0.44
40×240	3.0	7.3	0.06	0.12	0.21
80×480	24	58	0.31	0.53	1.2
160×960	202	565	1.38	6.15	12.5

Table 4.4: Execution times in seconds for the imbedding algorithm with multiple right hand sides applied to the cavity.

work for computing and factorizing C is clearly amortized over the total computation. Tables 4.1.2 and Table 4.1.2 show the same timings for the NACA0012 and the cavity problem.

4.1.3 The Finite Element Imbedding Algorithm

The implementation of the finite element imbedding algorithm is also based on a fast Helmholtz solver using FFTs, which is implemented much the same way as in the finite difference method. New here is the mesh generation, the assembly of the matrices from the element matrices and the iterative linear equation solver. We have implemented the mesh generation algorithm 3.5.1 in MATLAB and used it to generate the locally fitted meshes. For the iterative solution algorithm, we used Freund and Nachtigal's coupled two-term QMR [41, 42] implementation from QMRPACK available from NETLIB. Their code performs the matrix-vector multiplications via reverse communication, giving control back to the calling program whenever a multiplication with the system matrix or its transpose is needed. The matrix vector multiplies were then computed using the fast solver as described in Chapter 3.

One observation we should mention concerns the choice of the starting vector for the left Krylov subspace, which is a free parameter in the QMR method. The QMRPACK implementation gives the user the choice of supplying his own starting vector or having the code generate a one randomly. By choosing this vector to be the initial residual, which is what the algorithm uses as the *right* starting vector as well, the algorithm always converged faster than for the random initial left vector.

ellipse: $a = 0.8$, $b = 0.5$, $R_0 = 0.2$, $R = 1$				
$\vartheta_{inc} = 0^o$				
grid size	$k = 2\pi$	$k = 4\pi$	$k = 8\pi$	$k = 16\pi$
10×60	0.4 (25)	0.5 (27)	0.8 (43)	2.8 (159)
20×120	1.6 (25)	1.8 (28)	2.7 (42)	4.1 (66)
40×240	6.2 (26)	6.9 (29)	10.5 (44)	15.2 (63)
80×480	26.4 (25)	30 (29)	47.5 (45)	64.4 (61)
160×960	120.3 (26)	134 (29)	208.5(45)	287.6 (62)
$\vartheta_{inc} = 45^o$				
grid size	$k = 2\pi$	$k = 4\pi$	$k = 8\pi$	$k = 16\pi$
10×60	0.5 (31)	0.7 (39)	1.1 (64)	-
20×120	1.9 (31)	2.8 (45)	3.8 (62)	7.4 (118)
40×240	7.6 (32)	11.0 (46)	15.4 (65)	25.5 (107)
80×480	35.7 (34)	51.5 (49)	70.7 (67)	107.7 (102)
160×960	148.2 (32)	231.7(50)	321.6 (69)	513.2 (110)

Table 4.5: Times and iteration counts for the ellipse geometry

Table 4.5 shows the timings for the iterative algorithm applied to the ellipse test case for several wave numbers k and 0^o incidence presented in Chapter 3.

4.2 Parallel Version

Since both imbedding algorithms contain a large amount of potential coarse-grained parallelism, we have implemented them on an architecture well-suited for not all too tightly coupled parallel tasks.

4.2.1 The Parallel Architecture

The IBM SP1 is a distributed memory parallel computer whose processing nodes are (currently 8 to 64) IBM RS/6000 workstations. Each of these nodes has 32K of cache memory, 128Mb main memory and has a clock speed of 62.5 MHz, making it roughly equivalent with an IBM RS/6000 Model 370 workstation. These nodes can communicate either over Ethernet using the Internet Protocol or via a high performance all-to-all switch.

We have chosen to use IBM's Message Passing Library (MPL), which enables programs to take advantage of the fast switch. MPL enforces the SPMD (single program – multiple data) programming model, in which identical code runs on all the nodes, operating on different data.

4.2.2 Parallelizing the Fast Solver

As more of a programming exercise for learning to use the SP1 than in expectation of great performance, we began by parallelizing only the fast Helmholtz solver on an annulus. Potential parallelism in Algorithm 4.1.1 can be found by considering each of its three stages.

The first and third stages involve m independent FFT's, while the second consists of n independent tridiagonal solves. This would be an embarrassingly parallel situation, were it not for the fact that the data distribution of each stage is orthogonal to the previous one: the FFT's operate on the m grid circles $\{u_{i,j}\}_{j=1}^{n}$ while the tridiagonal solves operate on data and solution values on the radial grid lines $\{u_{i,j}\}_{i=1}^{m}$. This means that, if the FFT's and tridiagonal solves are evenly distributed across the computing nodes, there will be a lot of communication traffic between the stages.

After trying several other possibilities, the following way of dividing the work proved the most efficient. We assume we have $n_p = 2^\ell$ processing nodes at our disposal and think of the data and the unknowns as arranged in an $n \times m$ array, each column corresponding to a circular grid line.

Figure 4.1 shows the distribution of data and the communication patterns that arise for the case $m = 14$, $n = 22$ and $n_p = 4$. Figure 4.1 (a) shows the distribution of the columns among the processors. Each processor performs the forward FFTs of stage 1 and the backward FFTs of stage 3 on his columns only. Figure 4.1 (b) shows which subcolumns are communicated after the first stage. Figure 4.1 (c) shows the distribution of the rows for the second stage of the algorithm in which the tridiagonal systems are solved. Figure 4.1 (d) shows the communication pattern after the tridiagonal solves, when the data for the backward FFTs is communicated.

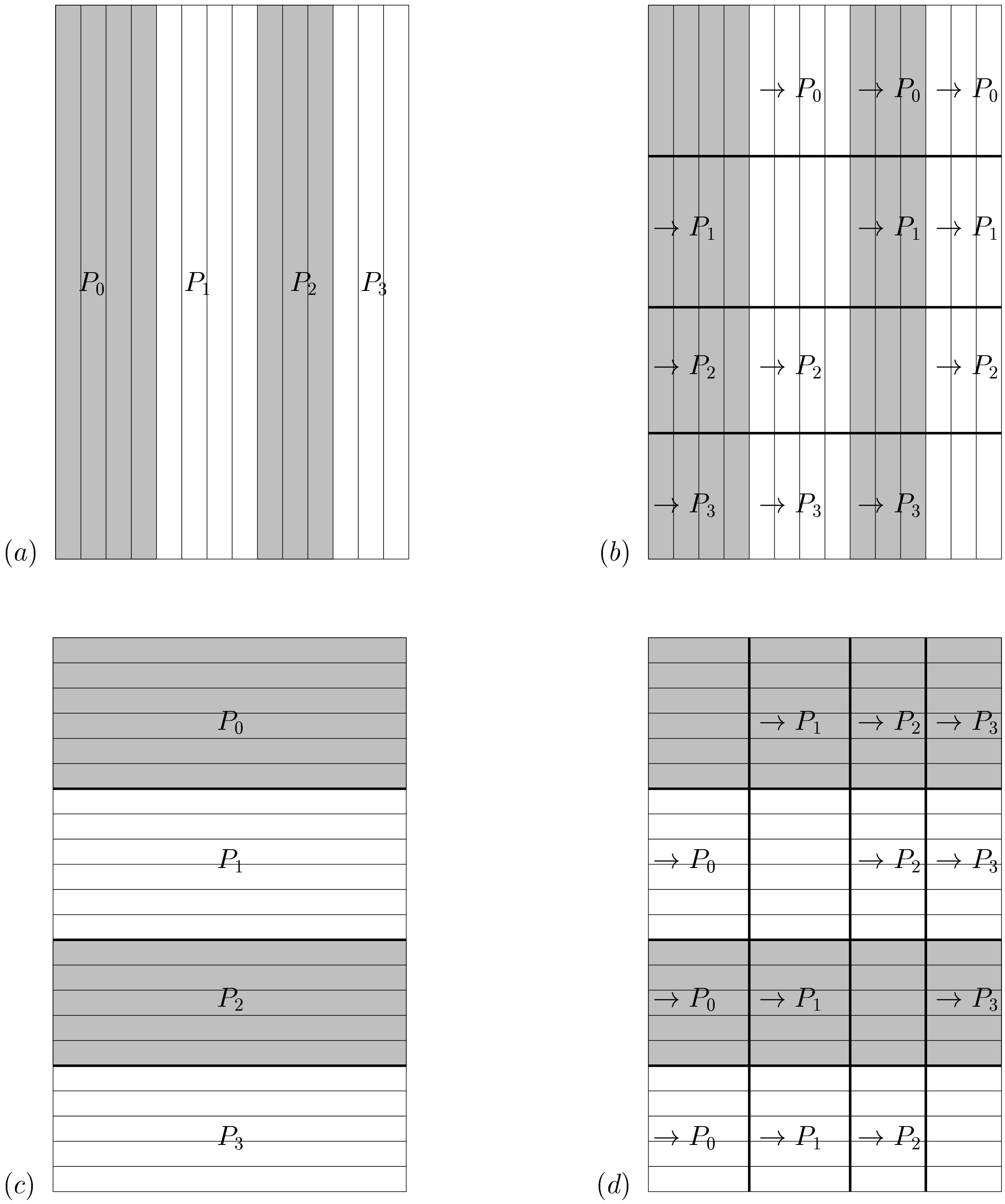

Figure 4.1: The distribution and communication of data in the parallel fast Helmholtz solver for four processors with $n = 22$ and $m = 14$.

grid	serial	$n_p = 2$	$n_p = 4$	$n_p = 8$
20×120	.004	.01	.012	.014
40×240	.014	.040	.030	.042
80×480	.290	.188	.130	.080
160×960	1.31	.70	.478	.54
320×1920	6.15	3.04	1.75	1.57

Table 4.6: Execution times for the fast Helmholtz solver on 1, 2, 4 and 8 processorns of the SP1

Table 4.6 shows the cpu times of the parallelized fast Helmholtz solver on 1, 2, 4 and 8 processors. We observe two things : first, a certain minimal problem size is necessary in order to take advantage of the parallel architecture. Second, we see that, for the larger problems, communication becomes a bottleneck so that, for 4 and 8 processors, the speedup degrades. This indicates that one fast solve is too fine-grained a task to work efficiently on this machine.

4.2.3 Parallelizing the Finite Difference Imbedding Code

In order to parallelize the finite difference imbedding code, we must parallalelize the main computatinal tasks : the generation of the capacitance matrix, the factorization of the capacitance matrix and the computation of the extra right hand sides. We will only look at the parallel computation of the capacitance matrix. The parallel computation of the additional right hand sides is trivial, as no communication at all is involved. The parallel solution of dense linear systems of equations on distributed memory machines is currently the subject of much research, and the implementation of such a solver would have been beyond the scope of the thesis. We point out, however, that there is a project currently underway under the name ScaLAPACK [25] headed by J. Dongarra of the Oak Ridge National Laboratory to develop portable, dense linear algebra routines running under the PVM message passing library. We opted for waiting until this package is available to parallelize the rest of the code.

Table 4.7 shows the computation times on 1, 2, 4, and 8 processors of the SP1 for the computation of the capacitance matrix for the ellipse problem for various grid

grid	1	2	4	8
20×120	.21	.14	.01	.27
40×240	1.47	.87	.49	.50
80×480	12.8	6.73	3.39	2.07
160×960	119	57.35	29.14	15.96

Table 4.7: Execution times for the parallel generation of the capacitance matrix on 1, 2, 4 and 8 processors

sizes. We took the serial code and added the scheduling of the work on the various processors and the message passing calls to the MPL library. Of the many variants we tested the following one was the only one to give the nearly linear speedup shown in Table 4.7. The columns of the capacitance matrix are grouped together in blocks belonging to the same fast solve, i.e. corresponding to discrete boundary points on the same grid circle. It is these blocks that are distributed equally to the various processors. One processor, $P0$, is designated to receive all the columns after they have been computed. The blocks of columns are in general of different length, usually decreasing from the inner grid circle to the outer. For this reason, the blocks are assigned to the processors cyclically rather than in contiguous blocks of columns. Before computing its columns, $P0$ makes a call to a non-blocking receive routine, specifying receive buffers for all the columns it is to receive in the course of the computation. This way, synchronization can be left to the message passing system and computation can be interleaved with communication as much as possible. All the other processors send each columns to $P0$ as soon as they receive it. Since $P0$ has to participate in more communication than the remaining processors, it receives a somewhat smaller workload than the others to achieve better load balancing.

4.2.4 Conclusion

We have seen that the fast solver itself is difficult to parallelize because of the orthogonal data distribution in the three phases of the algorithm. When the complete finite difference imbedding algorithm is parallelized, the main computational task of computing the capacitance matrix parallelizes quite well on the 2 to 8 processor runs we have performed. Using the factored capacitance matrix to compute the solutions for multiple right hand sides is a trivially parallel task. What remains is the factorization of the capacitance matrix, a task for which efficient portable software for distributed memory computers will soon be available.

Finally, for problems so large that a single grid will no longer fit into the memory of one computing node, a domain decomposition method would need to be added to the imbedding algorithm in order to parallelize the solution algorithm.

Appendix A

Difference Formulas for Discrete Dipoles

In this appendix we briefly describe the difference stencils used to approximate the normal derivative operator which forms the columns of the matrix W of discrete dipoles used in Chapter 2 to obtain well-conditioned capacitance matrices for exterior Dirichlet problems. We distinguish several cases for the location of an irregular mesh point with respect to the boundary $\partial\Omega$.

Consider a point $x \in \partial\Omega$ with polar coordinates (r_0, ϑ_0) and let α denote the angle between the exterior surface normal at x and the positive x-axis. Then the normal derivative of a function u at x is given by

$$\frac{\partial u(x)}{\partial n} = u_r \cos(\alpha - \vartheta_0) + \frac{u_\vartheta}{r_0} \sin(\alpha - \vartheta_0). \tag{A.1}$$

We approximate this expression using undivided differences.

At an irregular mesh point (r_i, ϑ_j), we define the surface normal to be the average of the surface normals at the intersection of $\partial\Omega$ and any of the grid lines connecting (r_i, ϑ_j) with $(r_i \pm \Delta r, \vartheta_j \pm \Delta\vartheta)$. To approximate (A.1), we will use values of the discrete solution at the five points of the difference stencil used for the Helmholtz operator subject to the condition mentioned in Chapter 2 that the difference stencils for the discrete dipoles involve only grid points in $\Omega_c^h \cup \Gamma^h$. If one restricts these points further to Ω_c^h, then the matrix $U^T W$, the first term in the capacitance matrix C, is a

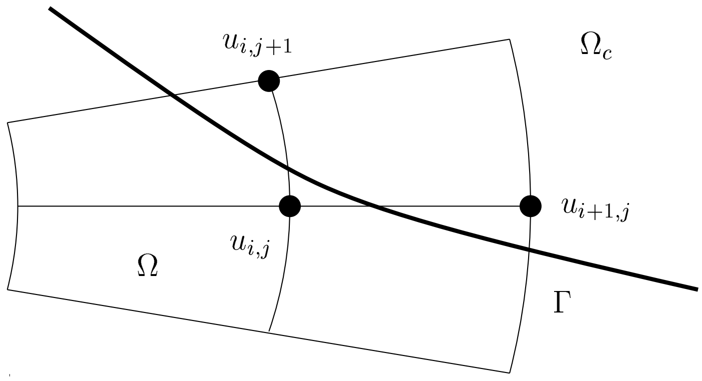

Figure A.1: The case of two stencil neighbors in Ω_c^h.

scaling of the identity and can thus be normalized to the identity, resulting in a closer analog to the second-kind Fredholm operator of the continuous case. We have found, however, that using the larger set $\Omega_c^h \cup \Gamma^h$ results in lower condition numbers for C.

Thus, we choose the difference formula for the normal derivative depending on which of the four stencil neighbors lie in Ω_c^h.

Figure A.1 shows an example situation of a grid point $(r_i, \vartheta_j) \in \Gamma^h$ whose neighbors (r_{i+1}, ϑ_j) and (r_i, ϑ_{j+1}) lie in Ω_c^h. In this case we approximate the radial derivative by $(u_{i+1,j} - u_{i,j})/\Delta r$ and the angular derivative by $(u_{i,j+1} - u_{i,j})/\Delta\vartheta$. Thus, if ℓ is the index of the point (r_i, ϑ_j) in Γ^h and $\mathrm{ind}(i,j)$ denotes the index of the same point in the large grid, we have

$$\begin{aligned}
W(\mathrm{ind}(i,j), \ell) &= -\cos(\alpha - \vartheta_j) - \frac{\sin(\alpha - \vartheta_j)}{r_i} \\
W(\mathrm{ind}(i+1,j), \ell) &= \cos(\alpha - \vartheta_j) \\
W(\mathrm{ind}(i,j+1), \ell) &= \frac{\sin(\alpha - \vartheta_j)}{r_i}.
\end{aligned}$$

The mesh widths Δr and $\Delta\vartheta$ don't appear since we use undivided differences. Analogous formulas are used in the case of one or three neighbors in Ω_c^h. In the case where only one neighbor lies in Ω_c, we also use solution values at the 'diagonal' neighbors $(r_{i\pm1}, \vartheta_{j\pm1})$.

Appendix B

Element Stiffness and Mass Matrices for Linear Triangles in Polar Coordinates

An annulus or a disk can also be discretized using linear triangles on the regular portion of the grid. A uniform triangulation is obtained. e.g. by halving each rectangle in a uniform rectangular partitioning along the same diagonal. Below, we give the element mass and stiffness matrices when the diagonal from the upper left to the lower right corner is chosen.

We denote the two differently oriented triangle types as type A and type B.

We enumerate the nodes in each element counter-clockwise beginning with the corner situated at the right angle. The local nodal basis functions are thus

$$\varphi_1(r,\vartheta) = 1 - \frac{r - r_i}{\Delta r} - \frac{\vartheta - \vartheta_j}{\Delta\vartheta} \tag{B.1}$$

$$\varphi_2(r,\vartheta) = \frac{r - r_i}{\Delta r} \tag{B.2}$$

$$\varphi_3(r,\vartheta) = \frac{\vartheta - \vartheta_j}{\Delta\vartheta} \tag{B.3}$$

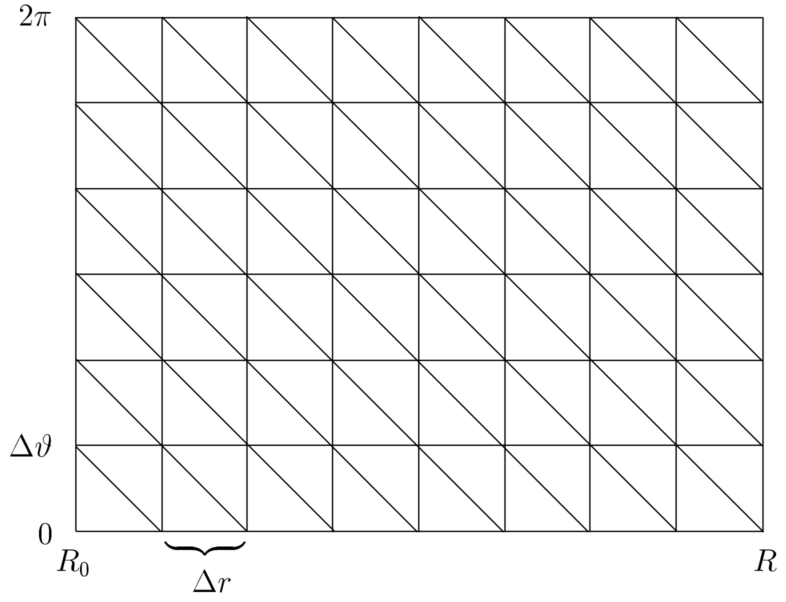

Figure B.1: Triangulation of the annulus in (r, ϑ) coordinates

for the type A triangles and

$$\varphi_1(r,\vartheta) = \frac{r - r_{i-1}}{\Delta r} + \frac{\vartheta - \vartheta_{j-1}}{\Delta\vartheta} - 1 \tag{B.4}$$

$$\varphi_2(r,\vartheta) = \frac{r_i - r}{\Delta r} \tag{B.5}$$

$$\varphi_3(r,\vartheta) = \frac{\vartheta_j - \vartheta}{\Delta\vartheta} \tag{B.6}$$

for those of type B. The element stiffness matrices are given by

$$K_A = \begin{pmatrix} \frac{r_i\Delta\vartheta}{2\Delta r} + \frac{\Delta\vartheta}{6} - \frac{1}{\Delta\vartheta} + \mu_i^A & -\left(\frac{r_i\Delta\vartheta}{2\Delta r} + \frac{\Delta\vartheta}{6}\right) & -\left(\frac{\mu_i^A}{\Delta r\Delta\vartheta} - \frac{1}{\Delta\vartheta}\right) \\ * & \frac{r_i\Delta\vartheta}{2\Delta r} + \frac{\Delta\vartheta}{6} & 0 \\ * & * & \frac{\mu_i^A}{\Delta r\Delta\vartheta} - \frac{1}{\Delta\vartheta} \end{pmatrix}$$

and

$$K_B = \begin{pmatrix} \frac{r_i\Delta\vartheta}{2\Delta r} - \frac{\Delta\vartheta}{6} + \frac{1}{\Delta\vartheta} - \mu_i^B & -\left(\frac{r_i\Delta\vartheta}{2\Delta r} - \frac{\Delta\vartheta}{6}\right) & -\left(\frac{1}{\Delta\vartheta} - \frac{\mu_i^B}{\Delta r\Delta\vartheta}\right) \\ * & \frac{r_i\Delta\vartheta}{2\Delta r} - \frac{\Delta\vartheta}{6} & 0 \\ * & * & -\frac{\mu_i^B}{\Delta r\Delta\vartheta} + \frac{1}{\Delta\vartheta} \end{pmatrix}$$

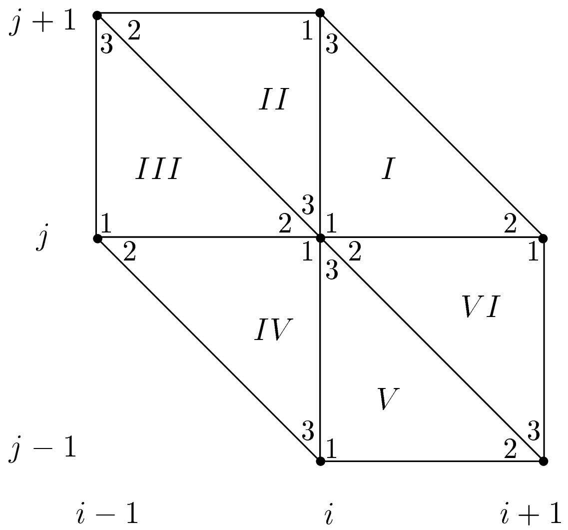

Figure B.2: Node i, j in the regular triangulation and its six neighboring elements; elements I,III and V are of type A, II,IV and VI are of type B

for triangles of the corresponding types. The asterisks indicate that the matrices should be completed symetrically and

$$\mu_i^A = r_{i+1} \log \frac{r_{i+1}}{r_i} \qquad \mu_i^B = r_{i-1} \log \frac{r_i}{r_{i-1}}.$$

The corresponding mass matrices are given by

$$M_A = \frac{\Delta r \Delta \vartheta}{12} \begin{pmatrix} r_i + \frac{\Delta r}{5} & \frac{r_i}{2} + \frac{\Delta r}{5} & \frac{r_i}{2} + \frac{\Delta r}{10} \\ * & r_i + \frac{3\Delta r}{5} & \frac{r_i}{2} + \frac{\Delta r}{5} \\ * & * & r_i + \frac{\Delta r}{5} \end{pmatrix}$$

and

$$M_B = \frac{\Delta r \Delta \vartheta}{12} \begin{pmatrix} r_i - \frac{\Delta r}{5} & \frac{r_i}{2} - \frac{\Delta r}{5} & \frac{r_i}{2} - \frac{\Delta r}{10} \\ * & r_i - \frac{3\Delta r}{5} & \frac{r_i}{2} - \frac{\Delta r}{5} \\ * & * & r_i - \frac{\Delta r}{5} \end{pmatrix},$$

respectively.

After assembling the matrices, i.e. collecting at each node the contributions from the neighboring elements, the global stiffness matrix is given by the Kronecker product

Bibliography

[1] V.K. Agapov and Yu.A. Kuznetsov. On some versions of the domain decomposition method. *Sov. J. Numer. Anal. Math. Modelling*, 3(4):245–265, 1988.

[2] G.P. Astrakhantsev. Method of fictitious domains for a second-order elliptic equation with natural boundary conditions. *U.S.S.R. Comput. Math. and Math. Phys.*, 18:114–121, 1978.

[3] G.P. Astrakhantsev. Numerical solution of the Dirichlet problem using a discrete analogue of the double-layer potential. *Sov. J. Numer. Anal. Math. Modelling*, 1(4):267–276, 1986.

[4] C. Atamian, G.V. Dinh, R. Glowinski, J. He, and J. Periaux. On some imbedding methods applied to fluid dynamics and electro-magnetics. *Comput. Methods Appl. Mech. Engrg.*, 91:1271–1299, 1991.

[5] C. Atamian, Q.V. Dinh, R. Glowinski, Jiwen He, and J. Périaux. Control approach to fictitious-domain methods application to fluid dynamics and electromagnetics. In R. Glowinski, Y.A. Kuznetsov, G. Meurant, J. Périaux, and O. Widlund, editors, *Fourth International Symposium on Domain Decomposition Methods for Partial Differential Equations*, number 51 in Proceedings in Applied Mathematics, pages 275–309. SIAM, 1990.

[6] C. Atamian and P. Joly. Une analyse de la méthode des domaines fictifs pour le problème de Helmholtz extérieur. *RAIRO Mathematical Modelling and Numerical Analysis*, 27(3):251–288, 1993.

[7] F.V. Atkinson. On Sommerfeld's "radiation condition". *Philos. Mag.*, 40:645–651, 1943.

[8] A. Bayliss, M. Gunzburger, and E. Turkel. Boundary conditions for the numerical solution of elliptic equations in exterior domains. *SIAM J. Appl. Math.*, 42:430–451, 1982.

[9] A. Bespalov. Application of fictitious domain method to the solution of the Helmholtz equation in unbounded domain. Technical Report 1797, INRIA, November 1992.

[10] A. Bespalov, Y. Kuznetsov, O. Pironneau, and M. Vallet. Fictitious domains with separable preconditioners versus unstructured adapted meshes. Technical Report 1614, INRIA, February 1992.

[11] P.E. Bjørstadt and O.B. Widlund. Solving elliptic problems on regions partitioned into substructures. In G. Birkhoff ans A. Schoenstadt, editor, *Elliptic Problem Solvers II*, pages 245–255, 1984.

[12] P.E. Bjørstadt and O.B. Widlund. Iterative methods for the solution of elliptic problems on regions partitioned into substructures. *SIAM J. Numer. Anal.*, 23(6):1097–1120, 1986.

[13] C. Börgers. The Neumann-Dirichlet domain decomposition method with inexact solvers on the subdomains. *Numer. Math.*, 55, 1989.

[14] C. Börgers. Domain imbedding methods for the stokes equations. *Numer. Math.*, 57:435–451, 1990.

[15] C. Börgers. A triangulation algorithm for fast elliptic solvers based on domain imbedding. *SIAM J. Numer. Anal.*, 27(5):1187–1196, October 1990.

[16] C. Börgers and O. B. Widlund. Finite element capacitance matrix methods. Technical Report 261, Computer Science Dept., New York University, 251 Mercer Street, New York, N.Y. 10012, 1986.

[17] C. Börgers and O. B. Widlund. On finite element domain imbedding methods. *SIAM J. Numer. Anal.*, 27(4):963–978, August 1990.

[18] J.J. Bowman, T.B.A. Senior, and P.L.E. Uslenghi. *Electromagnetic and Acoustic Scattering by Simple Shapes.* Hemisphere Publishing Corporation, 2 edition, 1987.

[19] M.O. Bristeau, R. Glowinski, and J. Périaux. Numerical simulation of high frequency scattering waves using exact controllability methods. Technical Report UH/MD-146, Univ. of Houston, Dept. of Mathematics, 1992.

[20] M.O. Bristeau, R. Glowinski, and J. Périaux. Exact controllability to solve the Helmholtz equation with absorbing boundary conditions. In P. Neittaanmaki, editor, *Proc. of the FEM50 Conf., Jyvaskyla, Sept. 93.* M. Dekker Inc., 1993.

[21] O. Buneman. A compact non-iterative Poisson solver. Technical Report 294, Stanford University Institute for Plasma Research, Stanford, Ca., 1969.

[22] B. Buzbee, G. Golub, and C. Nielson. On direct methods for solving Poisson's equation. *SIAM J. Numer. Analysis*, 7:627–656, 1970.

[23] B.L. Buzbee, F.W. Dorr, J.A. George, and G.H. Golub. The direct solution of the discrete Poisson equation on irregular regions. *SIAM J. Numer. Anal.*, 8:722–736, 1974.

[24] T.F. Chan and F. Saied. A comparison of elliptic solvers for general two-dimensional regions. *SIAM J. Sci. Statist. Comput.*, 6(3):742–760, 1985.

[25] J. Choi, J.J. Dongarra, and D.W. Walker. Scalapack I: Parallel factorization routines (LU, QR and Cholesky). Technical Report TM-2470, Oak Ridge National Laboratory, Mathematical Sciences Division, 1994.

[26] D. Colton and R. Kress. *Integral Equation Methods in Scattering Theory.* Wiley, New York, 1983.

[27] D. Colton and R. Kress. *Inverse Acoustic and Electromagnetic Scattering Theory*, volume 93 of *Applied Mathematical Sciences*. Springer-Verlag, 1992.

[28] P. Concus, G. H. Golub, and D. P. O'Leary. A generalized conjugate gradient method for solution of elliptic partial differential equations. In J.R. Bunch and D.J. Rose, editors, *Proc. Symp. on Sparse Matrix Computations*. Argonne National Lab.(Sept. 1975), Academic Press, New York, 1975.

[29] R. Dautray and J.L. Lions. *Mathematical Analysis and Numerical Methods for Science and Technology*. Springer-Verlag, Berlin-Heidelberg, 1988.

[30] E. J. Dean, Q.V. Dinh, R. Glowinski, Jiwen He, T.W. Pan, and J. Périaux. Least squares/domain imbedding methods for Neumann problems: Applications to fluid dynamics. In D.E. Keyes, T.F. Chan, G. Meurant, J.S. Scroggs, and R.G. Voig, editors, *Fifth International Symposium on Domain Decomposition Methods for Partial Differential Equation*, number 55 in Proceedings in Applied Mathematics, pages 451–475. SIAM, 1991.

[31] Q.V. Dinh, R. Glowinski, Jiwen He, V. Kwock, T.W. Pan, and J. Périaux. Lagrange multiplier approach to fictitious domain methods: Application to fluid dynamics and electro-magnetics. In D.E. Keyes, T.F. Chan, G. Meurant, J.S. Scroggs, and R.G. Voigt, editors, *Fifth International Symposium on Domain Decomposition Methods for Partial Differential Equations*, number 55 in Proceedings in Applied Mathematics, page Proceedings in Applied Mathematics. SIAM, 1991.

[32] F. Dorr. The direct solution of the discrete Poisson equation on a rectangle. *SIAM Rev.*, 12:248–263, 1970.

[33] M. Dryja. A capacitance matrix method for Dirichlet problem on polygonal region. *Numer. Math.*, 39:51–64, 1982.

[34] M. Dryja. A finite-element capacitance matrix method for the elliptic problem. *SIAM J. Numer. Anal.*, 20:621, 1983.

[35] M. Dryja. A finite element-capacitance method for elliptic problems on regions partitioned into subregions. *Numer. Math.*, 44:153–168, 1984.

[36] B. Engquist and A. Majda. Absorbing boundary conditions for the numerical simulation of waves. *Math. Comp.*, 31(139):629–651, 1977.

[37] B. Engquist and A. Majda. Radiation boundary conditions for acoustic and elastic wave calculations. *Comm. Pure Appl. Math.*, 32:313–357, 1979.

[38] S.A. Finogenov and Yu.A. Kuznetsov. Two-stage fictitious components method for solving the Dirichlet boundary value problem. *Sov. J. Numer. Anal. Math. Modelling*, 3(4):301–323, 1988.

[39] G.J. Fix and S.P. Marin. Variational methods for underwater acoustic problems. *J. Comput. Phys.*, 28:253–270, 1978.

[40] G.E. Forsythe and W.R. Wasow. *Finite-Difference Methods for Partial Differential Equations*. Wiley, 1960.

[41] R.W. Freund and N.M. Nachtigal. Implementation details of the coupled QMR algorithm. Technical Report 92.19, RIACS, 1992.

[42] R.W. Freund and N.M. Nachtigal. An implementation of the QMR method based on coupled two-term recurrences. *SIAM J. Sci. Comput.*, 15(2):313–337, March 1994.

[43] A. George. The use of direct methods for the solution of the discrete Poisson equation on non-rectangular regions. Technical Report STAN-CS-70-159, Computer Science Dept., Stanford University, Stanford, CA, 1970.

[44] D. Gilbarg and N.S. Trudinger. *Elliptic partial differential equations of second order*. Number 224 in Grundlehren der mathematischen Wissenschaften. Springer-Verlag, 2 edition, 1983.

[45] J. Giroire and J.C. Nedelec. Numerical solutions of an exterior Neumann problem using a double-layer potential. *Math. Comp.*, 32(144):973–990, 1978.

[46] D. Givoli. Non-reflecting boundary conditions. *J. Comput. Phys.*, 94:1–29, 1991.

[47] D. Givoli. *Numerical Methods for Problems in Infinite Domains*, volume 33 of *Studies in Applied Mechanics*. Elsevier, 1992.

[48] D. Givoli, L. Rivkin, and J.B. Keller. A finite-element method for domains with corners. *Internat. J. Numer. Methods Engrg.*, 35:1329–1345, 1992.

[49] R. Glowinski and T.W. Pan. Error estimates for fictitious domain/penalty/finite element methods. *Calcolo*, 29(1–2):125–141, 1992.

[50] C. I. Goldstein. The solution of exterior interface problems using a variational method with lagrange multipliers. *J. Math. Anal. Appl.*, 97:480–508, 1983.

[51] C.I. Goldstein. Numerical methods for Helmholtz-type equations in unbounded regions. In J.A. DeSanto, A.W. Saenz, and W.W. Zachary, editors, *Mathematical Methods and Applications of Scattering Theory*, volume 130 of *Lecture Notes in Physics*, pages 26–33. Springer, 1979.

[52] C.I. Goldstein. The finite element method with non-uniform mesh sizes applied to the exterior Helmholtz problem. *Numer. Math.*, 38:61–82, 1981.

[53] C.I. Goldstein. The finite element method with nonuniform mesh sizes for unbounded domains. *Math. Comp.*, 36(154):387–404, April 1981.

[54] C.I. Goldstein. A finite element method for solving Helmholtz type equations in waveguides and other unbounded domains. *Math. Comp.*, 39(160):309–324, October 1982.

[55] G.H. Golub. private communication, June 1994.

[56] W. Hackbusch. *Elliptic Differential Equations*, volume 18 of *Springer Series in Computational Mathematics*. Springer Verlag, 1992.

[57] W.W. Hager. Updating the inverse of a matrix. *SIAM Rev.*, 31(2):221–239, June 1989.

[58] I. Harari and T.J.R. Hughes. Analysis of continuous formulations underlying the computation of time-harmonic acoustics in exterior domains. *Comput. Methods Appl. Mech. Engrg.*, 97(1):103–124, 1992.

[59] I. Harari and T.J.R. Hughes. Galerkin/least-squares finite element methods for the reduced wave equation with non-reflecting boundary conditions in unbounded domains. *Comput. Methods Appl. Mech. Engrg.*, 98:411–454, 1992.

[60] I. Harari, T.J.R. Hughes, L.L. Thompson, K. Grosh, J.R. Stewart, and M. Malhotra. Recent developments in finite element methods in acoustics. *to appear in Archives of Computational Methods in Engineering*, 1995.

[61] R. W. Hockney. A fast direct solution of the discrete Poisson equation using Fourier analysis. *J. Assoc. Comput. Mach.*, 8:95–113, 1965.

[62] R. W. Hockney. POT4–A fast direct Poisson-solver for the rectangle allowing some mixed boundary conditions and internal electrodes. Technical report, IBM Thomas J. Watson Research Center, Yorktown Heights, NY 10598, May 1970.

[63] R.A. Horn and C.R. Johnson. *Topics in Matrix Analysis*. Cambridge University Press, 1991.

[64] G.C. Hsiao and W.L. Wendland. Domain decomposition via boundary element methods. Technical Report 92-14, Mathematisches Institut, Universität Stuttgart, 1992.

[65] D.S. Jones. Integral equations for the exterior acoustic problem. *Quart. J. Mech. Appl. Math.*, 27:129–142, 1974.

[66] S.N. Karp. A convergent 'farfield' expansion for two-dimensional radiation functions. *Comm. Pure Appl. Math.*, 14:427–434, 1961.

[67] J. B. Keller and D. Givoli. Exact non-reflecting boundary conditions. *J. Comput. Phys.*, 82:172–192, 1989.

[68] A. Kirsch. Generalized Boundary Value- and Control Problems for the Helmholtz Equation. Habilitation thesis, Göttingen, 1984.

[69] A. Kirsch. Surface gradients and continuity properties for some integral operators in classical scattering theory. *Math. Meth. Appl. Sc.*, 11:789–804, 1989.

[70] A. Kirsch. Remarks on some notions of weak solutions for the Helmholtz equation. *Appl. Anal.*, 14:7–24, 1992.

[71] A. Kirsch and P. Monk. Convergence analysis of a coupled finite element and spectral method in acoustic scattering. *IMA J. Numerical Analysis*, 9:425–447, 1990.

[72] A. Kirsch and P. Monk. An analysis of the coupling of finite element and nystrom methods in acoustic scattering. *IMA J. Num. Anal.*, 14(4), 1994.

[73] E.F. Knott, J.F. Schaeffer, and M.T. Tuley. *Radar Cross Section.* Artech House Inc., 1985.

[74] R. Kress. *Linear Integral Equations*, volume 82 of *Applied Mathematical Sciences.* Springer-Verlag, 1989.

[75] Yu.A. Kuznetsov and O.D. Trufanov. Two-stage fictitious components method for solving the wave Helmholtz equation. *Sov. J. Numer. Anal. Math. Modelling*, 3(5):373–391, 1988.

[76] N.N. Lebedev. *Special Functions and their Applications.* Dover, 1972.

[77] R.C. MacCamy and S.P. Marin. A finite element method for exterior interface problems. *Internat. J. Math. Math. Sci.*, 3(2):311–350, 1980.

[78] G.I. Marchuk, Yu.A. Kuznetsov, and A.M. Matsokin. Fictitious domain and domain decomposition methods. *Sov. J. Numer. Anal. Math. Modelling*, 1(1):3–35, 1986.

[79] E.D. Martin. A generalized capacity-matrix technique for computing aerodynamic flows. *Comput. & Fluids*, 2:79–97, 1974.

[80] M. Masmoudi. Numerical solution for exterior problems. *Numer. Math.*, 51:87–101, 1987.

[81] A. Mayo. The fast solution of Poisson's and the Biharmonic equations on irregular regions. *SIAM J. Numer. Anal.*, 21(2):285–299, 1984.

[82] W. L. Miranker. Uniqueness and representation theorems for solutions of $\Delta u + k^2 u = 0$ in infinite domains. *J. Math. Mech.*, 6(6):847–858, 1957.

[83] C. Müller. Zur Methode der Strahlungskapazität von H. Weyl. *Mathematische Zeitschrift*, 56(1):80–83, 1952.

[84] J.C. Nédélec and J. Planchard. Une méthode variationelle d'éléments finis pour la résolution numérique d'un problème extérieur dans R^3. *R.A.I.R.O.*, pages 105–129, 1973.

[85] Jindřich Nečas. *Les Méthodes Directes en Théorie des Equations Elliptiques.* Masson et Cie., Prague, 1967.

[86] D.P. O'Leary and O. Widlund. Capacitance matrix methods for the Helmholtz equation on general three-dimensional regions. *Math. Comp.*, 33(147):849–879, July 1979.

[87] W. Proskurowski. Numerical solution of Helmholtz's equation by implicit capacitance matrix methods. *ACM Trans. Math. Software*, 5:36–49, 1979.

[88] W. Proskurowski. Capacitance matrix methods–a brief survey. In *Elliptic Problem Solvers*, pages 391–398. Academic Press, 1981.

[89] W. Proskurowski and O. B. Widlund. On the numerical solution of Helmholtz's equation by the capacitance matrix method. *Math. Comp.*, 30:433–468, 1976.

[90] W. Proskurowski and O. B. Widlund. A finite element capacitance matrix method for the Neumann problem for Laplace's equation. *SIAM J. Sci. Statist. Comput.*, 1:410–425, 1980.

[91] H. Steve R. Lohner and J. Periaux, editors. *Proceedings of the Second International Workshop on Approximations & Numerical Methods for the Solution of Maxwell's Equations.* Wiley, to appear.

[92] F. Rellich. Über das asymptotische Verhalten der Lösungen von $\Delta u + \lambda u = 0$ in unendlichen Gebieten. *Jahresber. Deutsch. Math.-Verein.*, 53:57–65, 1943.

[93] F.W. Riegels. *Aerofoil Sections.* Butterworths, London, 1962.

[94] A.H. Schatz. An observation concerning Ritz-Galerkin methods with indefinite bilinear forms. *Math. Comp.*, 28(128):959–962, October 1974.

[95] A. Shieh. On the convergence of the conjugate gradient method for singular capacitance matrix equations from the Neumann problem of the Poisson equation. *Numer. Math.*, 29:307, 1978.

[96] A. Shieh. Fast Posson solvers on general two-dimensional regions for the Dirichlet problem. *Numer. Math.*, 31:405, 1979.

[97] A. Sommerfeld. Die Greensche Funktion der Schwingungsgleichung. *Jahresber. Deutsch. Math.-Verein.*, 21:309–353, 1912.

[98] A. Sommerfeld. *Electrodynamics*, volume III of *Lectures on Theoretical Physics.* Academic Press, 1952.

[99] J.R. Stewart and T.J.R. Hughes. An a posteriori error estimator and *hp*-adaptive strategy for finite element discretizations of the Helmholtz equation in exterior domains. in preparation.

[100] J.R. Stewart and T.J.R. Hughes. Adaptive finite element methods for the Helmholtz equation in exterior domains. In *1994 NRC Symposium on Large-Scale Structures in Acoustics and Electromagnetics*, 1994.

[101] P. N. Swarztrauber. The methods of cyclic reduction, fourier analysis and the facr algorithm for the discrete solution of Poisson's equation on a rectangle. *SIAM Rev.*, 19:490–501, 1977.

[102] P. N. Swarztrauber. Fast Poisson solvers. In Gene H. Golub, editor, *MAA Studies in Numerical Analysis*, volume 24, pages 319–369. Mathematical Association of America, 1984.

[103] P. N. Swarztrauber and R. A. Sweet. The direct solution of the discrete Poisson equation on a disk. *SIAM J. Numer. Analysis*, 10:900–907, 1973.

[104] F. Ursell. On the exterior problems of acoustics. *Proc. Cambridge Philos. Soc.*, 74:117–125, 1973.

[105] F. Ursell. On the exterior problems of acoustics ii. *Math. Proc. Cambridge Philos. Soc.*, 84:545–548, 1978.

[106] H. Weyl. Kapazität von Strahlungsfeldern. *Mathematische Zeitschrift*, 55(2):187–198, 1952.

[107] O. Widlund. On the use of fast methods for separable finite difference equations for the solution of general elliptic problems. In D.J. Rose and R.A Willoughby, editors, *Sparse Matrices and their Applications*, pages 121–131. Plenum Press, New York, 1972.

[108] O. Widlund. Capacitance matrix methods for Helmholtz's equation on general bounded regions. In *Meeting in Oberwolfach, Lecture Notes in Mathematics, vol.631*, pages 209–219. Springer-Verlag, New York, 1978.

[109] O.B. Widlund. Iterative methods for elliptic problems on regions partitioned into substructures. In R. Glowinski and J.L. Lions, editors, *Proc. 6th Intern. Conf. Comput. Meth. Sci. Eng.*, pages 33–45. Elsevier Science Publishers B. V. (North Holland), 1984.

[110] C. H. Wilcox. A generalization of theorems of Rellich and Atkinson. *Proc. Amer. Math. Soc.*, 7:271–276, 1956.

[111] C.H. Wilcox. An expansion theorem for electromagnetic waves. *Comm. Pure Appl. Math.*, 9:115–134, 1956.

[112] C.H. Wilcox. *Scattering Theory for the d'Alembert Equation in Exterior Domains*. Number 442 in Lecture Notes in Mathematics. Springer Verlag, 1975.

[113] E.L. Yip. A note on the stability of solving a rank-p modification of a linear system by the Sherman-Morrison-Woodbury formula. *SIAM J. Sci. Statist. Comput.*, 7(2):507–513, April 1986.

[114] D.P. Young, R.J. Melvin, M.B. Bieterman, F.T. Johnson, S.S. Samant, and J.E. Bussoletti. A locally refined rectangular grid finite element method: application to computational fluid dynamics and computational physics. *J. Comput. Phys.*, 92(1):1–66, 1991.